

**Equilibrium Climate Modeling with a one Dimensional Coupled  
Atmosphere-Ocean Model**

by  
Takmeng Wong and Graeme L. Stephens

Department of Atmospheric Science  
Colorado State University  
Fort Collins, Colorado



**Department of  
Atmospheric Science**

Paper No. 424

**EQUILIBRIUM CLIMATE MODELING  
WITH  
A ONE DIMENSIONAL COUPLED ATMOSPHERE-OCEAN MODEL**

by

Takmeng Wong and Graeme L. Stephens

Research supported by NSF Grant ATM-8415127

Principal Investigator: Graeme L. Stephens

Department of Atmospheric Science  
Colorado State University  
Ft. Collins, CO 80523

December 1987

Atmospheric Science Paper No. 424

## ABSTRACT

Understanding the variability of the Earth's climate is complicated by the mutual interactions that exist between the atmosphere and the oceans of the Earth. The purpose of the research described in this paper is to attempt to understand the rudiments of such interactions by constructing a simple 1-D atmosphere-ocean model in order to examine the sensitivity of the equilibrium of a coupled climate "system" to changes in the imposed external forcings.

This task is achieved by developing a simple ocean and atmospheric model separately then combining these models to simulate the annual/mean state of the atmosphere and the ocean system. The model atmosphere is based on the theory of radiative transfer and includes a parameterization of convection. The mixed layer ocean model, on the other hand, is constructed using the principles of conservation of thermal energy and turbulent kinetic energy. Independent calculations with the atmospheric model suggests that this model simulates the atmosphere temperature structure realistically. The ocean model, however, had to be modified to obtain reasonable results for annual/mean climatic simulations.

The coupled atmosphere-ocean model was constructed by combining the two separate models together using simple coupling processes developed for this research. Equilibrium studies were performed to allow a first order examination of the sensitivity of the coupled system to changes in atmospheric  $CO_2$  content, solar radiation input and clouds. It was demonstrated that atmospheric forcings are important parameters that can affect the equilibrium state of the coupled atmosphere-ocean system. Specifically, the simulations demonstrated that the thermal equilibrium structure of the atmospheric part of the coupled atmosphere-ocean model remained unchanged from those provided by the atmosphere model alone; the change in  $CO_2$  content of the atmosphere had a very little effect on the oceanic mixed layer depth and the change was basically associated with altering the oceanic mixed layer temperature. On the other hand the oceanic mixed layer depth and temperature were found to be sensitive to changes in solar energy input at top of the atmosphere as the increase/decrease of solar radiation was used to heat up/cool down the

modeled ocean and also pushed the oceanic mixed layer downward/upward against the natural buoyancy forces of the ocean. It was also demonstrated how clouds alter the oceanic mixed layer depth and temperature by changing the partitions of surface inputs radiation budget. The presence of cloud produced a negative effect on the oceanic mixed layer depth since it decreased the surface inputs of solar radiation, which was the primary source of energy for the ocean system. The oceanic mixed layer temperature, however, depended on the surface inputs of net radiation (solar plus infrared) and it increased/decreased as the net surface radiation increased/decreased.

This study represents a first step in development of an simple coupled atmosphere-ocean for the purpose of understanding climate and climate variability. In light of the limited results presented in this paper, recommendations are made on future refinements and applications of the model.

## ACKNOWLEDGEMENTS

We would like to thank the following individuals, Tom Greenwald, Paul Stackhouse, Robert Stone, and Dr. Si-chee Tsay for their constructive collaboration and editorial support. We also gratefully acknowledge the efforts of Susan Lini, who helped in preparing this paper.

This research was supported by the Atmospheric Sciences Section of the National Science Foundation under Contract ATM-8415127 and computer calculation were carried out using the super computer facilities at Colorado State University Computer Center.

## CONTENTS

<b>1 Introduction</b>	<b>1</b>
1.1 Mathematical climate modeling . . . . .	1
1.2 One-dimensional climate model of the earth-atmosphere system . . . . .	4
1.3 Ocean-atmosphere climate model . . . . .	4
1.3.1 Basic problems . . . . .	8
1.3.2 An early experiment . . . . .	8
1.3.3 Unanswered questions . . . . .	9
1.4 Thesis objectives and outline . . . . .	9
<b>2 One-dimensional model of the atmosphere</b>	<b>11</b>
2.1 Temperature change due to radiation . . . . .	11
2.1.1 General theory . . . . .	11
2.1.2 Shortwave and longwave radiative temperature changes . . . . .	12
2.2 Major constituents that influence radiative temperature profile . . . . .	13
2.2.1 Trace gases . . . . .	13
2.2.2 Rayleigh scatter . . . . .	13
2.2.3 Cloud . . . . .	18
2.3 The radiative transfer model . . . . .	18
2.3.1 The clear sky longwave model . . . . .	20
2.3.2 Inclusion of cloud into the longwave model . . . . .	25
2.3.3 Short wave model . . . . .	26
2.3.4 Cloud modeling in the shortwave spectrum . . . . .	30
2.4 Parameterization of dynamical effects . . . . .	33
<b>3 Simple model of the ocean</b>	<b>35</b>
3.1 Observational studies of the ocean temperature structure . . . . .	35
3.2 General theory of oceanic temperature structure . . . . .	38
3.3 One dimensional mixed layer ocean modeling . . . . .	38
3.3.1 Basic conservation laws of the mixed layer model . . . . .	39
3.3.2 Parameterizations for surface fluxes of sensible and latent heat, mean available turbulent kinetic energy, and radiation. . . . .	44
<b>4 Experiments with the atmospheric model</b>	<b>48</b>
4.1 Input conditions and computational procedures . . . . .	49
4.2 Response of the pure radiative atmosphere . . . . .	55
4.3 Modeling the troposphere with convective adjustment . . . . .	56
4.4 Atmospheric model with fixed relative humidity . . . . .	61
4.5 Model Sensitivities . . . . .	68
4.5.1 Solar input . . . . .	68

4.5.2	Carbon dioxide . . . . .	68
4.5.3	Surface albedo . . . . .	71
4.5.4	Cloud effects . . . . .	74
4.6	Summary of the model's performance . . . . .	75
<b>5</b>	<b>Performance of the ocean model.</b>	<b>78</b>
5.1	Input conditions and computational method. . . . .	78
5.2	Evaluation of the model's seasonal cycle. . . . .	80
5.2.1	The mixed layer depth. . . . .	80
5.2.2	The mixed layer temperature. . . . .	83
5.3	Annual/mean simulations. . . . .	85
5.3.1	Problems in running the annual model. . . . .	85
5.3.2	A hybrid annual model for studying the mean ocean condition. . . . .	85
5.4	Sensitivity experiments with the new ocean model. . . . .	86
5.4.1	Oceanic radiation parameterization. . . . .	86
5.4.2	Temperature gradient below the mixed layer . . . . .	89
5.4.3	Turbulent parameterization . . . . .	90
5.4.4	Solar and atmospheric radiation inputs . . . . .	90
5.4.5	Atmospheric wind speed, water vapor content, and temperature. . . . .	91
5.4.6	Summary of the new hybrid annual ocean model . . . . .	92
<b>6</b>	<b>Joint equilibrium atmosphere-ocean model</b>	<b>93</b>
6.1	Basic considerations in connecting the two systems . . . . .	94
6.1.1	The different structure of the two models . . . . .	94
6.1.2	The models' behavior . . . . .	94
6.2	Theory and assumptions of the coupled system . . . . .	97
6.2.1	Coupling methods . . . . .	97
6.2.2	Equilibrium state of the coupled system . . . . .	98
6.2.3	Energy conservation parameterization . . . . .	99
6.2.4	Definition of heat storage . . . . .	100
6.3	Performance of the coupled model . . . . .	103
6.3.1	Input values and method of computations . . . . .	103
6.3.2	Clear sky condition . . . . .	103
6.3.3	Sensitivity studies with $CO_2$ , solar constant, and cloud . . . . .	103
6.4	Summary of the equilibrium coupled model sensitivities and their climatic im- plications . . . . .	106
<b>7</b>	<b>Summary, conclusion, and recommendations</b>	<b>109</b>
7.1	1-D convective-radiative atmosphere model . . . . .	110
7.2	The performance of the model atmosphere . . . . .	111
7.3	Overview of the mixed layer ocean model . . . . .	112
7.4	Ocean model behavior . . . . .	112
7.5	Conclusions drawn from the joint equilibrium atmosphere-ocean model . . . . .	113
7.6	Recommendation for possible future research . . . . .	114
7.6.1	Possible future research topics . . . . .	115
7.6.2	Suggestions on future modeling and observational approach to the coupled atmosphere-ocean system . . . . .	116

<b>Reference</b>	<b>117</b>
<b>A On the numerical instability of the ocean model</b>	<b>120</b>
<b>B Construction of the hybrid annual/mean ocean mixed layer model</b>	<b>122</b>

## LIST OF FIGURES

1.1	Within historical time, the advance and retreat of glaciers have provided startling evidence of climate change . . . . .	2
1.2	Example of some possible feedback processes in a climate system (after Schneider, 1974). . . . .	3
1.3	Pure radiative equilibrium for various atmospheric absorbers. The distribution of gaseous absorbers at 35N in April are used. . . . .	5
1.4	Thermal equilibrium of various atmospheres with clouds (the critical lapse rate for convective adjustment . . . . .	6
1.5	Vertical distributions of temperature in radiative convective . . . . .	7
2.1	Normalized blackbody spectra representative of the sun . . . . .	14
2.2	The terrestrial infrared spectra and various absorption bands. . . . .	15
2.3	Spectral irradiance distribution curves related to the sun: . . . . .	16
2.4	On the average, of all the solar energy that reaches the . . . . .	17
2.5	Illustration of infrared upward and downward fluxes at level $Z$ . . . . .	22
2.6	Absorption spectrum of the water vapor rotational band and 15 . . . . .	24
2.7	Illustration of each term in equation 2.17. . . . .	28
2.8	Comparisons between the shortwave absorption, transmission and cloud albedo . . . . .	31
2.9	Values of solar absorptance $\alpha$ , solar albedo $\alpha$ , plotted against . . . . .	32
2.10	Temperature profile of actual atmosphere (solid curve), pure radiation . . . . .	34
3.1	Temperature Profile of the ocean. (after Thurman, 1981) . . . . .	36
3.2	The seasonal temperature cycle ( $^{\circ}\text{F}$ ) in . . . . .	36
3.3	Zonal sea surface temperature between 7/10/83 to 11/10/84 compiled using both surface and satellite data. . . . .	37
3.4	Schematic of the thermocline and the boundary . . . . .	40
4.1	Annual/mean mid-latitude temperature profile compiled by McClatchey et al., 1973. . . . .	50
4.2	Same as Figure 4.1, except for mixing ratio. . . . .	51
4.3	Same as Figure 4.1, except for ozone mixing ratio. . . . .	52
4.4	Approach to pure radiative equilibrium temperature from two initial isothermal atmosphere at 170k and 340k. . . . .	57
4.5	The change in the net flux difference between upward longwave and downward shortwave energy at the top of the model. . . . .	58
4.6	Temperature profile of the real atmosphere (solid curve) and pure radiative atmosphere model (dash curve). . . . .	59
4.7	Distribution of radiative equilibrium temperature. . . . .	60
4.8	Approach to radiative convective temperature profile from two initial isothermal atmosphere at 170k and 340k. . . . .	62

4.9	Temperature profile of actual atmosphere (solid curve), pure radiative atmosphere model (dash curve), and radiative convective atmosphere model (dot curve). . . . .	63
4.10	Vertical distribution of relative humidity (Mastenbrook, 1963; Murgatroyd, 1960; Telegadas and London, 1954) (after Manabe and Weatherald, 1967). . . . .	65
4.11	Vertical profiles of various equilibrium radiative heating rate. . . . .	66
4.12	Temperature profile from real atmosphere (solid), experiment 2 (dash), and experiment 3 (dot). . . . .	67
4.13	Solar input and surface temperature of radiative convective equilibrium. . . . .	69
4.14	Vertical distribution of radiative convective equilibrium temperature of the atmosphere for various values of solar input. . . . .	70
4.15	Vertical distributions of temperature in radiative convective equilibrium for various values of $CO_2$ content. . . . .	72
4.16	Vertical distributions of radiative convective equilibrium for various values of surface albedo. . . . .	73
4.17	Vertical distribution of radiative convective equilibrium temperature for various types of cloud condition. . . . .	76
5.1	The approach to steady state mixed layer depth for seasonal model. . . . .	81
5.2	The approach to steady state solution for sea surface temperature for seasonal model. . . . .	82
5.3	Isopleths of surface temperature in the Atlantic Ocean after Defant, 1961). . . . .	84
5.4	The approach to steady state mixed layer depth for hybrid annual/mean model. . . . .	87
5.5	The approach to steady state solution for sea surface temperature for hybrid annual/mean model. . . . .	88
6.1	Rate of heat storage ( $wm^{-2}$ ) in the atmosphere . . . . .	95
6.2	Northward flux of energy ( $10^{15}W$ ) in the atmosphere . . . . .	96
6.3	Schematic representation of energy adjustment process (method 1). . . . .	101
6.4	Same as Figure 6.3 except for method 2. . . . .	102

## LIST OF TABLES

2.1	Composition of the earth's atmosphere. (after Ahrens, 1982) . . . . .	12
2.2	Infrared emissivities (%). (after Sellers, 1965) . . . . .	21
2.3	List of gases and their correction methods. . . . .	23
2.4	Methods for emissivity calculation. . . . .	25
2.5	Annual mean daily solar insolation (watts/m <sup>2</sup> ). . . . .	29
2.6	Annual mean surface albedo (%). . . . .	29
2.7	Clean air shortwave parameterization schemes. . . . .	30
3.1	Solar Spectral Attenuation Length for oceanic water. (after Defant, 1961) . . .	47
4.1	Summary of different cases run with the atmosphere model. . . . .	48
4.2	Tabulated annual mid-latitude profile of air pressure(P), air temperature(T), air density(D), water vapor mixing ratio(Q), and ozone content(O <sub>3</sub> ). . . . .	53
4.3	The levels used in the model. . . . .	54
4.4	Equilibrium and change of equilibrium temperature (K) of the earth's surface corresponding to various CO <sub>2</sub> content of the clear atmosphere. . . . .	71
4.5	Equilibrium and change of equilibrium temperature (K) of the earth's surface corresponding to various values of the surface albedo. . . . .	74
4.6	Setups for the clouds studies . . . . .	75
4.7	Equilibrium temperature (K), downward energy budget . . . . .	75
5.1	Annual/mean inputs for the ocean model according to their categories. . . . .	79
5.2	Seasonal fluctuation for the atmospheric inputs. . . . .	80
5.3	The mixed layer/quasi-isothermal top layer temperature (°C) in the Atlantic Ocean (after Defant, 1961). . . . .	83
5.4	Annual sea surface temperature variations (°C) (after Defant, 1961). . . . .	83
5.5	Experiment setups and results for studying oceanic radiation extinction length. . . . .	89
5.6	Same as table 5.5 except for temperature gradient (lapse rate) below the mixed layer. . . . .	90
5.7	Same as table 5.5 except for turbulent parameterization constant. . . . .	90
5.8	Same as table 5.5 except for solar radiation input. . . . .	91
5.9	Same as table 5.5 except for atmosphere radiation input. . . . .	91
5.10	Same as table 5.5 except for atmosphere wind input. . . . .	92
5.11	Same as table 5.5 except for atmosphere water vapor content input. . . . .	92
5.12	Same as table 5.5 except for atmosphere temperature input. . . . .	92
6.1	Equilibrium ocean model under clear sky condition. . . . .	104
6.2	Same as table 6.1 except for various CO <sub>2</sub> content using Method 1. . . . .	104
6.3	Same as table 6.1 except for various CO <sub>2</sub> content using Method 2. . . . .	104
6.4	Same as table 6.1 except for various solar input using Method 1. . . . .	105

6.5	Same as table 6.1 except for various solar input using Method 2. . . . .	105
6.6	Cloud parameters and surface downward flux of radiation ( $W/m^2$ ) for different cloud studies. . . . .	106
6.7	Same as table 6.1 except for various cloud inputs using Method 1. . . . .	106
6.8	Same as table 6.1 except for various cloud inputs using Method 2. . . . .	106

## Chapter 1

### INTRODUCTION

Throughout man's history, natural climatic changes have been known to play an important role in determining the outcome of many civilizations (see Claiborne, 1970 and Schneider and Dickinson, 1974). The evidence of such climatic variation is illustrated in figure 1.1. The understanding of natural forcings which produce these changes is not simple since there are many interactions between various component of the climate system, which may or may not cancel each other, as illustrated in figure 1.2. Superimposed on this picture is the further complication that is introduced by the impact of anthropogenic materials and technologies (i.e., increasing level of carbon dioxide, methane, freon, fluorocarbons, deforestation, exploitation of the open ocean, etc.). A complete comprehension of these natural and anthropogenic induced climate changes is necessary since millions of people in today's society can be affected by climate variation.

#### 1.1 Mathematical climate modeling

Unfortunately, there is no comprehensive theory of climate to explain its variability nor are there physical models that can adequately simulate the complete climate system. The use of mathematical models of the earth's climate have proved to be useful in understanding and untangling the complex interactive processes referred to in figure 1.2. Many modeling approaches are available, ranging from a simple one-dimensional representation of the vertical radiative processes in the atmosphere (i.e., Manabe and Moller, 1961 and among others.) to very complex mathematical systems that describe the three-dimensional behavior of the entire system along with the thermodynamic processes that control the hydrological cycle and cryosphere (such as Manabe and Bryan, 1969 for example).

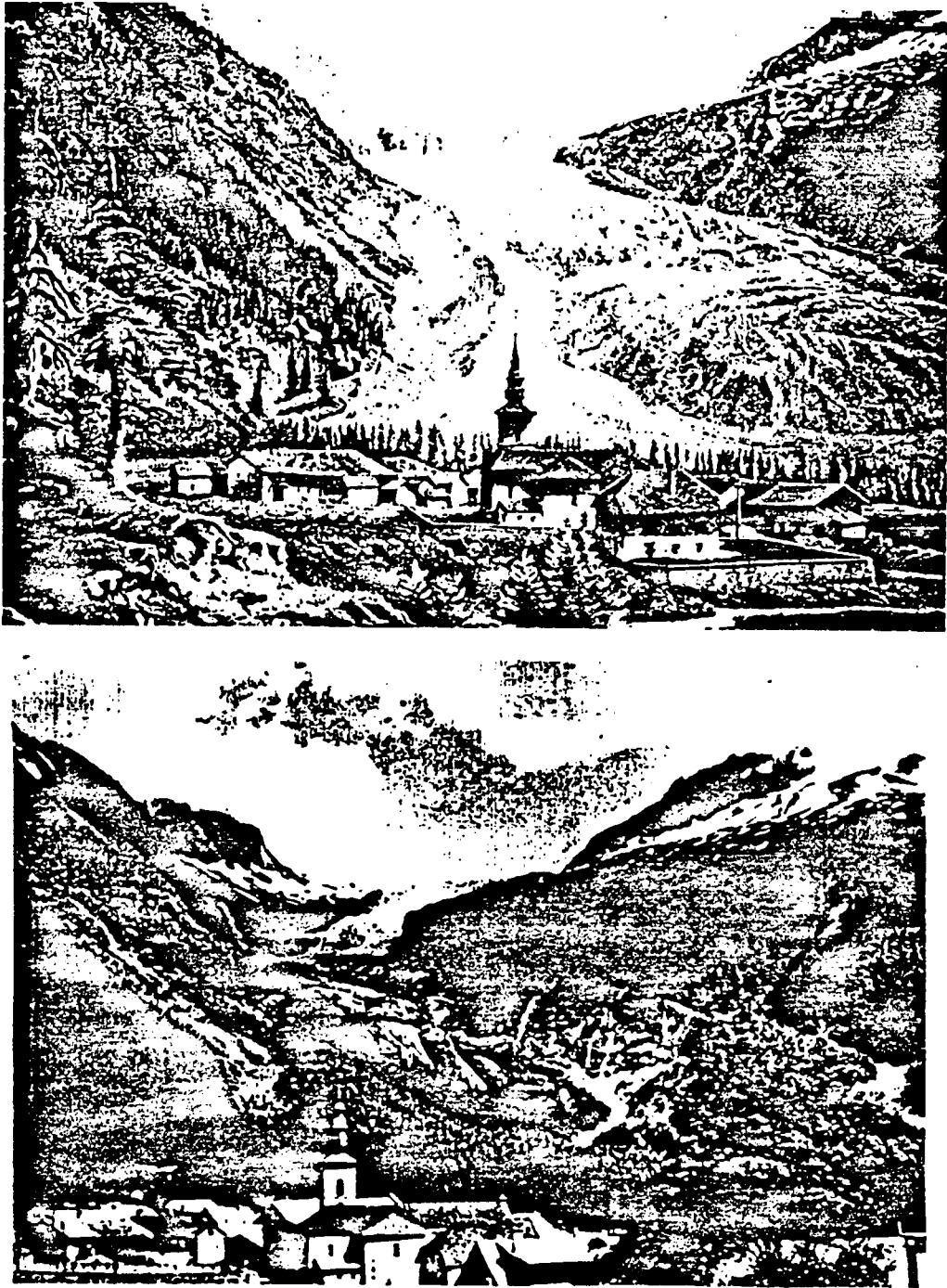


Figure 1.1: Within historical time, the advance and retreat of glaciers have provided startling evidence of climate change, as can be seen from these two pictures of the Argentinere Glacier (Top: An etching made in 1855, and Bottom: a photograph of same scene taken in 1966) (after Schneider, 1974).



Since simpler models isolate the important physical processes that determine the broad features of the climate, they are used frequently in climate studies not only to access the sensitivity of the simple hypothetical climate system to changes in climate forcing but also to provide a suitable framework on which parameterizations for the more elaborate models can be developed. The simplest models of climate are essentially one dimensional, with the dependence on other dimensions being simply parameterized or neglected.

## 1.2 One-dimensional climate model of the earth-atmosphere system

One-dimensional (1-D) climate model is intended to model the vertical structure of various radiative fluxes and temperature assuming some form of globally averaged radiative and convective heat transfer processes. Such a model is used to provide some insight into the relationship between a hypothetical climate and specific external forcings. Many of the pioneering works in the study of climate were performed using this type of model. Manabe and Moller (1961) for example employed such a model to demonstrate the importance of atmospheric gases, such as  $CO_2$ ,  $O_3$ , and  $H_2O$ , in maintaining the radiative balance of the global system (see figure 1.3). In a following study, Manabe and Strickler (1964) further introduced the feedback processes between dynamics (through convection) and radiative effects and explained their roles in maintaining the observed tropospheric temperature profile of the atmosphere. The same study also suggested that the possibility that high cirrus cloud might warm the earth surface (see Fig. 1.4). This study, however, did not consider the effect of moisture-temperature feedback, which can be important in the real atmosphere. This feedback process was later incorporated into the model by Manabe and Weatherald (1967). Their results suggested that the increasing  $CO_2$  content of the atmosphere can lead to a significant warming effect at the earth surface (see Fig. 1.5). Although these studies are no doubt classical works, they are somewhat incomplete due to the absence of the ocean system.

## 1.3 Ocean-atmosphere climate model

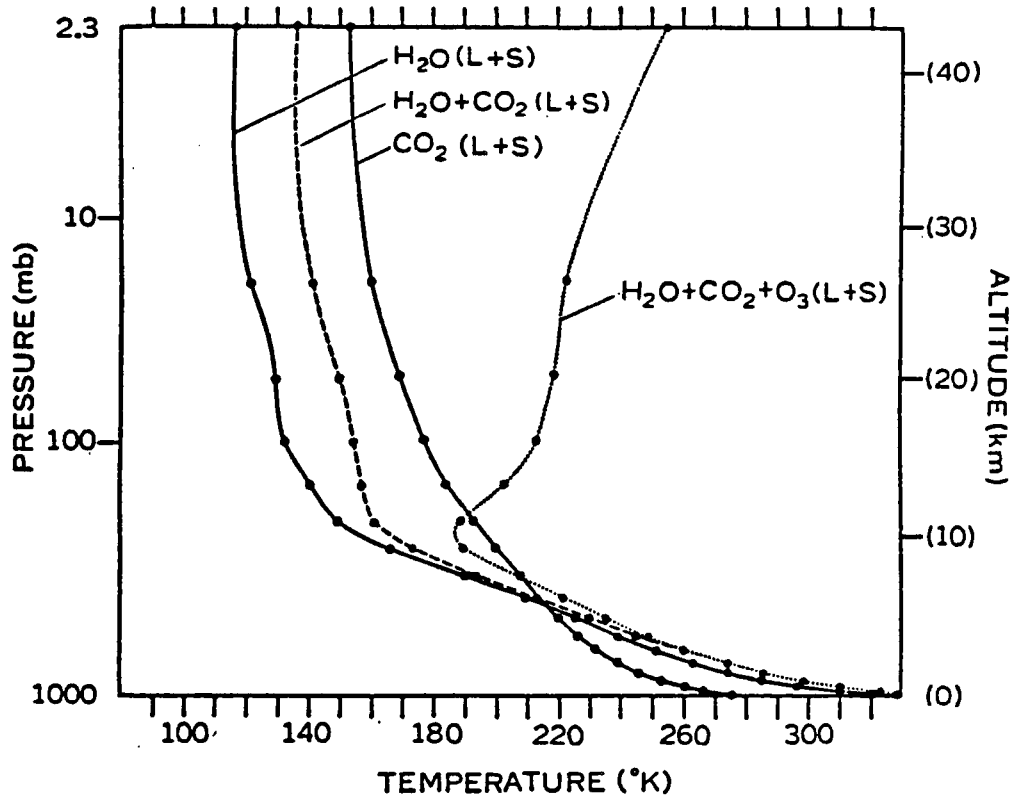


Figure 1.3: Pure radiative equilibrium for various atmospheric absorbers. The distribution of gaseous absorbers at 35N in April are used.  $S_e = 2 \text{ ly min}^{-1} \cos \bar{\xi} = 0.5$ ,  $\tau = 0.5$ . No clouds. (L+S) means that the effects of both longwave radiation and solar radiation are included (after Manabe and Strickler, 1964).

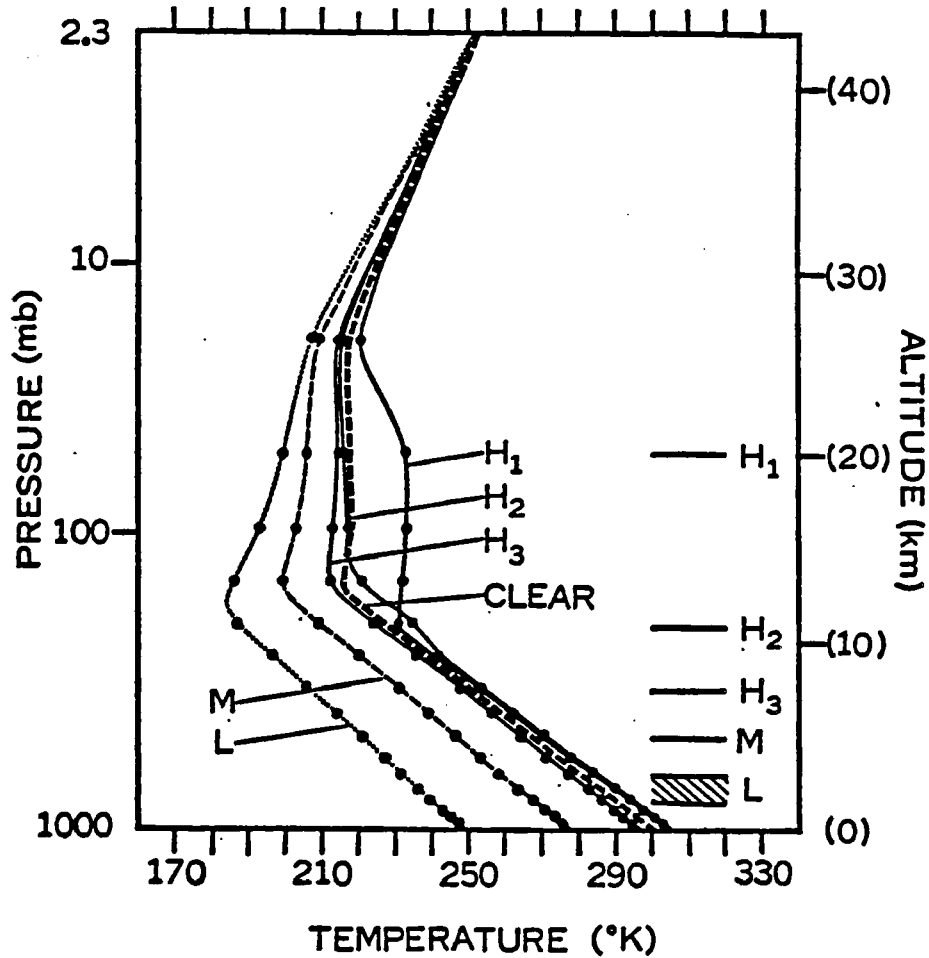


Figure 1.4: Thermal equilibrium of various atmospheres with clouds (the critical lapse rate for convective adjustment is  $6.5 \text{ deg km}^{-1}$ ). On the right-hand side of the figure the height of overcast clouds used for each computation is shown,  $H_1, H_2$ , and  $H_3$  denoting high clouds,  $M$  and  $L$  denoting middle and low clouds. As a reference, the equilibrium curve of the clean atmosphere is shown by a thick dashed line (after Manabe and Strickler, 1964).

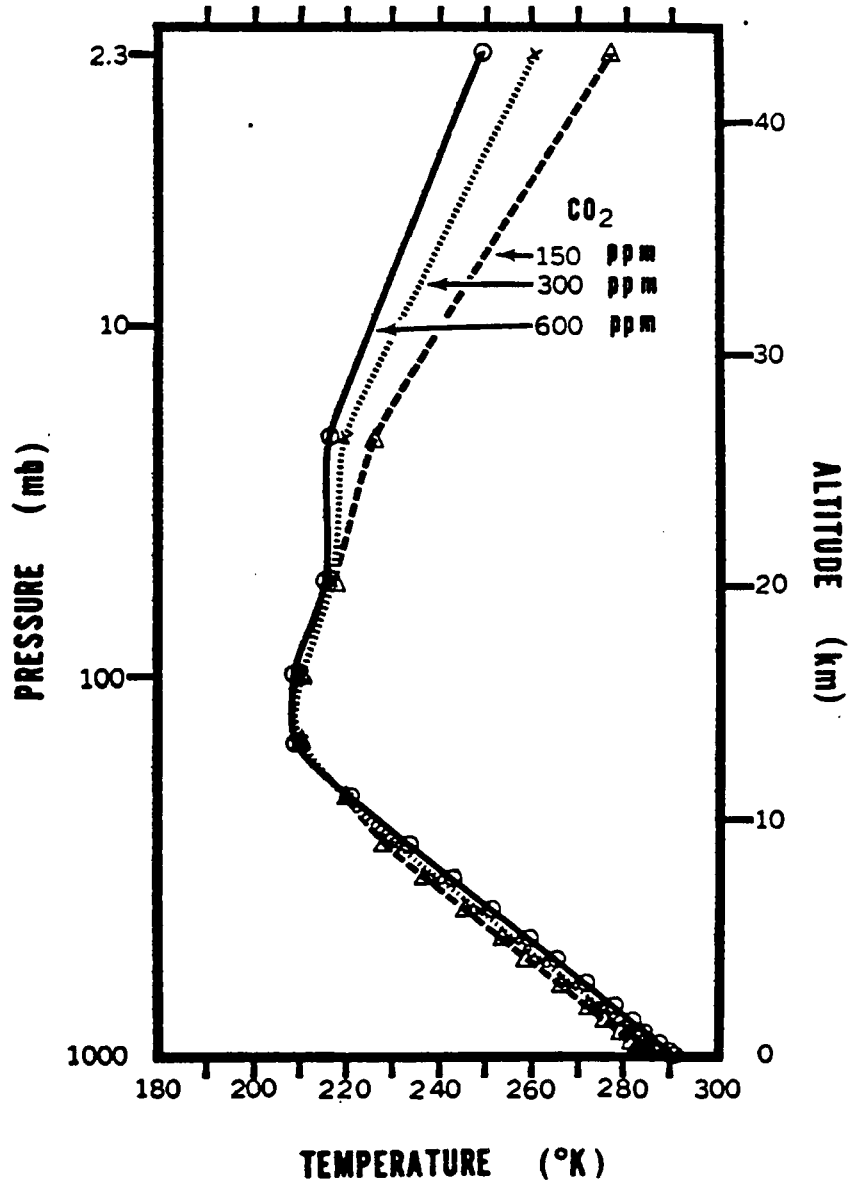


Figure 1.5: Vertical distributions of temperature in radiative convective equilibrium for various values of CO<sub>2</sub> content (after Manabe and Weatherald, 1969).

### 1.3.1 Basic problems

The lack of an ocean component in the early climate studies is largely due to the fact that the ocean system is not largely understood at that time. Even today, the complete structure of the deep ocean are still very much unknown due to lack of observational data. Many of the existing 3-D ocean models rely on theoretical considerations along with some limited amount of observational data in the upper ocean. It is still uncertain whether these models can be used realistically to simulated oceanic structure on a climatic timescale.

These are not the only problems encountered in coupling an ocean to an atmospheric model. We are faced with even a more difficult problem when we consider the thermal relaxation time associate these two "systems". Estimation of the atmospheric thermal relaxation time is about one year while the ocean system operates on 100's or even 1000's of years. It is therefore impractical to run numerical models (usually with time step of less than 3 minutes for a 3-D atmosphere model) over such a long period of time. In addition to this, the different physical properties at the air-sea boundary (such as latent and sensible heat transfer) also add to the uncertainty of coupling an ocean and atmosphere model.

### 1.3.2 An early experiment

Manabe and Bryan (1969) have made the first attempt at jointly modeling the atmosphere, ocean, and cryosphere to study the equilibrium state of a model climate system under annual/mean conditions. The results of this 3-D climate model indicated important effects that depended specifically on the interactions between the atmosphere and ocean. They found that:

1. a drastic reduction of modeled rainfall over the tropical ocean resulted from equatorial upwelling that altered the ratio of land-sea precipitation,
2. the ocean is very important in reducing the meridional atmospheric temperature by transporting heat poleward. This transport helped to decrease the magnitude of eddy kinetic energy in the atmosphere,

3. the air mass modification by the energy exchange between the model ocean and atmosphere creates a favorable place for the development of cyclones off the east coast of the continents in high latitudes, and
4. the coupled model suggested that the deep oceanic circulations could be important for climate variations on a timescale of over 100's years.

### 1.3.3 Unanswered questions

The problem encountered in the studies by Manabe and Bryan (1969) is that they were unable to obtain a true equilibrium state of the entire system. The question of whether their results can be used to infer the true equilibrium condition of the coupled system remains an open issue to debate even today. Beside this main problem, the model results are extremely complicated to analyze since many physical processes are coupled together, therefore making it difficult to estimate the significance of an individual process. Thus there is a need to construct some simpler model to examine the structure of the equilibrium state of the coupled atmosphere-ocean system and its sensitivity to any possible imposed external change.

### 1.4 Thesis objectives and outline

There are five main objectives in this thesis:

1. A 1-D convective radiative model of the atmosphere will be developed based on solving the equation of radiative transfer and by parameterizing the effect of dynamics (specifically of convection). The model should be able to simulate the temperature profile of the atmosphere under annual/mean conditions of solar energy input, clouds, and different atmospheric absorbers. This model is presented in Chapter 2.
2. This 1-D model of the atmosphere must be properly tested to insure its reliability. This is done in Chapter 4 where a series of experiments are conducted to simulate both the radiative and convective properties of the model atmosphere and its sensitivity to different solar inputs, carbon dioxide levels, surface albedo values, and cloud forcings.

3. A simple 1-D mixed layer model of the ocean will be formulated based on kinetic turbulent theory and conservation of energy with a simple parameterization for absorption of radiation in the ocean. The aim of this model is to simulate the temperature structure of the ocean realistically. This objective is pursued in Chapter 3 of this thesis.
4. The ocean model will be tested to determine its limitations and abilities. Sensitivities of the model ocean to different forcings (such as oceanic solar radiation extinction rates, turbulent parameterization, temperature lapse below the mixed layer, atmosphere wind speed, atmosphere temperature, atmosphere moisture, and surface radiation inputs) will be performed. This is carried out in Chapter 5.
5. The 1-D model atmosphere and ocean are coupled together in Chapter 6 of the thesis to investigate the equilibrium condition of the coupled system. Some simple coupling processes and assumptions will be proposed to allow first order examination of the equilibrium system. Sensitivities experiments will also be presented. The research describe in this chapter constitutes much of the original work of this thesis.

## Chapter 2

### ONE-DIMENSIONAL MODEL OF THE ATMOSPHERE

A simple one-dimensional (1-D) numerical model of the atmosphere is constructed in this chapter with the specific purpose of simulating the atmospheric temperature profile. The model is based on radiative transfer theory with dynamical effects incorporated using a parameterization scheme.

#### 2.1 Temperature change due to radiation

##### 2.1.1 General theory

The change in radiative temperature at any layer in the atmosphere is caused by imbalance of the radiative inputs and outputs from that layer. This imbalance results from the differences in absorption, reflection and transmission of the constituents that make up the atmosphere. A summary of the most common atmospheric constituents (neglecting water and ice) is presented in table 2.1.

The conservation law describing the local rate of change of the radiative temperature at any single vertical point with height  $Z'$  in the atmosphere is

$$\left[ \frac{d}{dt} T(Z') \right]^G = \frac{g}{C_p} \left[ \frac{d}{dp} F_n(Z') \right]^G = \frac{-1}{\rho_a C_p} \left[ \frac{d}{dz} F_n(Z') \right]^G \quad (2.1)$$

where superscript  $G$  stands for different atmospheric constituents,  $p$  is air pressure,  $\rho_a$  is the air density,  $C_p$  is specific heat of air at constant pressure,  $Z$  is height,  $t$  is time,  $T(Z')$  is radiative temperature at the point  $Z'$ , and  $dF_n(Z')$  is the local change in net radiative flux at point  $Z'$ . This net flux term is given by

$$F_n(Z') = F_{up}(Z') - F_{dn}(Z') \quad (2.2)$$

Table 2.1: Composition of the earth's atmosphere. (after Ahrens, 1982)

Constituent	Percent by Volume
Nitrogen ( $N_2$ )	78.0800
Oxygen ( $O_2$ )	20.9500
Argon ( $A$ )	0.93000
Carbon dioxide ( $CO_2$ )	0.03000
Water vapor ( $H_2O$ ) *	0. -4.
Neon ( $Ne$ )	0.00180
Ozone ( $O_3$ ) *	0.00050
Helium ( $He$ )	0.00050
Hydrogen ( $H_2$ )	0.00020
Carbon monoxide ( $CO$ )*	0.00001
Sulfur dioxide ( $SO_2$ )*	0.00001
Nitrogen dioxide ( $NO_2$ )*	0.00001
Particles (dust, soot, etc.)*	0.00001

\*Highly variable constituents

where  $up$  and  $dn$  represent the upward and downward flux of the radiation at the point  $Z'$ . The physical interpretation of equation (2.1) can be stated simply as the local rate of change of the radiative temperature at the point  $Z'$  in the atmosphere is governed by the flow of radiation into and out of that point (or by the local gradient of net flux at that point). If the net amount of radiation is diverging from a given point, that point loses energy and cools. Conversely, if the net flux is converging into that point, the point experiences radiative warming.

In finite difference form, equation (2.1) can be written as

$$\left[ \frac{\Delta T}{\Delta t} \right]^G = \frac{g}{C_p} \left[ \frac{\Delta F}{\Delta p} \right]^G = \frac{-1}{\rho_a C_p} \left[ \frac{\Delta F}{\Delta z} \right]^G \quad (2.3)$$

where now  $\frac{\Delta F}{\Delta p}$  or  $\frac{\Delta F}{\Delta z}$  applies to some layer of finite thickness of  $\Delta p$  or  $\Delta z$  and  $\frac{\Delta T}{\Delta t}$  represents the change in temperature per time step. Thus the local rate of change in temperature can now be calculated by using flux values at the layer boundaries and  $\frac{\Delta T}{\Delta t}$  can be interpreted as being a mean layer or layer-center quantity.

### 2.1.2 Shortwave and longwave radiative temperature changes

Solar radiation received at the earth is concentrated in the visible and near-infrared portions of the electromagnetic spectrum, while the radiation emitted by the earth and its

atmosphere is largely confined to the infrared region. This feature permits the study of solar effects on the radiative temperature profile of the atmosphere to be made independently from those of the earth and its atmosphere. Figure 2.1 shows the normalized blackbody curves for solar and planetary energy and further highlights this point. There with this in mind, the rate of change of radiative temperature at any layer in the atmosphere can be separated into its short and longwave components by

$$\left[\frac{\Delta T}{\Delta t}\right]^G = \left[\frac{\Delta T}{\Delta t}\right]_{SW}^G + \left[\frac{\Delta T}{\Delta t}\right]_{LW}^G \quad (2.4)$$

## 2.2 Major constituents that influence radiative temperature profile

### 2.2.1 Trace gases

While most of the constituents presented in table 2.1 have distinct absorption features over the short and long wave spectrum, only the trace gases  $H_2O$ ,  $CO_2$ , and  $O_3$  have a dominant effect on the radiative heating. Figure 2.2 provided an example of the measured longwave emission spectrum of earth's atmosphere obtained from Nimbus 4 satellite. The absorption bands which mainly contribute to longwave radiation of the atmosphere are defined in the figure to be those of  $6.3\mu m$  vibration band, the rotation band and the continuum region all associated with water vapor, the  $15\mu m$  band of carbon dioxide and the  $9.6\mu m$  band of ozone. In the short wave spectral region, the absorption is mainly due to ozone and water vapor with somewhat weaker contribution by carbon dioxide as illustrated in figure 2.3. In view of this, only the radiative temperature change resulting from these three gases will be modeled in the present study.

### 2.2.2 Rayleigh scatter

In addition to absorption by trace gases, Rayleigh scatter by gas molecules (i.e., by  $N_2$  and  $O_2$ ) is also important to the radiative energy budget of our climate system, and together they account for 6 percent of the total reflected solar radiation at the top of the atmosphere (shown in figure 2.4). This process is included in the model developed for this study.

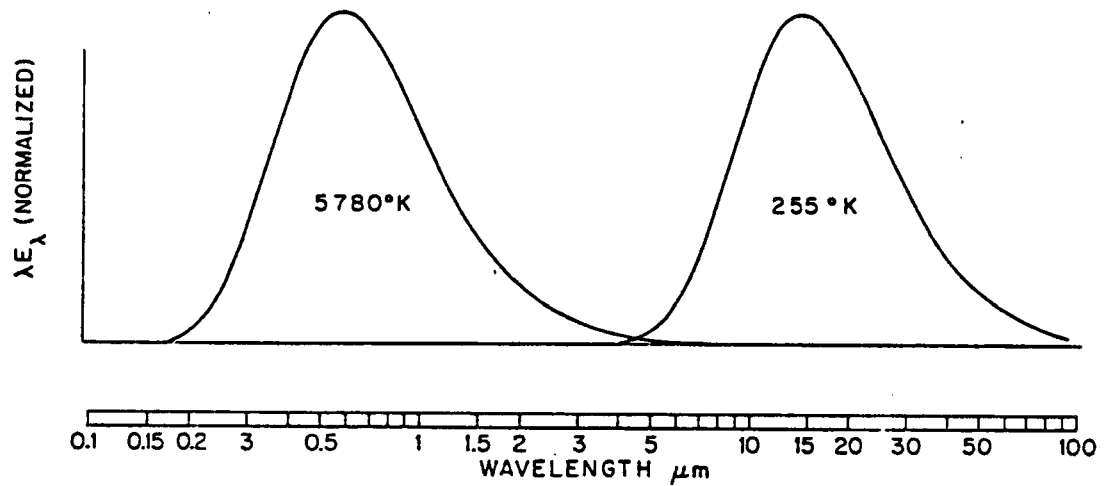


Figure 2.1: Normalized blackbody spectra representative of the sun (left) and earth (right), plotted on a logarithmic wavelength scale. The ordinate is multiplied by wavelength in order to make area under the curves proportional to irradiance. [Adapted from R. M. Goody. "Atmospheric Radiation." Oxford Univ. Press (1964), p.4.], (after Wallace and Hobbs, 1979)

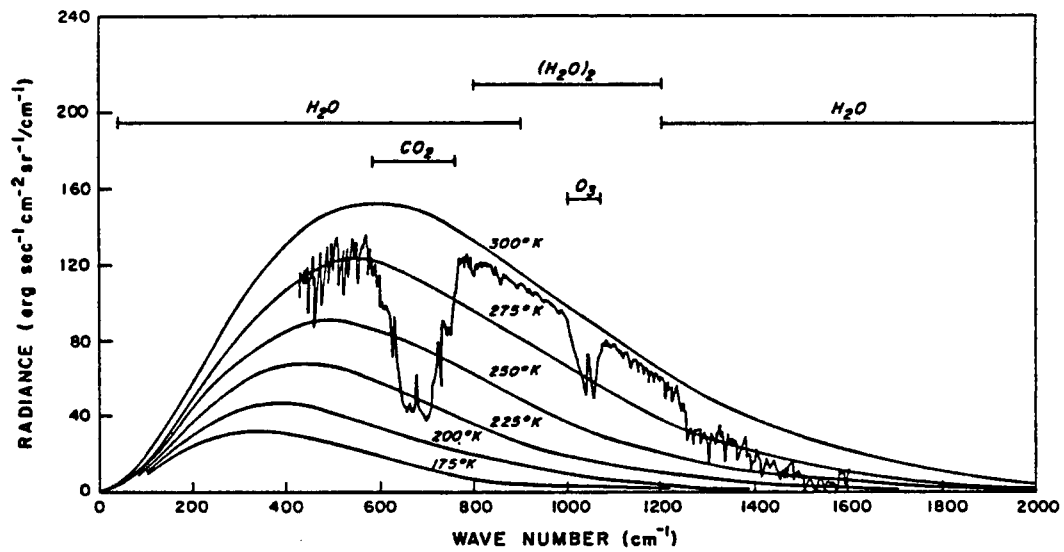


Figure 2.2: The terrestrial infrared spectra and various absorption bands. Also shown is an actual atmospheric emission spectrum taken by the Nimbus IV IRIS instrument near Guam at 15.1 N and 215.3 W on April 27, 1970. (after Liou, 1980)

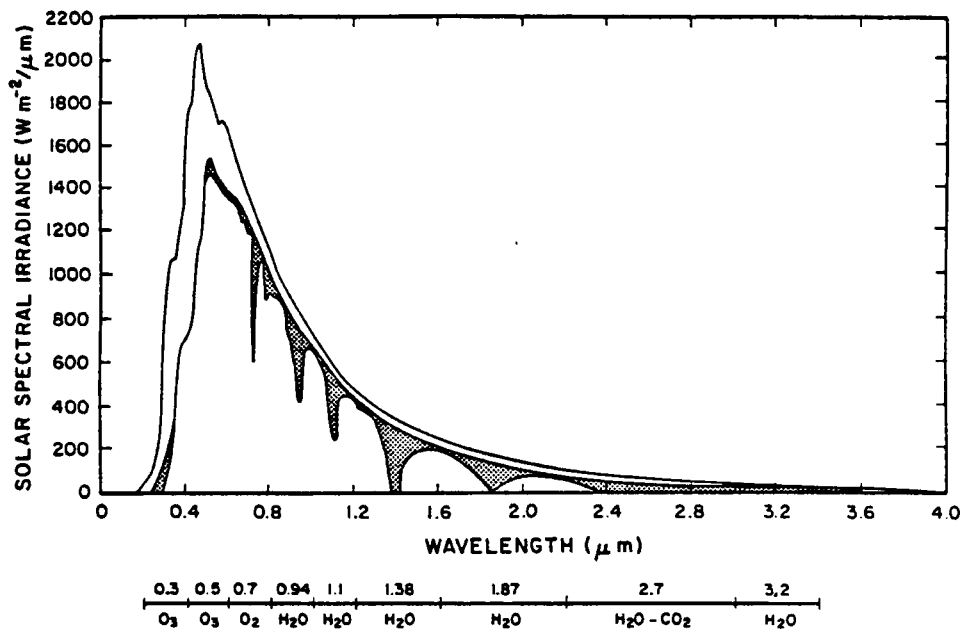


Figure 2.3: Spectral irradiance distribution curves related to the sun: (1) the observed solar irradiance at the top of the atmosphere (after Thekaekara, 1976) and (2) solar irradiance observed at sea level. The shaded areas represent absorption due to various gases in a clear atmosphere. (after Liou, 1980)

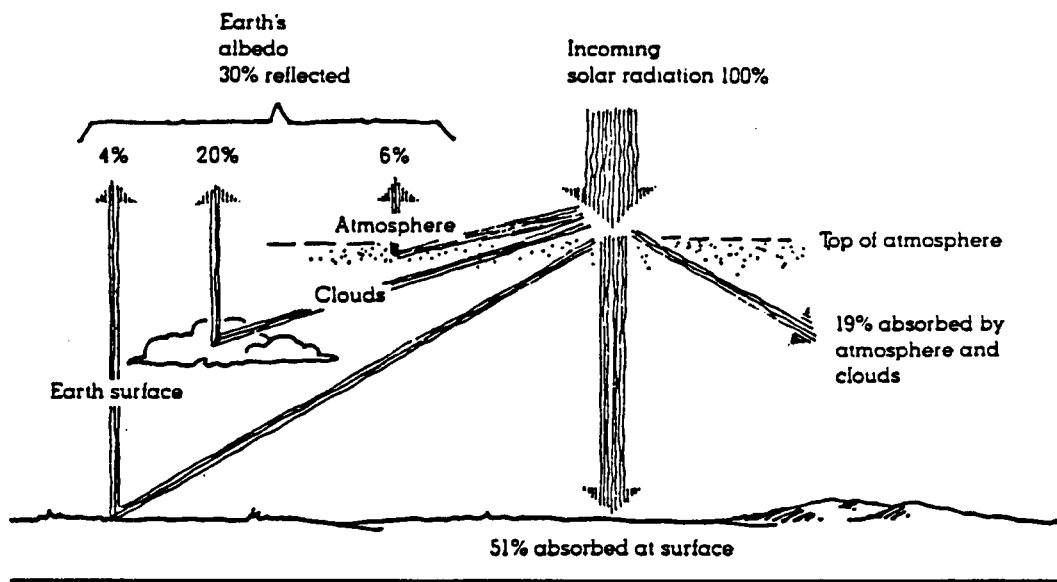


Figure 2.4: On the average, of all the solar energy that reaches the earth's atmosphere, about 30 percent is reflected back to space, 19 percent is absorbed by the atmosphere and clouds, and 51 percent is absorbed at the surface. (after Ahrens, 1981)

### 2.2.3 Cloud

The scatter and absorption effects of cloud droplets/crystals in both the shortwave and longwave spectrum have a significant impact in the transfer of radiation through the atmosphere. These processes are included in this study using simple parameterizations.

### 2.3 The radiative transfer model

This section discusses how the net flux and flux divergence terms that appear in equation (2.1) and (2.2) are calculated from radiative transfer equations. A simple radiative transfer model adopted from that used by Stephens and Webster (1979) is used and is described in the following section.

Before describing this model, it is necessary to introduce some preliminary concepts of radiative transfer. The equation describing the transfer of monochromatic radiation through an absorbing, emitting, and scattering medium can be found in many introductory atmospheric radiation texts. In its most general form,

$$\underline{\zeta} \cdot \nabla I_\nu = -\rho K_{ext,\nu}(P, T) \cdot [I_\nu - S] \quad (2.5)$$

where  $\rho$  is the density of gas,  $K_{ext,\nu}(P, T)$  is the spectral volume extinction coefficient of the medium, which is a function of temperature and pressure,  $I_\nu$  is the monochromatic intensity field of the radiation,  $\underline{\zeta}$  is the spherical coordinate's unit vector and  $S$  represents the source of radiation within the medium.

Equation (2.5) states that the divergence or leakage of radiation from a beam of direction  $\underline{\zeta}$  as it passes along some path of the atmosphere is caused by the attenuation of radiation within the medium plus the addition of radiation from internal (or external) sources.

In the usual cartesian coordinate system, (2.5) can be transformed under the assumption of a plane-parallel, horizontal homogeneous atmosphere to

$$\mu \frac{d}{dZ} I_\nu(Z, \mu, \phi) = -\rho K_{ext,\nu} I_\nu(Z, \mu, \phi) + \rho K_{ext,\nu} (1 - \bar{\omega}_o) B_\nu(T) +$$

$$\rho K_{ext,\nu} \frac{\bar{\omega}_o}{4\pi} \int_0^{2\pi} \int_{-1}^1 P(\mu, \phi, \mu', \phi') I_\nu(Z, \mu', \phi') d\mu' d\phi'$$

$$+ \frac{\tilde{\omega}_o}{4} F_o P(\mu, \phi, \mu_o, \phi_o) \text{ext} \left( \frac{- \int_z^\infty \rho K_{\text{ext}, \nu} dZ'}{\mu_o} \right) \quad (2.6)$$

where the spatial derivatives along the horizontal surface are zero and where the cosine of the zenith angle ( $\mu$ ) and the azimuthal angle ( $\phi$ ) result from the coordinate transformation.  $\tilde{\omega}_o$  is the single scattering albedo which describes the amount of scattering to the total extinction of the single particles (or of a small volume of particles),  $P$  is the phase function which describes the probability of scattering associated with each of the scatter angle, and  $B_\nu(T)$  is the spectral Plank emission function at temperature  $T$  and wave number  $\nu$ ,  $\mu_o$  is the cosine of the sun zenith angle,  $\phi_o$  is the azimuthal angle of the sun, and  $F_o$  is the solar constant at top of the atmosphere. The first term on the right hand of (2.6) is the "sink" for radiation due to attenuation within the atmosphere while the remaining terms of the right hand side represents the "sources" of radiation. These include emission, scattering from the surrounding atmosphere, and the effects of scattering of the collimated solar flux which is treated as a separate source of radiation.

Equation (2.6) is the general equation of radiative transfer suitable for a 1-D study of the atmosphere. The net flux can be calculated directly by solving (2.6) for intensity and integrating to give the fluxes

$$\begin{aligned} F_n(Z) &= \int_0^\infty \int_0^1 I_\nu(Z, \mu, \phi) \mu d\mu d\nu - \int_0^\infty \int_0^{-1} I_\nu(Z, \mu, \phi) \mu d\mu d\nu \\ &= F_{up}(Z) - F_{dn}(Z) \end{aligned} \quad (2.7)$$

The radiative heating/cooling rate can finally be found by substituting (2.7) into (2.1).

In practice, it is very difficult to solve (2.6) and carry out the subsequent integrations of (2.7) without using an enormous amount of computer time. Some simplification is thus required in order to incorporate radiative processes into complicated climate models. Since the simplifications used here are those frequently encountered in radiation models, only a brief account is given here. A more detailed description of the methods and the assumption made can be found in Stephens (1984).

### 2.3.1 The clear sky longwave model

Molecular and aerosol scattering can generally be neglected for problems of clear sky longwave radiative transfer. Cloud droplets, on the other hand, tend to be larger than aerosol particles and of a size comparable to the wavelength of radiation. Despite this however, the scattering effects of these droplets are also small when compared to the more dominant effects of absorption (e.g., Yamamoto, 1970 and Stephens, 1984). These characteristic allows the simplification of the general radiative transfer theory of previous section to a problem associated only with absorption and emission. Also assuming azimuthal symmetry, such that the radiation field is the same around any given zenith angle, (2.6) reduces to the following equation for a clear sky atmosphere

$$\mu \frac{d}{dZ} I_{\nu}(Z, \mu) = -\rho K_{ext, \nu} I_{\nu}(Z, \mu) + \rho K_{ext, \nu} B_{\nu}(T) \quad (2.8)$$

which can be separated into equations for the upward and downward components as

$$\begin{aligned} \mu \frac{d}{dZ} I_{up, \nu}(Z) &= -\rho K_{ext, \nu} I_{up, \nu}(Z) + \rho K_{ext, \nu} B_{\nu}(T) \quad ; \mu > 0 \\ \mu \frac{d}{dZ} I_{dn, \nu}(Z) &= \rho K_{ext, \nu} I_{dn, \nu}(Z) - \rho K_{ext, \nu} B_{\nu}(T) \quad ; \mu < 0 \end{aligned} \quad (2.9)$$

where

$$\begin{aligned} I_{up, \nu}(Z) &= I_{\nu}(Z, \mu) \\ I_{dn, \nu}(Z) &= I_{\nu}(Z, -\mu) \end{aligned} \quad (2.9a)$$

The solutions for the total upward and downward flux for the entire infrared spectrum at some level  $Z$  can be obtained by performing integration on (2.9) over height, zenith angle, and wave number. Following Stephens (1984), these flux equations are

$$\begin{aligned} F_{up}(Z) &= \int_0^{\infty} \pi B_{\nu}(Z=0) \tau_{\nu}^f(Z, Z=0) d\nu + \int_0^{\infty} \int_0^Z \pi B_{\nu}(Z') \frac{d\tau_{\nu}^f}{dZ'} dZ' d\nu \\ F_{dn}(Z) &= \int_0^{\infty} \int_Z^{\infty} \pi B_{\nu}(Z') \frac{d\tau_{\nu}^f}{dZ'} dZ' d\nu \end{aligned} \quad (2.10)$$

where  $\tau_{\nu}$  is the monochromatic diffuse transmission function defined by

$$\tau_{\nu}^f = 2 \int_0^1 \tau_{\nu}(Z, Z', \mu) \mu d\mu$$

$$\tau_\nu(Z, Z', \mu) = \exp\left(\frac{-1}{\mu} \int_{u(Z)}^{u(Z')} K_{ext,\nu}(P, T) du\right) \quad (2.11)$$

$$du = \rho dZ$$

where  $u$  is the optical path length, which defines amount of materials in a column of air.

In obtaining (2.10), assumptions have been made about the upward and downward intensity field at the surface and the top of the atmosphere, respectively. At the surface the upward intensity field is assumed to be the result of the black body emission from the surface. This assumption is justified since the earth surface is very close to being a black body for infrared wavelength as illustrated in table 2.2. The downward intensity at the top of the atmosphere is set to zero.

Table 2.2: Infrared emissivities (%). (after Sellers, 1965)

Surface	Emissivity
Water	92-96
Snow	82-99
Ice	96
Frozen Sand	93-94
Dry Sand	84-90
Wet Sand	95
Gravel	91-92
Dry Concrete	71-90
Moist Concrete	95-98
Desert	90-91
Grass	90
Pine Forest	90

The interpretation of (2.10) is that the upward flux at some level  $Z$  is the combination of the transmitted surface flux and the integrated contributions from all the layers below the level  $Z$ . The downward flux results only from the integral contribution of fluxes from all the layers above level  $Z$ . Figure 2.5 illustrates of each of the terms in (2.10).

The infrared cooling rate due to different gases can be obtained by combining and differentiating equation (2.10) with the appropriate transmission function for each gas and using (2.1) and (2.2). However, there are several major problems in applying (2.10) directly to the atmosphere. These problems arises from the nested integrations within (2.10). The

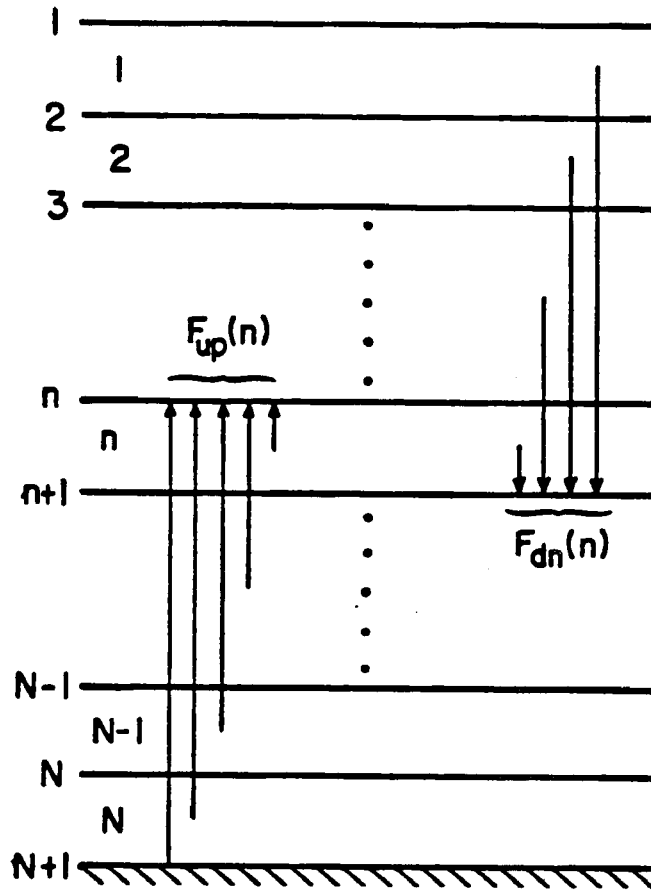


Figure 2.5: Illustration of infrared upward and downward fluxes at level  $Z$ .

most difficult and challenging problems of (2.10) are to represent the integration for optical paths and spectral intervals. The general treatments for these two problems involve the use of sophisticated parameterization schemes to approximate these integrals.

### Integration over optical path

The difficulty of summation over optical path arises from the fact that  $K_{ext,\nu}$  depends on both pressure and temperature. The use of a constant  $K_{ext,\nu}$  in evaluating (2.11) is not appropriated for the real atmosphere where large variations of pressure and temperature exists along any given path. The problem is further complicated by the fact that most of the absorption data are measured in laboratories at fixed temperature and pressure.

To overcome this problem, approximation methods are used. All these methods have a common assumption that the absorption along a nonhomogeneous path can be approximated by absorption along a homogeneous path with some factors of correction for non-homogeneity. There are several approximation methods available. Careful examination of each method is necessary to obtain the best possible solution for a specific purpose. A discussion of these methods is given by Stephens (1984). Table 2.3 summarizes the adopted approximations used in the study to correct optical paths.

Table 2.3: List of gases and their correction methods.

Gas	Correction Method
$H_2O$	Simple 1 parameter scaling
$CO_2$	Curtis-Godson 2 parameters
$O_3$	High order 4 parameters

### Spectral integration

The other problem in applying (2.10) to the real atmosphere is the need to deal with the integration over all spectral intervals containing those absorption lines important to the atmospheric temperature profile. The rapid change in the absorption coefficient  $K_{ext,\nu}$  with wave number in the vibration and rotation bands of the infrared spectrum is illustrated in figure 2.6. Since line-by-line calculations are impractical for climate study, this study must rely on an alternative parameterization scheme.

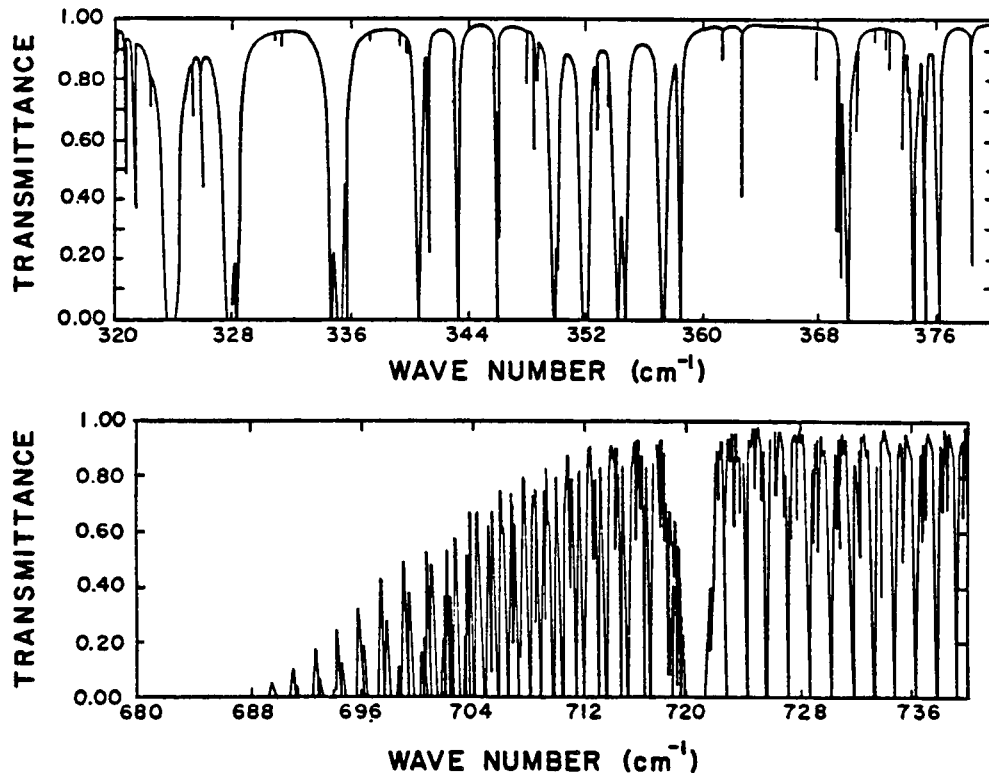


Figure 2.6: Absorption spectrum of the water vapor rotational band and 15  $\mu m$  carbon dioxide band at high resolution (after McClatchey and Selby, 1972).

In this study, the broadband flux emissivity approach is used to approximate the integration over wave number. The main advantage of this method is to remove the wave number integral from (2.10), and to simplify the flux calculations by only requiring the summation over layers. Details of the derivation of emissivity can be found in Stephens (1984). The broadband flux emissivity ( $\epsilon$ ) equations have the following form:

$$F_{up}(Z) = \sigma T_g^4 + \int_0^Z \epsilon'(Z, Z') \frac{d(\sigma T^4(Z'))}{dZ'} dZ'$$

$$F_{dn}(Z) = \int_Z^\infty \epsilon'(Z, Z') \frac{d(\sigma T^4(Z'))}{dZ'} dZ' \quad (2.12)$$

The solution of fluxes are obtained using (2.12) with an emissivity determined previously as a function of corrected optical path. Table 2.4 shows the methods used to generated clear sky emissivity values for each gas in this study.

Table 2.4: Methods for emissivity calculation.

Gas	Method
$O_3$	Rodgers (1975)
$CO_2$	Goody's random model (1964)
$H_2O$	Rodgers (1967)
$\epsilon$ type correction	Stephens and Webster (1979)

### 2.3.2 Inclusion of cloud into the longwave model

Clouds dramatically affect the radiative balance in the atmosphere and thus require inclusion in the climate model. As point out in the early section, the most important contributions of cloud to the longwave radiation is in its ability to absorb radiation. In this study, these clouds absorption effects are parameterized according to Stephens and Webster (1981). The clouds are allowed to exist only in one layer of the atmosphere. They are assumed to be plane-parallel and horizontally homogeneous. No attempt has been made to include multiple cloud layers or broken cloud layers. The fluxes from the cloud boundaries are calculated by

$$F_{up}(\text{cloud top}) = F_{up}(0)(1 - \epsilon_c) + \epsilon_c \sigma T_c^4$$

$$F_{dn}(\text{cloud base}) = F_{dn}(0)(1 - \epsilon_c) + \epsilon_c \sigma T_c^4 \quad (2.13)$$

where  $F_{up,dn}(0)$  are the incident cloud-base and cloud-top fluxes determined from (2.12),  $T_c$  is the mean cloud temperature,  $\epsilon_c$  is the effective cloud emittance which is parameterized using total liquid water content of the cloud ( $W_c$ ) after Stephens (1978) and Paltridge and Platt (1981) by:

$$\begin{aligned}\epsilon_c &= 1.0 - \exp(-0.1 * W_c) && \text{low, middle cloud} \\ \epsilon_c &= 1.0 - \exp(-0.56 * W_c) && \text{cirrus cloud}\end{aligned}\quad (2.14)$$

### 2.3.3 Short wave model

For the short wave radiation field, scattering and absorption by cloud and air molecules, and to a less extent aerosol, are important sources of radiative heating. Thus (2.6) for radiative transfer equation can be simplified to

$$\begin{aligned}\mu \frac{d}{dZ} I_\nu(Z, \mu, \phi) &= -\rho K_{ext,\nu} I_\nu(Z, \mu, \phi) + \\ \rho K_{ext,\nu} \frac{\tilde{\omega}_o}{4\pi} \int_0^{2\pi} \int_{-1}^1 P(\mu, \phi, \mu', \phi') I_\nu(Z, \mu', \phi') d\mu' d\phi' &+ \\ \frac{\tilde{\omega}_o}{4} P(\mu, \phi, \mu_o, \phi_o) \exp\left(-\frac{1}{\mu_o} \int_Z^\infty \rho K_{ext,\nu} dZ'\right) &\end{aligned}\quad (2.15)$$

which is more complicated than the reduced form of equation for the longwave spectrum since it requires summation over all zenith angles and azimuth angles. A simplification of this equation is necessary for more efficient use of computer time for climate studies. If we are only interested in flux quantities then (2.15) can be used in the form of a two stream (two radiation beam) model to simulate the upward and downward radiation field. The two stream azimuthally independent form of (2.15) is given by the following set of equations (after Liou, 1981)

$$\begin{aligned}\mu \frac{d}{d\tau} I_{up,\nu}(\tau) &= -I_{up,\nu}(\tau) + \frac{\tilde{\omega}_o}{2} (1 + gg) I_{up,\nu}(\tau) + \frac{\tilde{\omega}_o}{2} (1 - gg) I_{dn,\nu}(\tau) \\ &\quad - F_o \frac{\tilde{\omega}_o}{4} (1 - 3gg\mu\mu_o) \exp(-\tau/\mu_o) \\ \mu \frac{d}{d\tau} I_{dn,\nu}(\tau) &= I_{dn,\nu}(\tau) - \frac{\tilde{\omega}_o}{2} (1 + gg) I_{dn,\nu}(\tau) - \frac{\tilde{\omega}_o}{2} (1 - gg) I_{up,\nu}(\tau) \\ &\quad - F_o \frac{\tilde{\omega}_o}{4} (1 + 3gg\mu\mu_o) \exp(-\tau/\mu_o)\end{aligned}\quad (2.16)$$

and

$$dr = \frac{\rho K_{ext,\nu} dZ}{\mu_0}$$

where the new variable  $gg$  is the asymmetry factor, which describes the pattern of scattering along the forward and backward direction and  $dr$  is the change in optical depth, which defines the change in optical material in a vertical column of air. The radiative fluxes can be calculated by solving these two differential equations.

In this study, the form of solution to (2.16) is adopted from the recursive scheme of Stephens (1979). This scheme is based on the interaction principle of Grant and Hunt (1968) and it has the form

$$\begin{aligned} F_{up}(Z) &= \frac{T_r(Z) F_{up}(Z+1)}{1 - R_e(1, Z) R_e(Z)} + V_{up}\left(Z + \frac{1}{2}\right) \\ F_{dn}(Z) &= R_e(1, Z+1) F_{up}(Z+1) + V_{dn}\left(Z + \frac{1}{2}\right) \end{aligned} \quad (2.17)$$

$$\begin{aligned} R_e(1, Z+1) &= R_e(Z) + T_r(Z)^2 R_e(1, Z) (1 - R_e(1, Z) R_e(Z)) \\ V_{dn}\left(Z + \frac{1}{2}\right) &= \frac{T_r(Z) V_{dn}\left(Z - \frac{1}{2}\right)}{1 - R_e(1, z) R_e(Z)} \\ V_{up}\left(Z + \frac{1}{2}\right) &= \frac{R_e(Z) V_{dn}\left(Z - \frac{1}{2}\right)}{1 - R_e(1, z) R_e(z)} \end{aligned} \quad (2.18)$$

where  $R_e(1, Z+1)$  is the reflection of a composite of layers formed by adding two layers whose reflections are  $R_e(1, Z)$ , and  $R_e(Z)$ . Thus  $R_e(1, Z)$  represents the multiple reflections from all layers above level  $Z+1$ .  $V_{up}(Z + \frac{1}{2})$  represents the fluxes transmitted from the upper boundary which undergoes scattering down to the level  $Z+1$ , and  $V_{dn}(Z + \frac{1}{2})$  represents the fluxes reflected from the layers below, which undergoes scattering back up to the level  $Z+1$ . Figure 2.7 gives an illustration of these terms. The radiative fluxes at any level  $Z$  can be recursively computed using (2.17) and (2.18) once the boundary conditions and the  $R_e$  and  $T_r$  operators are defined.

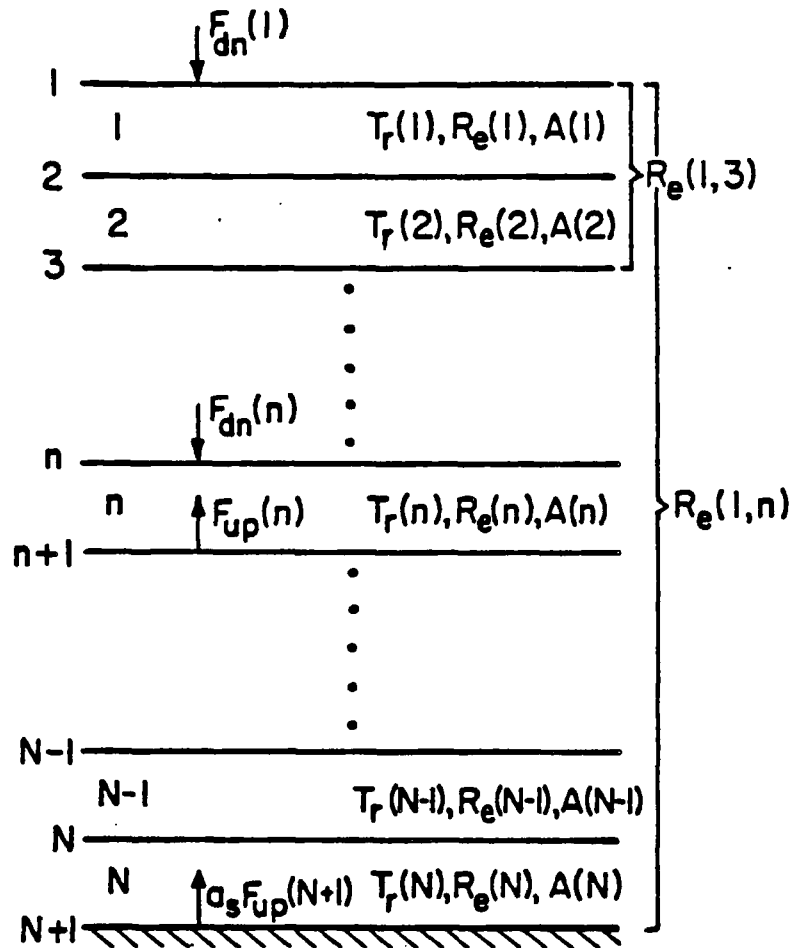


Figure 2.7: Illustration of each term in equation 2.17.

### Boundary conditions

The boundary terms in (2.17) and (2.18) include  $R_e(1, 1)$ ,  $V_{up}(\frac{1}{2})$ ,  $F_{dn}(1)$ , and  $F_{up}(Z + 1)$ . At the upper boundary  $R_e(1, 1)$ , represents the multiple scattering from all layers above level 1, and is zero since there is no atmosphere above this level.  $V_{dn}(\frac{1}{2})$  is equal to  $F_{dn}(1)$  at the top of the atmosphere for the same reason where  $F_{dn}(1)$  represents the amount of solar insolation at the top of the atmosphere. This term is specified using mean annual daily insolation. Table 2.5 lists typical values of  $F_{dn}(1)$  as a function of latitude.

Table 2.5: Annual mean daily solar insolation (watts/m<sup>2</sup>).

Latitude	Solar Insolation
0	430.0
35	350.0
65	180.0

The lower boundary condition  $F_{up}(Z + 1)$  is given by the following:

$$F_{dn}(\text{ground level}) = A_g F_{up}(\text{ground level}) \quad (2.19)$$

where  $A_g$  is the lower boundary surface albedo. It is specified using a typical annual surface value. Table 2.6 lists some typical values for albedo as a function of latitude.

Table 2.6: Annual mean surface albedo (%).

Latitude	Albedo
0	10.0
35	15.0
65	25.0

### Parameterization of absorption and reflection in clear sky

The  $R_e$  and  $T_r$  operators in (2.17) and (2.18) can be used to define the absorption within the layer by

$$A(z) = 1 - R_e(z) - T_r(z) \quad (2.20)$$

For general radiative transfer problems, these terms can be calculated using highly accurate methods known as doubling. However, this is impractical for climate modeling

studies and parameterization schemes are required. In this study, a parameterization of these quantities is used to generate these terms as function of the corrected optical path ( $u$ ). The shortwave absorption and reflection for the clear sky case is parameterized using the method of Lacius and Hansen (1974) and Sasamori et al., (1972). These calculations are performed in two shortwave bands, the visible ( $0.3\mu m < < 0.7\mu m$ ) and the near infrared ( $0.7\mu m < < 4.0\mu m$ ). The formulas for these parameterizations are given in table 2.7.

Table 2.7: Clean air shortwave parameterization schemes.

Band	Gas	Formula
Visible	$O_3$	$\frac{0.0218U(O_3)}{1.0+0.042U(O_3)+0.000323U(O_3)^2}$ $+ \frac{1.082U(O_3)}{(1+138.6U(O_3))^{0.28}} + \frac{0.0658U(O_3)}{(1+103.6U(O_3))^3}$
	$SCA$	$\frac{0.219}{1+0.816\mu_0}$
Near IR	$H_2O$	$\frac{2.9U(H_2O)}{(1+141.5U(H_2O))^{0.835}+5.925U(H_2O)}$
	$CO_2$	$2.35 \times 10^{-3}(U(CO_2) + 0.0129)^{0.26} - 7.5 \times 10^{-4}$

#### 2.3.4 Cloud modeling in the shortwave spectrum

The shortwave absorption and scattering by cloud is very important to the energy budget of the atmosphere as discussed in an earlier section. Thus proper parameterization of these parameters is necessary. These shortwave absorptions and scatterings are known to be strong functions of cloud optical depth (which measure the amount of optically active materials within the cloud), the incident sun angle, and the single scattering albedo (which is the ratio scattering to total extinction for a single particle) of the cloud. These new parameters, in term, are related to the cloud liquid/ice water path. In this study we will parameterize the absorption and scattering by cloud after Stephens (1978) and Paltridge and Platt (1981) by relating them to the cloud liquid/ice water path. Figure 2.8 and 2.9 show some typical values of water and ice cloud absorption and reflection as a function of cloud liquid/ice water path.

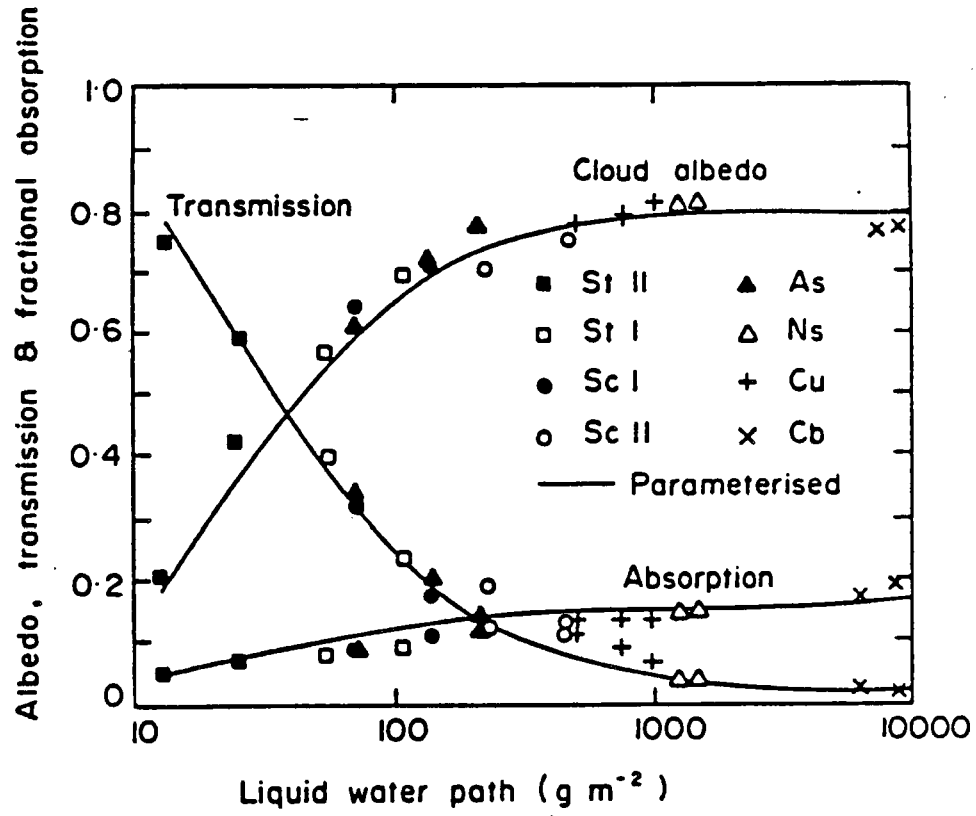


Figure 2.8: Comparisons between the shortwave absorption, transmission and cloud albedo as determined by the theoretical model for the given water cloud types (illustrated points) and the parameterized scheme (solid lines). The cosine of the solar zenith angle ( $\mu_0$ ) is 0.8 and a zero surface albedo ( $\alpha_s$ ) is assumed (after Stephens, 1978).

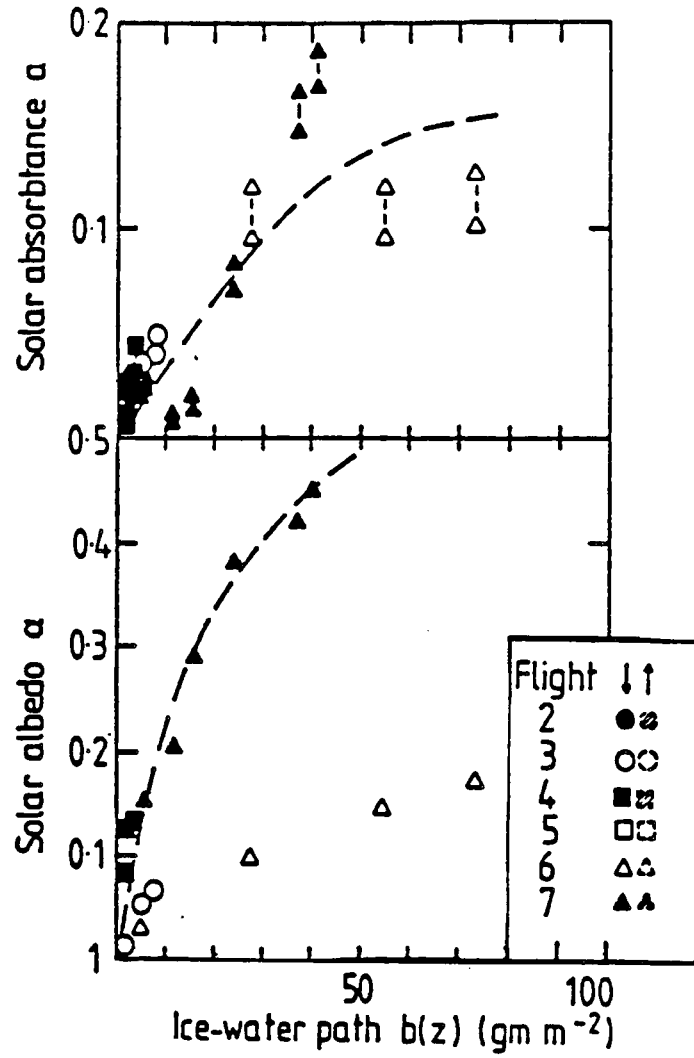


Figure 2.9: Values of solar absorptance  $\alpha$ , solar albedo  $\alpha$ , plotted against ice-water path for cirrus (ir) cloud. (after Paltridge and Platt, 1981)

## 2.4 Parameterization of dynamical effects

According to the study by Manabe and Strickler (1964), a pure radiative climate model has a tendency to produce unrealistic tropospheric temperature profile due to the absence of dynamical effects. They found that by incorporating dynamical effects the model produced a more realistic temperature profile of the atmosphere. In this study, the convective adjustment process with a fixed amount of relative humidity is incorporated into the model. The parameterization scheme assumes that convective adjustment occurs whenever the calculated radiative lapse rate exceeds the observed moist-adiabatic lapse rate. That is, dynamic overturning transfers the excess heat at the surface to the free atmosphere. If the calculated lapse rate is below the critical lapse rate, overturning is suppressed by turning off the convective adjustment process, and the atmosphere is assumed to be stable. Figure 2.10 shows the U.S. standard atmosphere and the resultant atmosphere temperature profiles for our radiative climate model with and without convective adjustment process and fixed amount of relative humidity. The present of convection in the model definitely helps to simulate a more realistic tropospheric temperature profile. More detail of these results will be presented in Chapter 4 of this thesis.

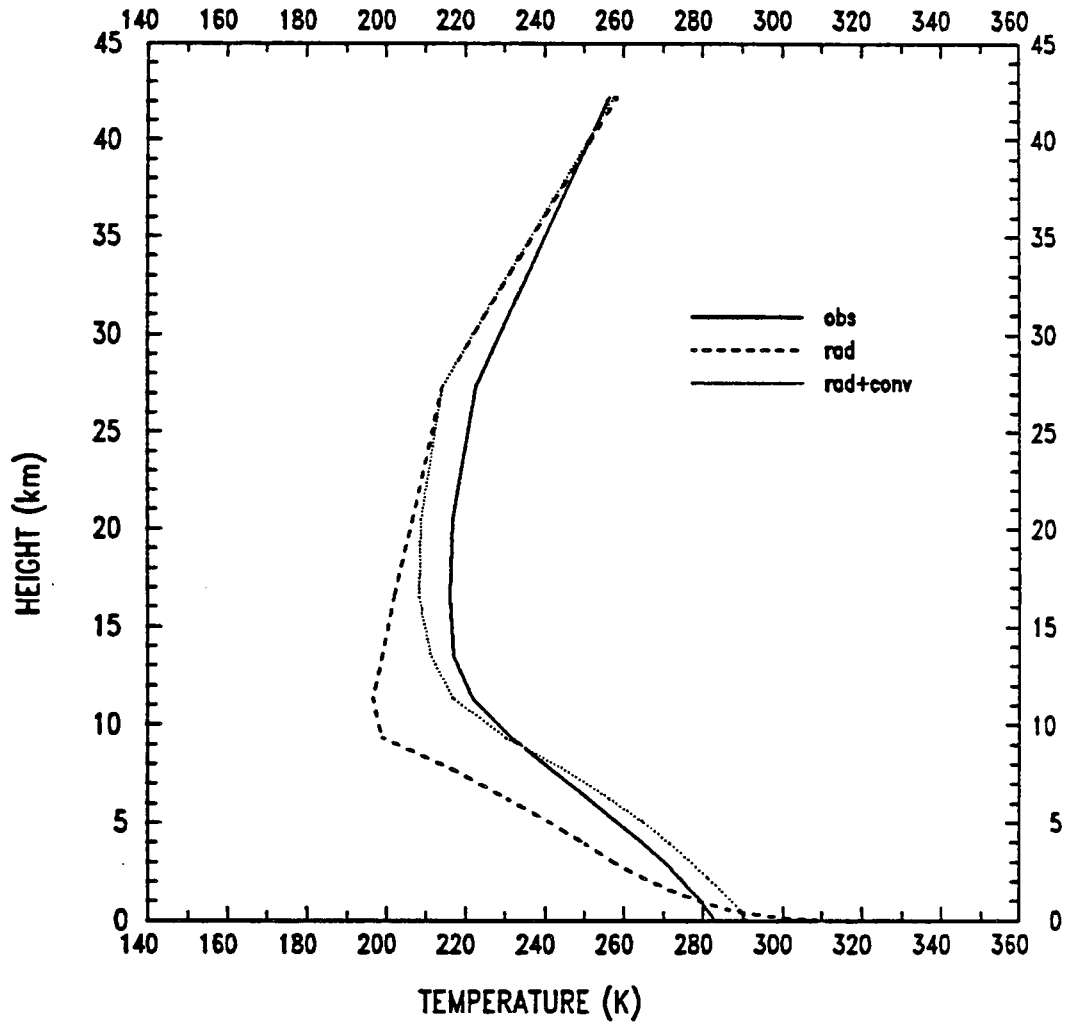


Figure 2.10: Temperature profile of actual atmosphere (solid curve), pure radiation atmosphere model (dash curve), and radiative convection atmosphere model (dot curve).

## Chapter 3

### SIMPLE MODEL OF THE OCEAN

The ocean is an important part of the earth's climate system. The combination of its high heat capacity and mixing act as a thermal energy reservoir which stabilizes the atmospheric circulation above it. Therefore, careful considerations of this system are necessary for studying long term climatic variations. In this chapter, a simple one-dimensional model of the ocean will be constructed to simulate the vertical temperature profile of the ocean and the response of this profile to external forcings. The model is based on a simple mixed layer formulation and thus only represents a bulk global ocean condition.

#### 3.1 Observational studies of the ocean temperature structure

Many early observational works have provided invaluable clues to the structure of our ocean. It is known that the oceanic temperature profile can be separated into two regimes: the well mixed layer and the deep ocean layer. The well mixed layer is located at the upper 20m to 200m of the ocean where the temperature remains relatively constant. On the other hand, the deep ocean layer, which covers the rest of the vertical structure, is characterized by a general decrease of temperature with depth. Figure 3.1 shows such structure for three different latitudinal locations. Furthermore, these studies indicate that this structure is not constant in time. The mixed layer generally increases in thickness after July to a maximum depth in February. It then decreases back to its minimum value in July. Accompanied with these changes, the mixed layer/surface temperature usually decreases (increases) in value with increasing (decreasing) mixed layer thickness. Figure 3.2 and 3.3 show some examples of this cyclic feature.

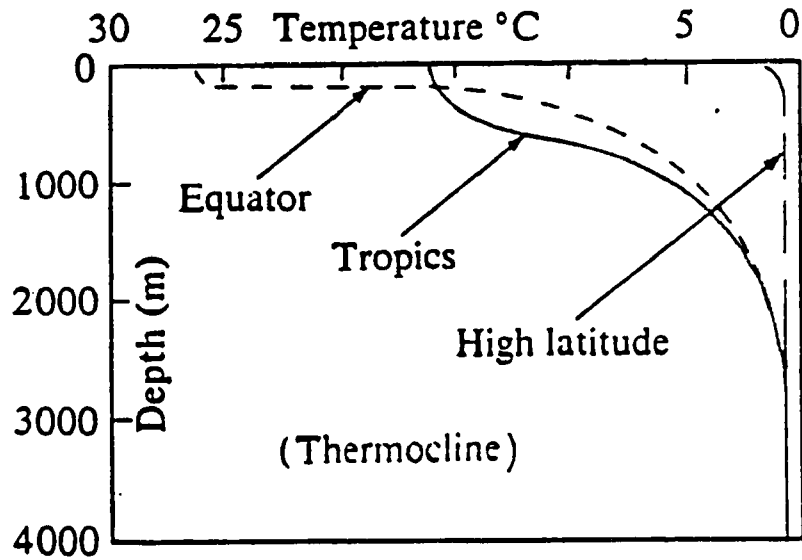


Figure 3.1: Temperature Profile of the ocean. (after Thurman, 1981)

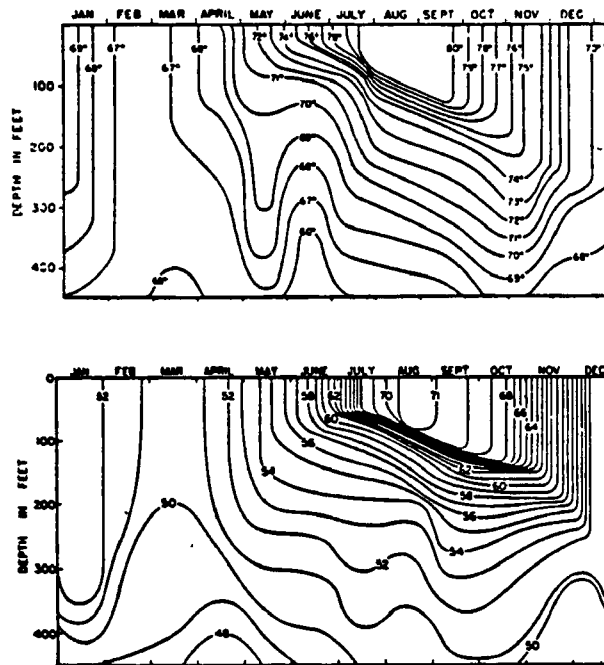


Figure 3.2: The seasonal temperature cycle (°F) in (a) the Bermuda area, (b) the North Pacific. (From Summary Technical Report of Division 6, N.D.R.C., Washington, 1946). (after Kraus and Turner, 1967)

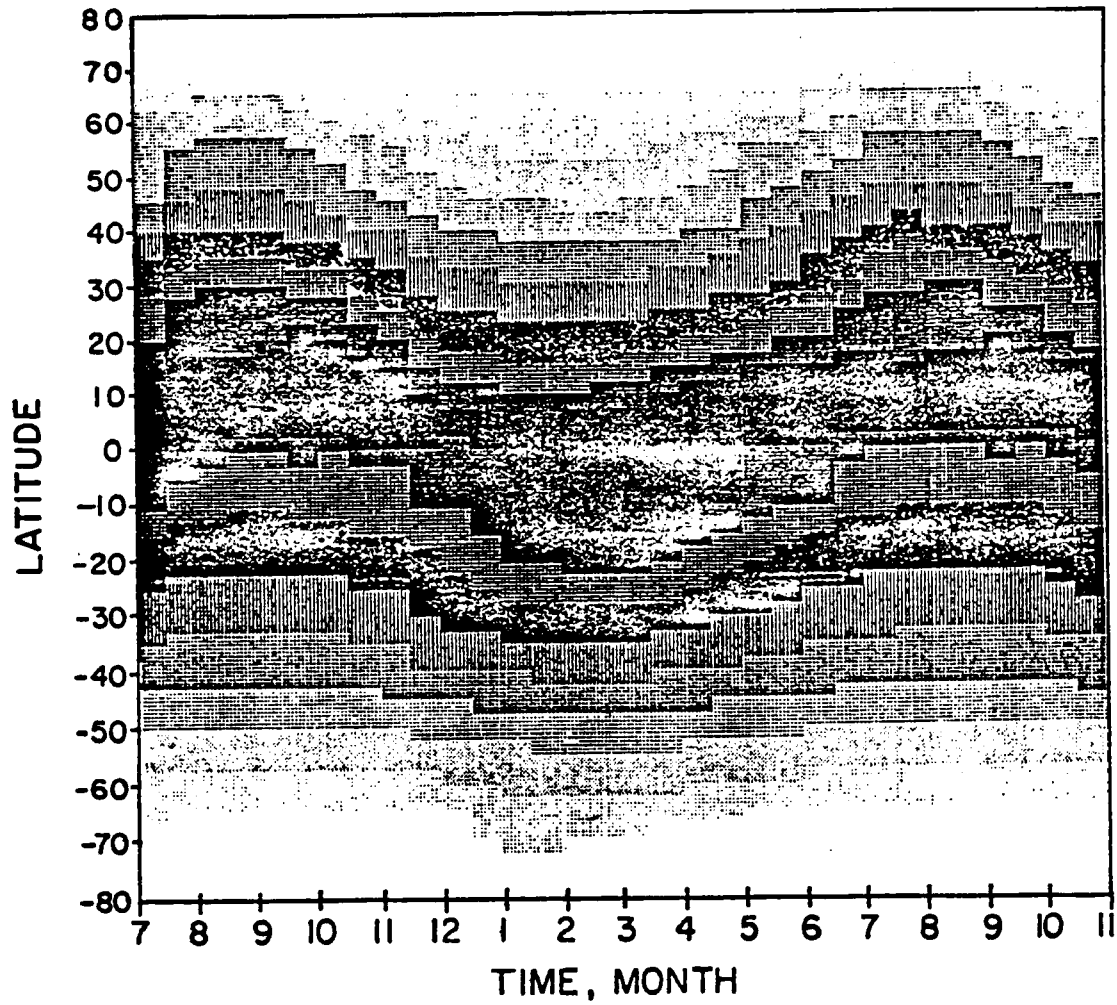


Figure 3.3: Zonal sea surface temperature between 7/10/83 to 11/10/84 compiled using both surface and satellite data.

### 3.2 General theory of oceanic temperature structure

The most generally accepted theory of oceanic temperature structure was first proposed by Kraus and Turner (1968). Using the results from an experiment and a simple one dimensional model, Kraus and Turner hypothesized that the behavior of the oceanic temperature profile was the product of the solar radiation, the buoyancy force of the combination of the water, and the turbulent mixing within the mixed layer that arises from the wind stress associated with the atmospheric circulation. Their theory is briefly summarized in the following paragraph.

The solar radiation that enters into the ocean is strongly absorbed in the first 10m of the ocean. This strong absorption in turn heats up the surface water. Consequently, the turbulent mixing created by atmospheric wind stress mixes the heated surface water with the colder water below. This mixing process in turn creates a homogeneous/constant temperature layer of water which has a temperature between that of the surface and the deep ocean water. This mixing will continue as long as the wind stress at the surface supplies enough energy to mix the entire mixed layer downward against the buoyancy force of the water itself. At some point in the ocean, the mixed layer will stop to advance, and a state of equilibrium will be established between the radiation, turbulence mixing, and the natural buoyancy force of the water. Thus changes in this profile with time can be explained by the simple balance of these forces.

### 3.3 One dimensional mixed layer ocean modeling

In the search for a simple one-dimensional ocean model for this thesis, the focus was placed primarily on finding a simple ocean model which was capable of being coupled to the atmosphere. The original Kraus and Turner model would have been an excellent choice for this study; however it did not include realistic atmospheric inputs as the boundary conditions. Instead, a modified version of a model developed by Denman (1973) was used in this study.

The model assumes the ocean to be incompressible, stably stratified, and horizontally homogeneous. The upper mixed layer is an idealized, vertically homogeneous layer

bounded at the bottom by a temperature discontinuity as shown in figure 3.4. The heat and mechanical energy inputs at the upper and lower boundaries, or at any point within the mixed layer, are assumed to be redistributed uniformly throughout the layer by turbulent diffusion. The timescale of this redistribution is assumed to be small compared to the times over which the processes of interest occur in this model. Below the lower interface, a stable temperature profile and an advective vertical velocity are specified.

### 3.3.1 Basic conservation laws of the mixed layer model

The one-dimensional mixed layer model is based on principles of thermal and turbulent kinetic energy. The conservation law governing the vertical transfer of thermal energy within any layer in the ocean is

$$\frac{\partial T}{\partial t} = -w \frac{\partial T}{\partial Z} + \frac{\partial}{\partial Z} \overline{w'T'} + \frac{1}{\rho_o C_p} \frac{\partial F_n}{\partial Z} \quad (3.1)$$

where  $w$  is the vertical motion,  $w'T'$  is the vertical turbulence flux of temperature,  $C_p$  and  $\rho_o$  are the specific heat and the density of water, respectively,  $F_n$  is the net solar flux, and  $Z$  is height, measuring positive upward. Physically, this law states that the change of oceanic temperature at any layer with time is the result of vertical advection of temperature by vertical motion into the layer, local divergence of vertical heat flux, and vertical divergence of short wave radiative flux within that layer.

The law describing the conservation of turbulent kinetic energy in the ocean can be approximated by

$$\overline{-u'w'} \frac{\partial u}{\partial z} - \frac{\partial}{\partial z} \left[ \overline{w' \left( \frac{p'}{\rho_o} + \frac{C^2}{2} \right)} \right] = \alpha g \overline{w'T'} + \epsilon \quad (3.2)$$

where  $C^2 = u'^2 + v'^2 + w'^2$ ,  $\frac{C^2}{2}$  is the turbulent kinetic energy,  $\epsilon$  is the dissipation of turbulent energy,  $u'$  and  $v'$  are the fluctuation of the  $x$  and  $y$  components of the horizontal velocity,  $p'$  is the pressure fluctuation, and  $\alpha$  is the thermal expansion coefficient of water. The left hand side of the equation represents the source of turbulent energy due to shear production, pressure gradient production, and transport of turbulent energy. The right side is the sink for turbulent energy due to buoyancy and viscous dissipation.

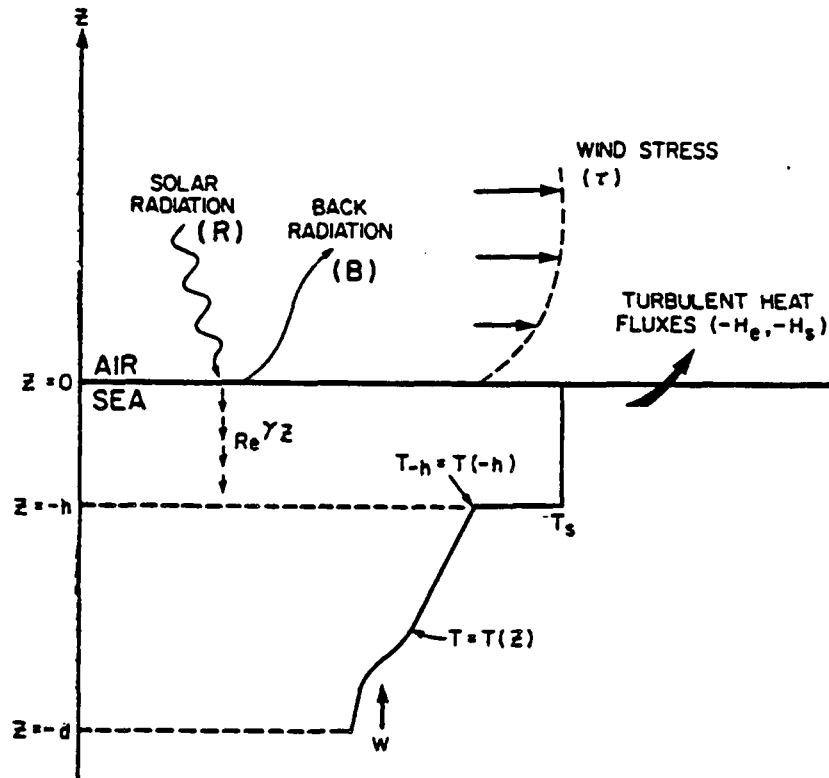


Figure 3.4: Schematic of the thermocline and the boundary inputs assumed in the model. The mixed layer parameters are: the thickness  $h$ ; the temperature  $T_s$ ; and the extinction coefficient  $\gamma$ , for the incident solar radiation  $r$ . Other boundary conditions are the wind stress  $\tau$ , the back radiation  $-B$ ; the latent and sensible fluxes of heat  $-(H_e + H_s)$  at the upper surface; the temperature  $T_{-h}$ , immediately below the layer; and the vertical velocity  $w$  below the layer. (after Denman, 1973)

The equations governing the change in surface/mixed layer temperature, the mixed layer depth, and the temperature just below the mixed layer can be obtained by integrating (3.1) and (3.2) over the entire mixed layer region and combining their results with proper boundary conditions at the top and bottom of the mixed layer. At the upper boundary of the mixed layer, the turbulent heat flux is equal to the net heat transfer through the ocean surface, i.e.,

$$\overline{w'T'}|_{z=0} = -(H_e + H_s + F_{nd,ir}) / (\rho_o C_p) \quad (3.3)$$

where  $H_e$  and  $H_s$  are the downward fluxes of latent and sensible heat at the surface, and  $F_{nd,ir}$  is the net downward longwave flux at the sea surface. The vertical velocity  $w$  at the surface is zero.

The lower boundary condition assumes that the turbulent heat flux is proportional to the temperature different across the boundary and the entrainment rate of the mixed layer into the lower stable layer. If the entrainment rate is less than or equal to zero, the turbulent heat flux is to be zero. This lower boundary can be expressed by

$$\overline{w'T'}|_{z=h} = -H \left( w + \frac{dh}{dt} \right) (T_s - T_{-h}) \quad (3.4)$$

where  $T_s$  is the mixed layer temperature,  $T_{-h}$  is the temperature just below the mixed layer,  $\frac{dh}{dt}$  is the rate of change of the boundary's vertical displacement, and  $H$  is the Heaviside step function having the properties

$$H = \begin{cases} 0 & , \text{ if } w + \frac{dh}{dt} \leq 0 ; \quad \text{no entrainment} \\ 1 & , \text{ if } w + \frac{dh}{dt} > 0 ; \quad \text{entrainment mixing} \end{cases} \quad (3.5)$$

Using the above techniques and boundary conditions, two sets of governing equations are obtained which describe the evolution of the mixed layer during two different situations.

#### Equations for heat-dominated regime

The first set of equations, i.e.  $H = 0$ , represents the condition when the entrainment rate is zero at the base of the mixed layer. This condition occurs when there are weak surface winds and strong solar radiation. It is referred to by Denman (1973) as the heat-dominated regime and this regime is a representative of the conditions from spring to fall.

The set of equations for this regime is

$$\frac{dT_s}{dt} = \frac{(F_{nd,ir}^* + H_e^* + H_s^* + F_n^*(0)) - F_n^*(-h)}{h} \quad (3.6)$$

$$\begin{aligned} \frac{dh}{dt} = & \frac{1}{H_e^* + H_s^* + F_{nd,ir}^* + F_n^*(0) + F_n^*(-h)} \left\{ 2 \frac{d(G - D)^*}{dt} \right. \\ & - h \frac{d}{dt} (H_e^* + H_s^* + F_{nd,ir}^*) + 2 \frac{d}{dt} \left[ \int_{-h}^0 F_n^*(z) dz \right] \\ & \left. - h \frac{d}{dt} F_n^*(0) - h \frac{d}{dt} F_n^*(-h) \right\} \quad (3.7) \end{aligned}$$

where the transformation

$$(F_n^*, H_e^*, H_s^*, F_{nd,ir}^*) = \frac{(F_n, H_e, H_s, F_{nd,ir})}{\rho_o C_p}$$

$$(G - D)^* = - \frac{(G - D)}{\rho_o \alpha g}$$

have been used and  $\alpha$  is the thermal expansion coefficient of water.

Equation (3.6) states that the change of mixed layer/surface temperature is controlled by the downward fluxes of sensible and latent heat, net solar radiation, and net downward flux of longwave radiation at the surface. If there is more downward energy available to the mixed layer, it will heat up. This temperature change is also inversely proportional to the mixed layer depth. Thus, the thinner the mixed layer, the faster it will heat up. Equation (3.7) states that the change in mixed layer thickness is governed by a set of complicated processes, which includes the rate of change of turbulent heat fluxes, radiative forcing, and wind stress energy supplied by the atmosphere. The new term  $G$  represents the generation of turbulent kinetic energy by wind stress, and  $D$  represents the viscous dissipation of turbulent energy. These two terms are derived from the equation of turbulent kinetic energy. The entire term  $G - D$  represents the mean available turbulent kinetic energy in the mixed layer.

### Equations for the wind-dominated regime

The second set of equations represents the other condition when there is entrainment below the mixed layer and  $H = 1$ . This occurs when there are strong surface winds and weak solar radiation. This condition is referred to as the wind-dominated regime by Denman (1973) and it represents the ocean condition from fall to spring. These equations are

$$\frac{dT_s}{dt} = \frac{2}{h^2} \left[ -(G - D)^* + h (H_e^* + H_s^* + F_{nd,ir}^* + F_n^*(0)) - \int_{-h}^0 F_n^*(Z) dZ \right] \quad (3.8)$$

$$\left( w + \frac{dh}{dt} \right) = \frac{2 \left[ (G - D)^* + \int_{-h}^0 F_n^*(Z) dZ \right] - h \left[ (H_e^* + H_s^* + F_{nd,ir}^* + F_n^*(0) + F_n^*(-h)) \right]}{h (T_s - T_{-h})} \quad (3.9)$$

$$\frac{dT_{-h}}{dt} = - \left( w + \frac{dh}{dt} \right) \frac{\partial T_{-h}}{\partial Z} + \frac{\partial F_n^*(-h)}{\partial Z} \quad (3.10)$$

where now (3.8) is similar to (3.6) with the exception of a few extra terms. The rate of mixed layer/surface temperature change is now also negatively proportional to the available turbulent kinetic energy. The mixed layer temperature decreases with increasing mean available turbulent kinetic energy since the turbulent energy can mix the mixed layer to the deeper and colder water. Thus the mixed layer governed by (3.9) is completely different in character from (3.7). The change in mixed layer depth is now controlled by the mean available turbulent kinetic energy and the upward turbulent heat flux at the surface. If there is more turbulent energy or if the mixed layer losses its thermal energy to the atmosphere, the mixed layer will increase in thickness and decrease in temperature. The thickness changes are also inversely proportional to the mixed layer depth and temperature difference across the bottom boundary of the mixed layer. Thus the larger the temperature jump across the bottom mixed layer boundary, the more difficult it is to increase the thickness of the layer, because it will have to overcome a larger buoyancy force of the water. Finally (3.10) describes the evolution of the temperature just below the mixed

layer. This temperature is governed by the net flux of radiation, entrainment rate and the temperature gradient below the mixed layer.

### Equations for the global/annual average condition

The equations above are only valid for a specific time of the year. In order to describe a global/annual average condition, the equations for the two different regimes must be combined into a single set of equations. This creates a problem in the present application when annual/mean inputs are to be used in an attempt to determine the annual/mean mixed layer temperature and depth. A hybrid annual/mean model is formulated in chapter 5 to overcome this problem.

### 3.3.2 Parameterizations for surface fluxes of sensible and latent heat, mean available turbulent kinetic energy, and radiation.

Equation (3.6), (3.7) and (3.8) - (3.10) are not a closed-set of equations since  $H_e$ ,  $H_s$ ,  $F_{n,ir}$ ,  $G - D$ , and the solar radiation terms are still unknown. In order to close the equations, parameterization closure schemes are applied.

#### Sensible and latent heat fluxes

Even though many methods are available for parameterizing the transfer of latent and sensible energy across the ocean surface, there are few that will actually satisfy the requirements for climate simulation. In this paper the simple parameterization schemes by Seigel (1977) are used. These schemes are based on bulk aerodynamic theory and have the following forms

$$\left. \begin{aligned} H_s &= -\rho_a C_p CD (T_{sst} - T_{air}) u \\ H_e &= -(0.26 + 0.077u) (0.98e(sst) - e(air)) \frac{L}{10} \end{aligned} \right\} \quad (3.11)$$

where  $T_{sst}$  and  $T_{air}$  are the sea surface temperature and the temperature at the lowest atmospheric layer, respectively,  $u$  is the wind speed at 10m above the sea surface,  $CD$  is the drag coefficient and is related to the wind speed  $u$  by

$$CD = (1.0 + 0.07u) \times 10^{-3} \quad (3.12)$$

$CD$  is a dimensionless number if  $u$  is given in m/sec,  $e(sst)$  and  $e(air)$  are the saturation vapor pressure of the sea surface and the water vapor pressure of the lowest atmospheric layer in millibars, respectively,  $L$  is the latent heat of vaporization, 0.98 accounts for the sea surface vapor pressure being 2% less than that of fresh water, and 0.26 is omitted if  $(e(sst) - e(air))$  is negative.

### Mean available turbulent kinetic energy

The generation of turbulent kinetic energy  $G$  can be parameterized in terms of the wind stress  $\tau$ . According to Denman (1973), who modified the work of Kraus and Turner (1968), the rate of work by wind stress,  $E_a$ , at 10m height is given by

$$E_a = \tau U_{10} = \rho_a CD U_{10}^3 \quad (3.13)$$

where  $\rho_a$  is the density of air. By assuming that the wind and wave fields are statistically stationary, the same wind stress  $\tau$  acts on the water below. A velocity scale appropriate to the underlying water,  $w^*$ , is then

$$w^* = (\tau/\rho_o)^{\frac{1}{2}} = (\rho_a/\rho_o)^{\frac{1}{2}} CD U_{10} \quad (3.14)$$

(3.14) can be used to estimate the rate of turbulent energy transfer downward at some depth below the surface,  $E_w$ , (or the mean available turbulent energy for mixing in the layer) by

$$G - D = E_w \simeq w^* \tau = (\rho_a/\rho_i)^{\frac{1}{2}} CD U_{10} = (\rho_a/\rho_o)^{\frac{1}{2}} CD^{\frac{1}{2}} E_a \quad (3.15)$$

Equation (3.15) is consistent with the suggestion of Turner (1969) that the turbulent energy available for mixing within the layer is produced at a rate that is approximately a constant fraction  $m$  of the rate of downward transfer of turbulent energy from the wind field at 10m

$$G - D = m u_{10} \tau = m E_a \quad (3.16)$$

### Radiation in the mixed layer

Although it is possible to calculate the radiative fluxes for the entire coupled ocean-atmosphere system using a unified 2-stream theory, this study has chosen to use a simple radiation parameterization scheme for the ocean, because it can be easily incorporated into the mixed layer formulation. According to Defant (1961) the net flux of solar radiation at any level in the ocean can be spectrally decomposed as

$$F_n(Z) = \sum_{i=1}^n F_{n,i}(Z) \exp(Z/\xi_i) \quad (3.17)$$

where  $F_{n,i}$  is the surface net flux of spectral solar radiation and  $\xi_i$  is the attenuation length for the  $i$  spectral band. Table 3.1 shows the spectral breakdown of these attenuation lengths for solar wavelengths. For this study, the solar radiation is decomposed only into two bands to match the formulation used for the atmosphere model. The formula for the net flux of solar radiation in the ocean is then represented by

$$F_n(Z) = F_{n,vis}(Z) \exp(Z/\xi_{vis}) + F_{n,nir}(Z) \exp(Z/\xi_{nir}) \quad (3.18)$$

where  $F_{n,vis}$  and  $F_{n,nir}$  are the surface net flux of radiation in the visible band and the near infrared band, respectively, and these terms are given by the atmospheric model.  $\xi_{vis}$  and  $\xi_{nir}$  are the attenuation lengths for the visible band and near infrared band of solar radiation, respectively. The value of these two terms is dependent on the turbidity of the ocean.

The downward net flux of infrared radiation at the surface is another important term in the mixed layer formulation. This term is parameterized by assuming the ocean radiates upward to the atmosphere as a blackbody for infrared wavelengths, with a sea surface/mixed layer temperature. This upward flux is then subtracted from the downward flux of infrared radiation of the lowest atmospheric model level to obtain the net upward infrared flux of radiation,  $F_{nd,ir}$ :

$$F_{nd,ir} = F_{dn,ir,atm} - \sigma T_{sst}^4 \quad (3.19)$$

where  $\sigma$  is stefan-boltzmann constant and  $F_{dn,ir,atm}$  is the downward flux of atmospheric infrared radiation.

Table 3.1: Solar Spectral Attenuation Length for oceanic water. (after Defant, 1961)

Wavelength ( $\mu m$ )	$\xi_i$ (m)
0.2-0.6	34.849
0.6-0.9	2.2661
0.9-1.2	$3.1486 \times 10^{-2}$
1.2-1.5	$5.4831 \times 10^{-3}$
1.5-1.8	$8.3170 \times 10^{-3}$
1.8-2.1	$1.2612 \times 10^{-3}$
2.1-2.4	$3.1326 \times 10^{-3}$
2.4-2.7	$7.8186 \times 10^{-3}$
2.7-3.0	$1.4427 \times 10^{-3}$

Equations (3.6), (3.7) or (3.8) to (3.10), which represent the time evolution of the mixed layer, can now be solved by using the above parameterizations once the attenuation lengths, the temperature profile of the deep ocean, the vertical velocity below the mixed layer, the fraction of surface turbulent kinetic energy, and the atmospheric wind speed at 10m above the sea surface are specified.

## Chapter 4

### EXPERIMENTS WITH THE ATMOSPHERIC MODEL

In order to assess the performance of the atmospheric model, four sets of simple experiments were conducted with different versions of the same atmospheric model. In the first experiment the temperature profile of a static clear atmosphere containing the annual mean amount of gaseous absorbers at 35 N and a fixed amount of absolute humidity is studied. The effects of dynamical processes as modeled by convective adjustment and their relationship to the tropospheric temperature profile will be investigated in experiment 2. The importance of these dynamical forcings in maintaining a realistic temperature profile will become clear in this chapter. In experiment 3 we will further relax the initial condition by allowing variation of water vapor in the model through fixing a constant value of relative humidity. Experiment 4 contains a set of sensitivity studies for the fixed relative humidity and convectively adjusted atmosphere under various conditions. Table 4.1 gives a summary of these experimental setups.

Table 4.1: Summary of different cases run with the atmosphere model.

Case	Radiation	Dynamic	Rel. Hum.	Sensitivity
1	Yes	No	No	No
2	Yes	Yes	No	No
3	Yes	Yes	Yes	No
4	Yes	Yes	Yes	Yes

The main objectives of experiment 1 to 3 are to compute the equilibrium temperature profiles of the atmosphere (these profiles are defined when the net incoming solar radiation is equal to the net outgoing longwave radiation at the top of the atmosphere.) and to evaluate these results by comparing them with the actual annual/mean temperature profile (shown in figure 4.1) at 35 N as given by McClatchey et al., (1973). Evaluation

of experiment 4 will be made by comparing the results with other studies (i.e., Manabe and Strickler, 1964, Manabe and Weatherald, 1967). A final summary of the performance of the model and its reliability in simulating the atmospheric temperature structure is provided at the end of this chapter.

#### 4.1 Input conditions and computational procedures

Unless stated otherwise, the following values will be used as inputs to initialize the atmosphere model. The annual solar input is set at  $350 \text{ W/m}^2$ . The annual mean profiles of water vapor and ozone at 35 N are given according to McClatchey et al., (1973). The water vapor profile, shown in figure 4.2, is a monotonically decreasing function of height to above 16 km (100 mb). The maximum value of water vapor at the surface is about 7 g of water vapor per 1000 g of air. The ozone profile, shown in figure 4.3, is very different from that of water vapor's. It increases with height and has a maximum value at about 32 km (9 mb). A complete listings of these profile is provided in table 4.2. The carbon dioxide in the model is fixed at 0.00456 percent by weight (300 ppm by volume). The values of 0.15 and 0.494 are assigned to the surface albedo and the cosine of the mean sun zenith angle, respectively. Two isothermal clear sky atmospheres at 170 K and 340 K are used to start the experiments. All experiments are performed on a 19 levels model atmosphere proposed by Manabe and Strickler (1964) and the positions of these levels are shown in table 4.3. The equilibrium temperature profiles from the experiments are then computed as the asymptotic solutions to the initial value problem as specified by the above input conditions with a time step of 8 hours. The convergence criterion for the experiments without the convective adjustment is specific such that the absolute difference between the net outgoing longwave radiation and the net incoming shortwave radiation at the top of the model is less than or equal to  $0.05 \text{ W/m}^2$ . For those experiments which include convective adjustment, the convergence criterion follows after Manabe and Strickler (1964) and requires that the rate of change in temperature for consecutive time steps at any layers in the atmosphere is less than or equal to an equivalent change of 0.001 K/day.

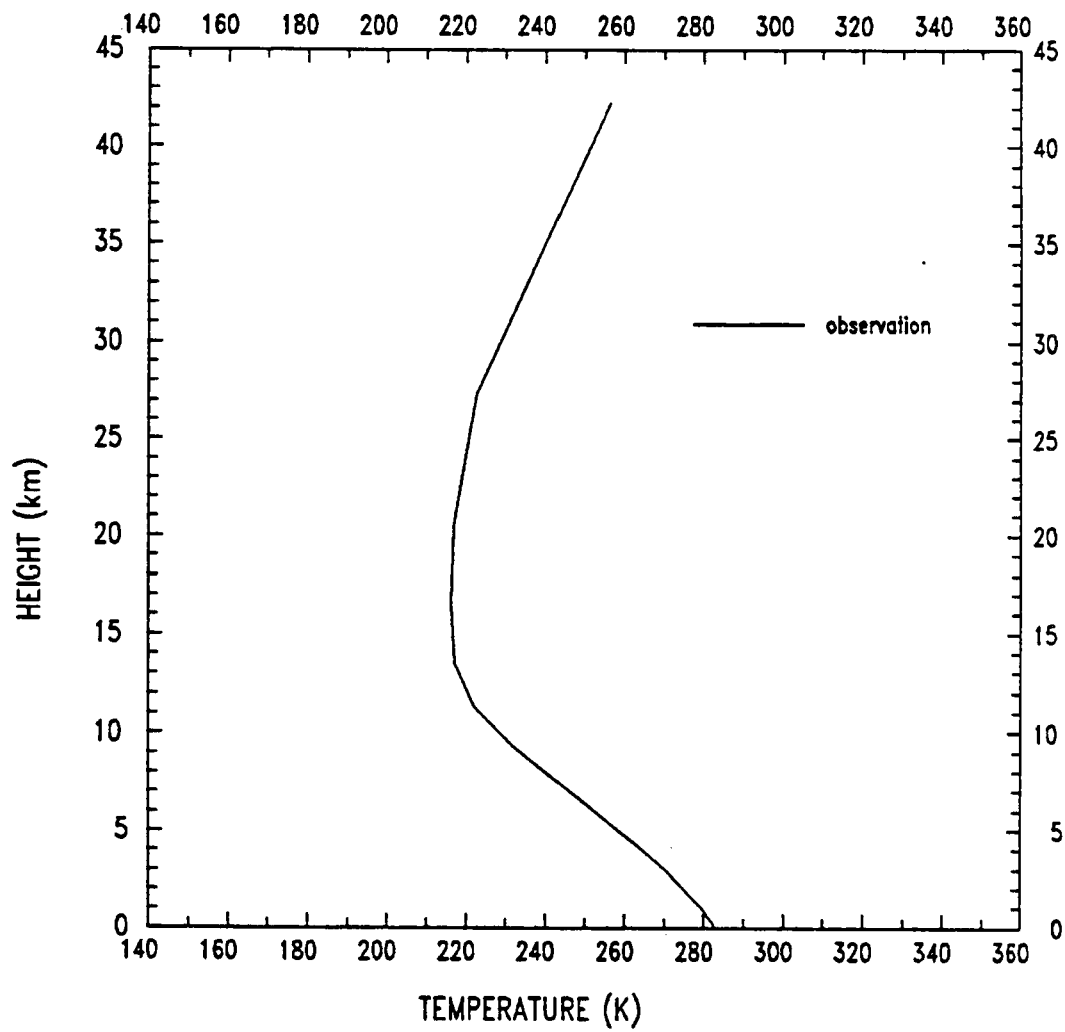


Figure 4.1: Annual/mean mid-latitude temperature profile compiled by McClatchey et al., 1973.

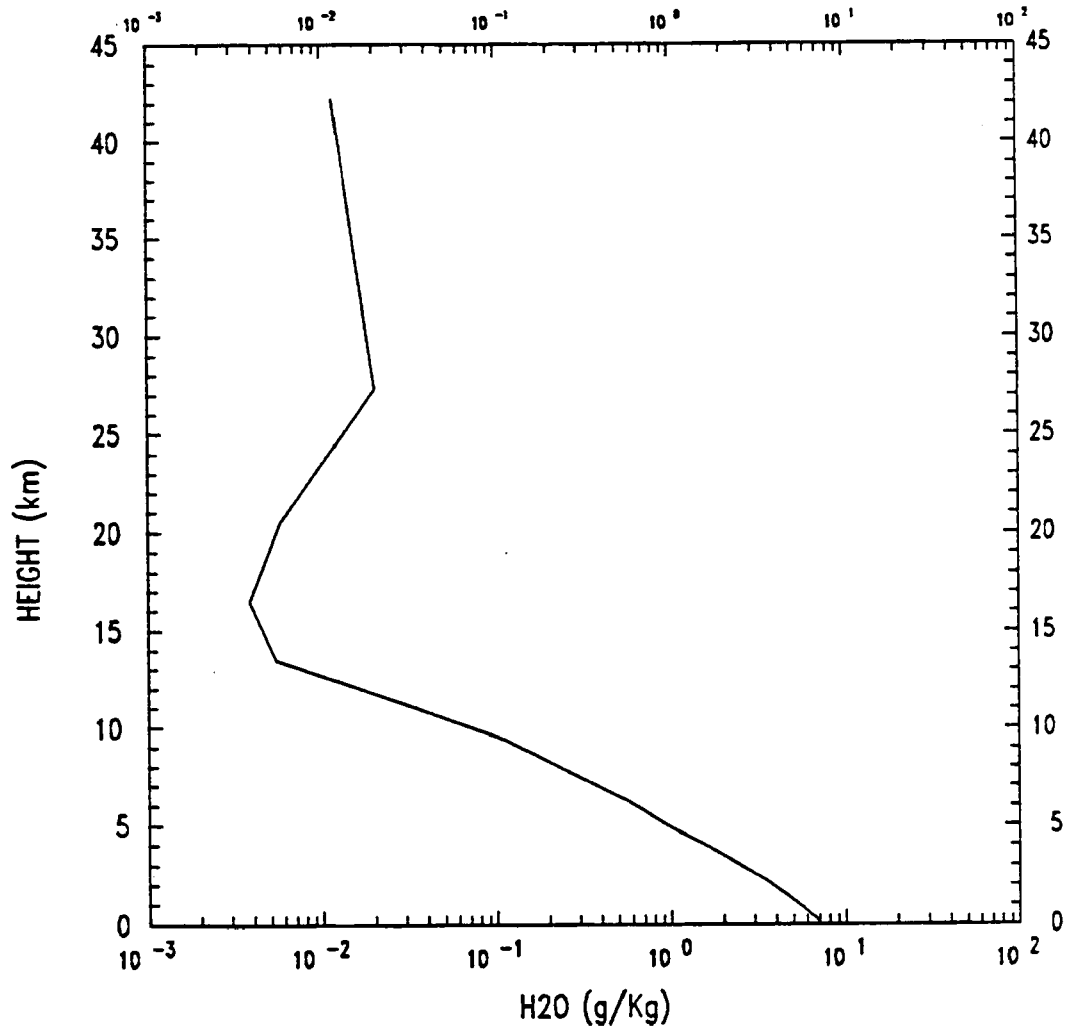


Figure 4.2: Same as Figure 4.1, except for mixing ratio.

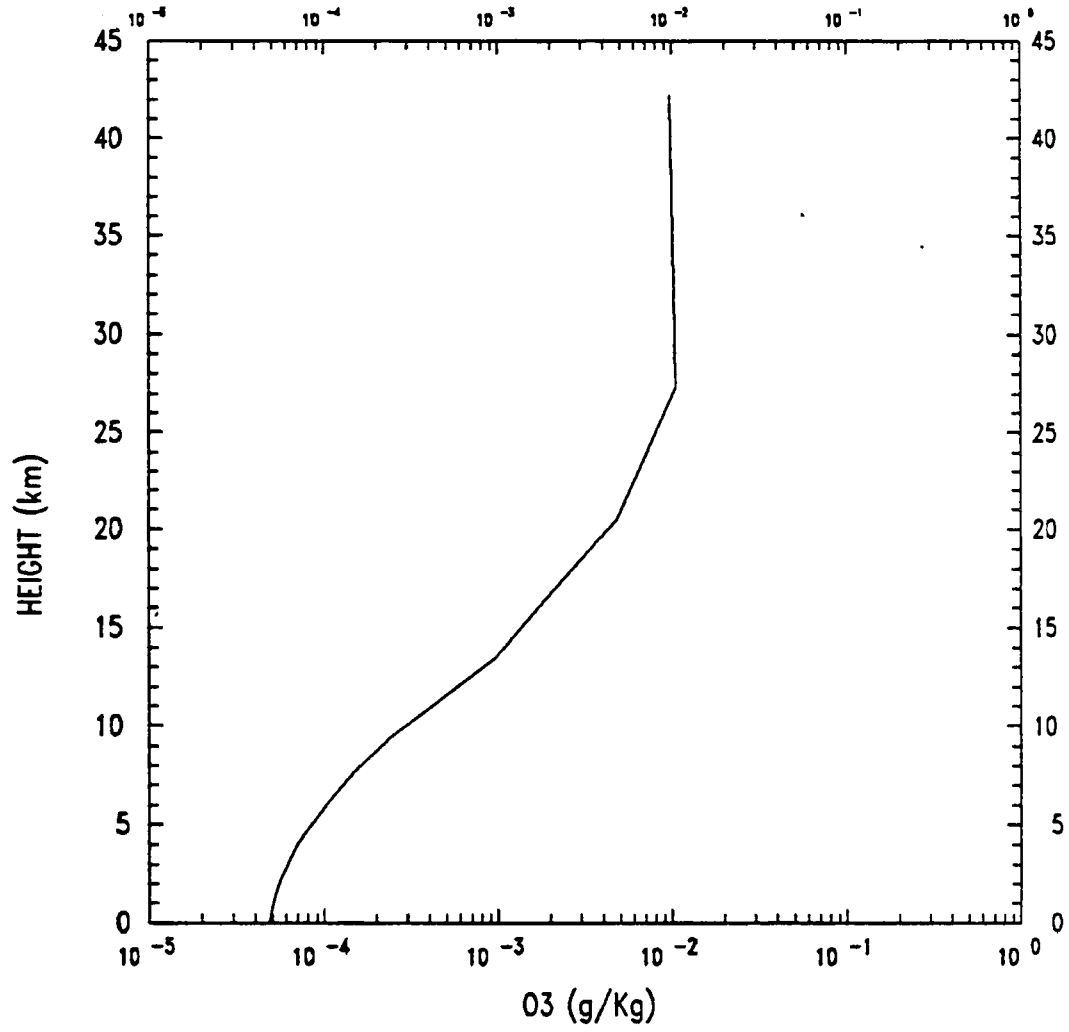


Figure 4.3: Same as Figure 4.1, except for ozone mixing ratio.

Table 4.2: Tabulated annual mid-latitude profile of air pressure(P), air temperature(T), air density(D), water vapor mixing ratio(Q), and ozone content(O<sub>3</sub>).

H(Km)	P(mb)	T(K)	D(Kg/m <sup>3</sup> )	Q(g/Kg)	O <sub>3</sub> (g/Kg)
42.2	2.270	256.2	0.003	0.012	0.00975
27.3	19.68	222.7	0.029	0.020	0.01041
20.5	52.51	217.0	0.084	0.006	0.00479
16.5	98.72	216.3	0.159	0.004	0.00189
13.5	156.2	217.1	0.251	0.005	0.00096
11.3	223.0	222.0	0.349	0.028	0.00046
9.34	297.0	231.5	0.447	0.113	0.00024
7.69	376.2	241.7	0.542	0.264	0.00015
6.27	458.4	250.7	0.637	0.551	0.00011
5.02	541.6	258.2	0.730	0.928	0.00008
3.94	623.8	264.7	0.821	1.605	0.00007
2.99	703.0	270.2	0.906	2.478	0.00006
2.20	777.0	274.0	0.986	3.547	0.00006
1.54	843.7	277.0	1.059	4.531	0.00005
0.99	901.3	279.4	1.123	5.381	0.00005
0.58	947.5	280.9	1.173	6.137	0.00005
0.30	980.3	282.0	1.208	6.676	0.00005
0.10	997.7	282.5	1.227	6.960	0.00005
0.00	1000.	282.6	1.229	7.000	0.00005

Table 4.3: The levels used in the model.

Full Level	Half Level	Height(Km)	Pressure(mb)
	1/2	$\infty$	0.000
1		42.2	2.270
	1 1/2	32.5	8.920
2		27.3	19.68
	2 1/2	23.2	34.30
3		20.5	52.51
	3 1/2	18.3	74.08
4		16.5	98.72
	4 1/2	14.9	126.2
5		13.5	156.2
	5 1/2	12.3	188.6
6		11.3	223.0
	6 1/2	10.3	259.3
7		9.34	297.0
	7 1/2	8.49	336.1
8		7.69	376.2
	8 1/2	6.96	417.0
9		6.27	458.4
	9 1/2	5.64	500.0
10		5.02	541.6
	10 1/2	4.47	583.0
11		3.94	623.8
	11 1/2	3.45	663.9
12		2.99	703.0
	12 1/2	2.59	740.7
13		2.20	777.0
	13 1/2	1.86	811.4
14		1.54	843.7
	14 1/2	1.25	873.8
15		0.99	901.3
	15 1/2	0.77	925.9
16		0.58	947.5
	16 1/2	0.43	965.7
17		0.30	980.3
	17 1/2	0.21	991.1
18		0.10	997.7
	18 1/2	0.00	1000.
19		0.00	1000.

## 4.2 Response of the pure radiative atmosphere

In this section only the radiative forcing considered in section 2.3 will be included. The effects of "convection" will be discussed in the next section.

Using the input conditions of section 4.1, calculations by a pure radiative atmospheric model described in section 2.3 with fixed absolute humidity prescribed according to figure 4.2 were carried out and a radiative equilibrium state was obtained. Figure 4.4 shows the model's approach to pure radiative equilibrium from the initial isothermal atmosphere of 170 K and 340 K. It takes about 445 days to reach equilibrium for both cases. The approach to equilibrium temperature profiles are most rapid at the beginning of the integration due to large differences between the net incoming solar radiation and the net outgoing longwave radiation as shown in figure 4.5. As the differences in these fluxes become smaller as time integration proceeds, the change in the temperature profiles also decreases. The equilibrium temperature profiles are reasonably well established for both cases after 200 days of integration and slowly converge to the same final profile. The absolute differences between the net incoming and net outgoing net flux at the top of the model at this time is about  $4.2 \text{ W/m}^2$  after 200 days of integration. However, it will take another 245 days for them to reach the convergence criterion stated in section 4.1. The absolute difference in surface temperature between 200 and 445 days is about 0.4 K and the final equilibrium surface temperature computed by the model is about 310.6 K. At the end of integration, the difference in surface temperature between the two atmospheres is less than 0.01 K. The final equilibrium temperature profile of this model shows a super-adiabatic temperature lapse rate throughout the entire troposphere, specially near the surface. The temperature profile has an inversion at 11 Km (220 mb) indicating the tropopause level and the temperature at this level is about 196.6 K. Figure 4.6 shows the temperature profile of the model and of actual atmosphere. The major differences between the two profiles are found in the troposphere. The surface temperature predicted by the model is too warm compared to the actual atmosphere with a lapse rate that is too large leading to a much colder tropopause temperature and a much lower tropopause height compared to the actual atmospheric temperature profile. All these unrealistic values indicate that processes, other

than radiation, are at work in the troposphere to lower both the surface temperature and modify the radiative tropospheric lapse rate. The computed lapse rate in the stratosphere, on the other hand, is reasonably well predicted by the model. This feature indicates that the stratosphere must be in very close equilibrium with the radiation forcing. These findings are not new. When compared to the first successful study of radiative equilibrium temperature profile by Manabe and Moller (1961), our model agrees well with their results (shown in figure 4.7). The small disagreements between the two models can be accounted for by differences in both the initial inputs and the gaseous absorption data used in the parameterizations. Overall, this experiment demonstrates that the model performs very poorly in simulating the actual atmospheric temperature profile. It seems very clear from this experiment that an explicit representation of dynamical effects in the troposphere is necessary to obtain realistic temperature profile in the model.

#### 4.3 Modeling the troposphere with convective adjustment

In this section, the dynamical effect due to overturning of air by convection is incorporated into the model according to the convective parameterization presented in section 2.4.

Using the input conditions of experiment 1 and setting a convective lapse rate in the troposphere to be the moist adiabatic value, a radiative convective calculation was performed with fixed absolute humidity. The approach to equilibrium temperature profile from the same initial profiles of experiment 1 is given in figure 4.8. The two different initial profiles again converge into one final equilibrium temperature profile as in experiment 1. However, the time for convergence is much faster for this study and it only takes about 312 days to reach the thermal equilibrium state with the given convergence criterion. At this time the absolute difference in net flux at the top of the model atmosphere is about  $0.27 \text{ W/m}^2$ . The equilibrium surface temperature computed by the model is about 291.1 K. At the end of integration the difference in surface temperature between the two initially isothermal temperature atmospheres is less than 0.01 K. Figure 4.9 shows the temperature profile of the real atmosphere and those for the modeled atmosphere

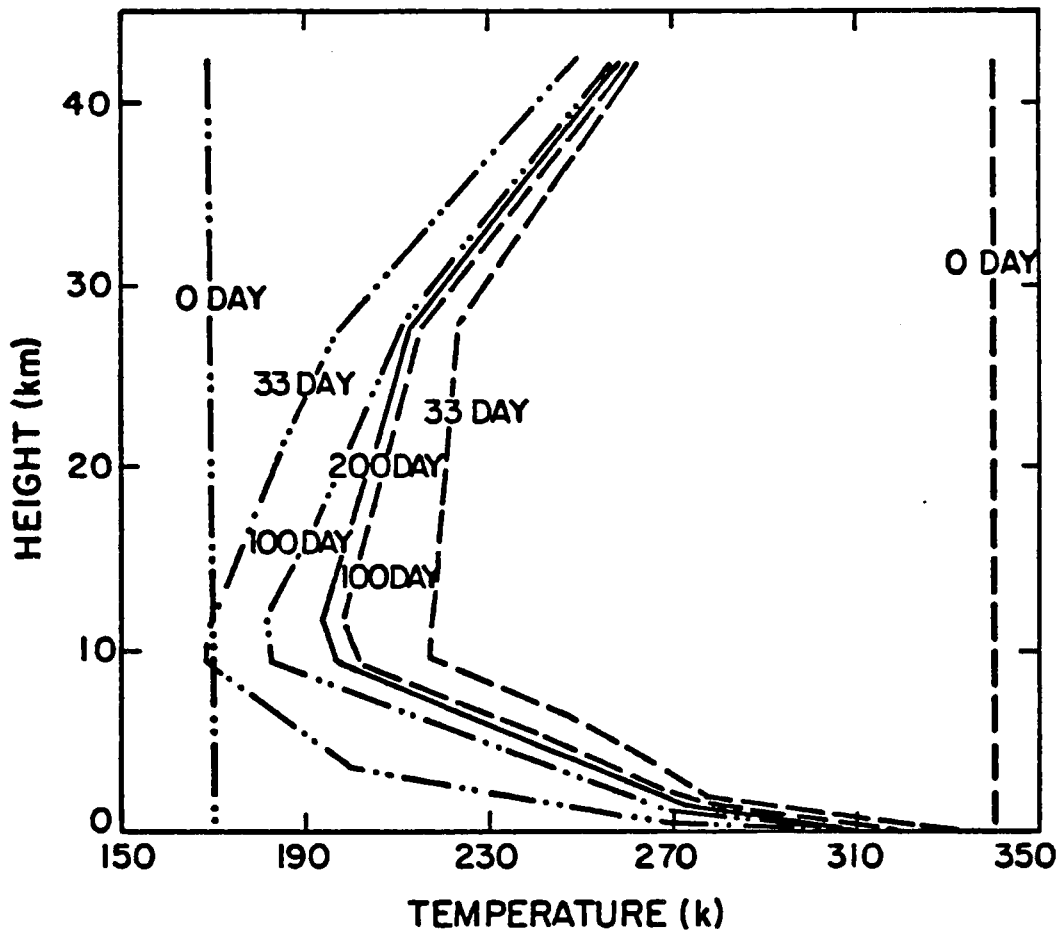


Figure 4.4: Approach to pure radiative equilibrium temperature from two initial isothermal atmosphere at 170k and 340k.

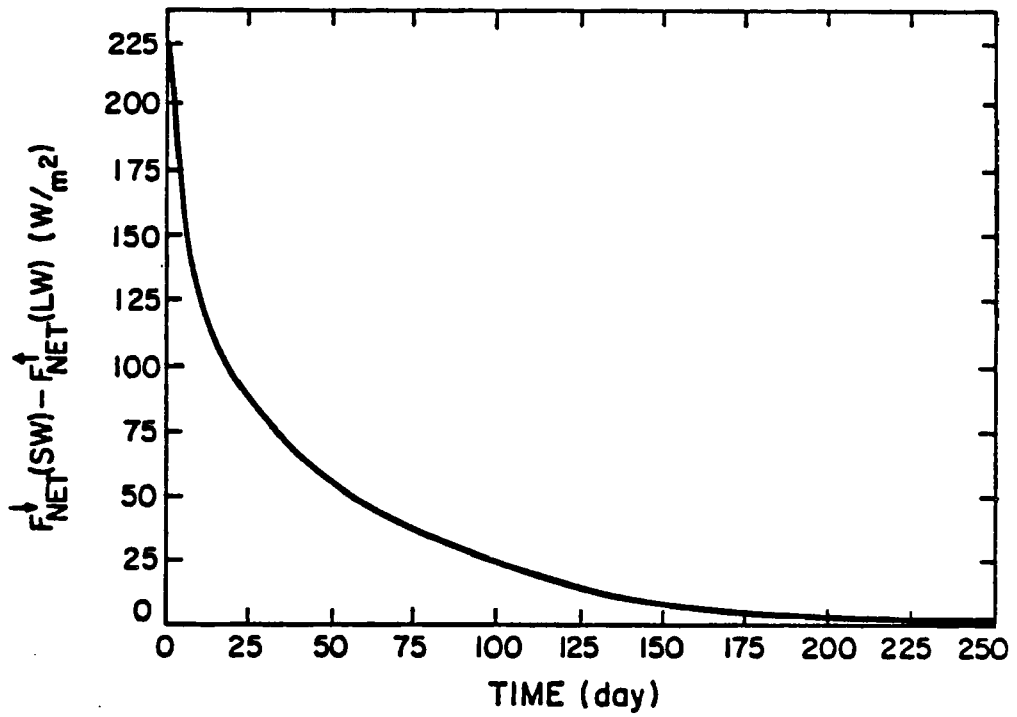


Figure 4.5: The change in the net flux difference between upward longwave and downward shortwave energy at the top of the model.

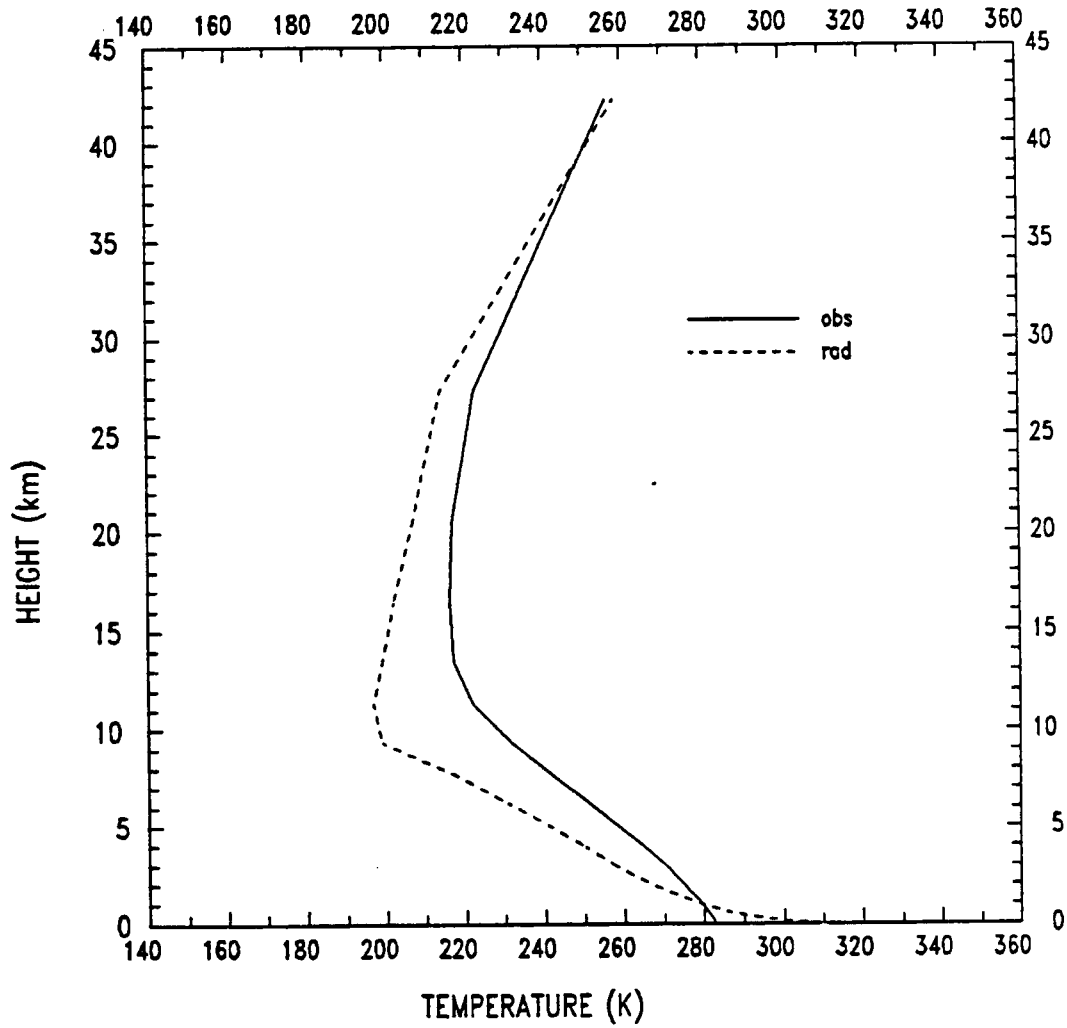


Figure 4.6: Temperature profile of the real atmosphere (solid curve) and pure radiative atmosphere model (dash curve).

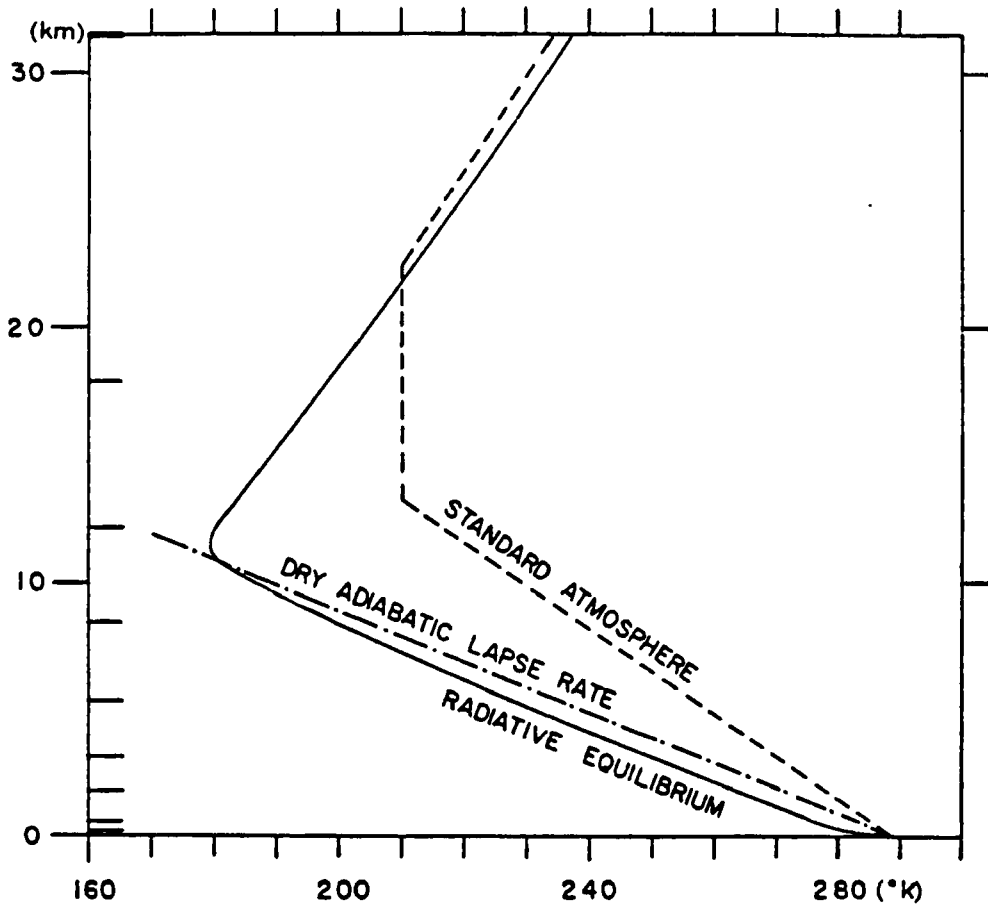


Figure 4.7: Distribution of radiative equilibrium temperature. The amount of sunshine, the distributions of gases, and surface temperature at 30° N in April were used ( $\delta = 0.03^{\circ}\text{C}/\text{day}$ ). The line of standard atmosphere and that of dry adiabatic lapse rate are also shown for the sake of comparison (after Manabe and Moller, 1961).

with and without convective adjustment. For the model with convective adjustment, the calculated tropospheric temperature profile is very realistic and arises from the convective parameterization in the model which allows the excess energy at the surface to be redistributed throughout the atmosphere. The model predicted tropopause is at 16.5 km (100 mb). The corresponding model temperature at the tropopause is about 208.4 K. These values are in very close argument with the actual atmosphere shown for comparison. The temperature at the tropopause and at the surface are still slightly lower and higher than the real atmospheric values respectively. These results again agree well with the first convective adjustment study of Manabe and Strickler (1964). Overall the model does very well in predicting the actual temperature profile.

#### 4.4 Atmospheric model with fixed relative humidity

In this section, we will relax our initial condition by allowing the water vapor to vary in the atmosphere thereby making the model more realistic.

In experiment 2, the vertical distribution of the absolute humidity was fixed throughout the computation of equilibrium temperature, and its dependence upon atmospheric temperature was not taken into consideration. However, the absolute humidity in the actual atmosphere strongly depends upon temperature. Thus a model atmosphere with a fixed absolute humidity is not very realistic for studying climate and its variations. In this experiment, we will allow the absolute humidity to vary in the model according to Manabe and Wetherald (1967) by fixing the relative humidity for the atmosphere according to a prescribed profile. This assumption of a constant relative humidity is supported by the 1-D hydrological radiation model results of Sarachik (1978) which show the atmosphere will tend to restore a certain climatological distribution of relative humidity responding to the change of temperature. The relative humidity profile in this experiment is fixed according to Manabe and Weatherald (1967) and is shown in figure 4.10. This profile can be expressed as

$$h = h_* \frac{\frac{P}{P(1000mb)} - 0.02}{1.0 - 0.02} \quad (4.1)$$

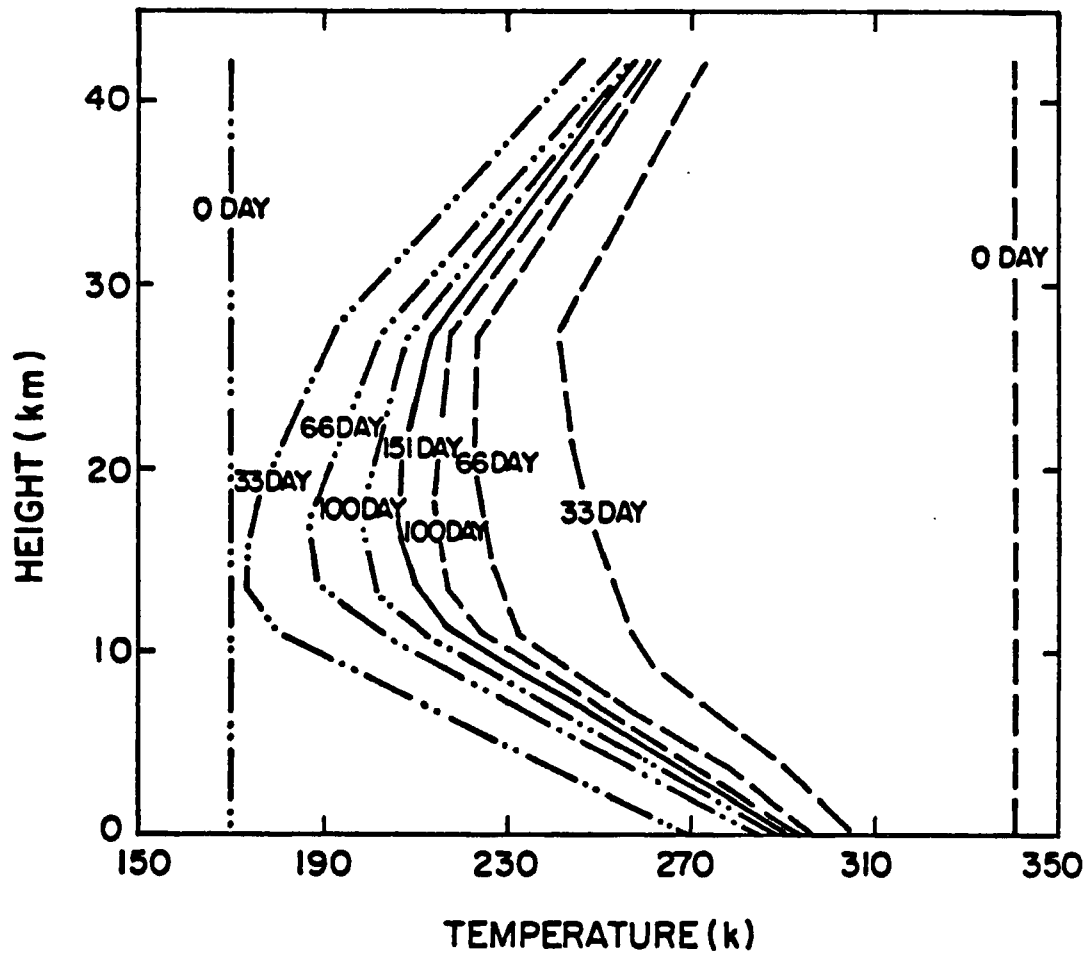


Figure 4.8: Approach to radiative convective temperature profile from two initial isothermal atmosphere at 170k and 340k.

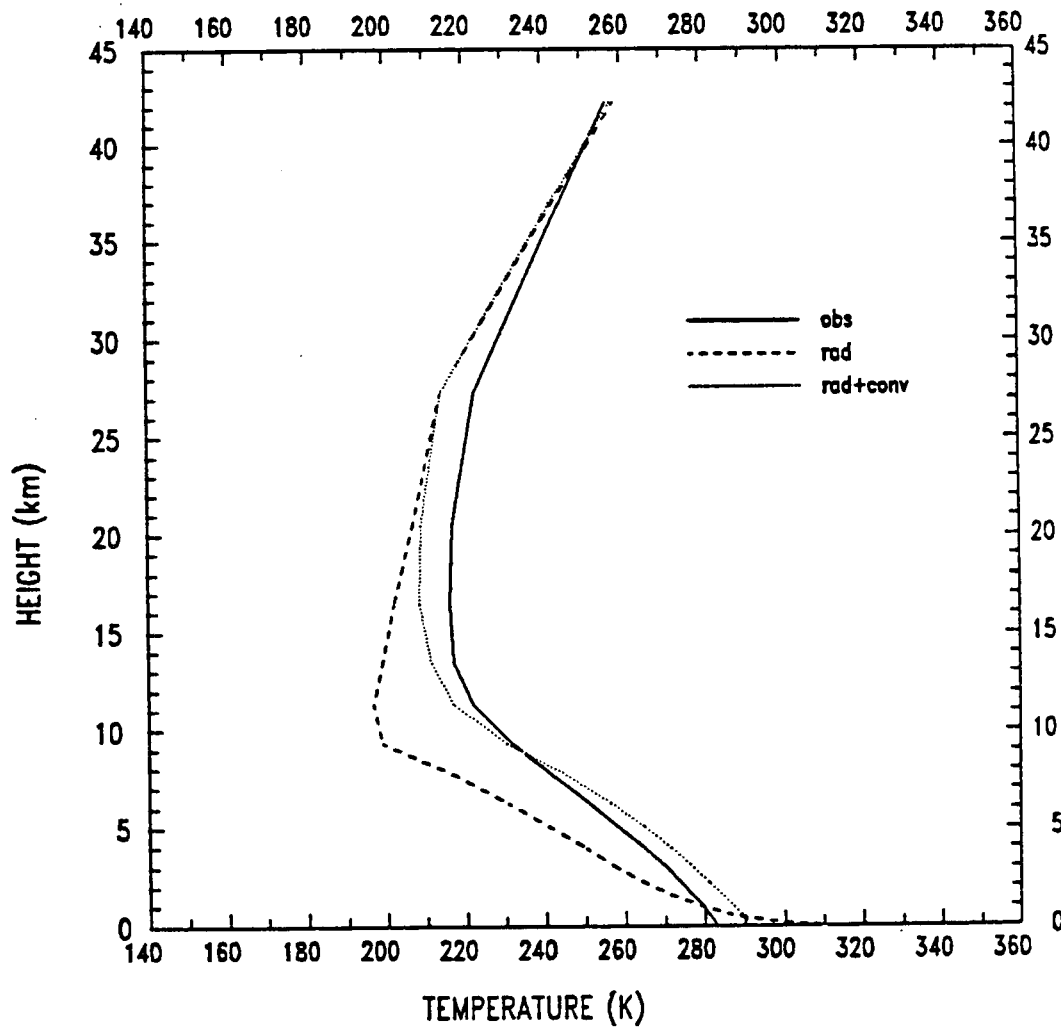


Figure 4.9: Temperature profile of actual atmosphere (solid curve), pure radiative atmosphere model (dash curve), and radiative convective atmosphere model (dot curve).

where  $h_*$  is the relative humidity at the earth's surface, and it has a value of 0.77 (or 77 percent). The corresponding mixing ratio is computed by

$$r(T, h) = \frac{0.622he_s(T)}{P - he_s(T)} \quad (4.2)$$

Furthermore, if the mixing ratio drops below 0.0015 g/Kg, a constant value of 0.0015 g/Kg is assumed for the layer. This conditional statement, following Manabe and Weatherald (1967), is used to avoid unrealistic high water vapor content that would be otherwise result in the model stratosphere.

The equilibrium temperature profile is calculated using the same input conditions as the previous experiments. The behavior of this experiment is very similar to experiment 2 and only final model results will be discussed. The model takes about 533 days to reach the equilibrium state. This integration period is about 1.7 time longer than that of experiment 2 and it is caused by the fact that the dependence of the outgoing radiation of the atmosphere with a given distribution of relative humidity depends less on the atmospheric temperature than does that of an atmosphere with a given distribution of absolute humidity, therefore, the speed of approach towards the equilibrium state is significantly less. The final predicted surface temperature, tropopause temperature, and tropopause height are 293.6 K, 219.3 K and 16.5 Km, respectively. These values are in good agreement with the actual atmosphere and with the model of Manabe and Weatherald (1967). The contributions to the equilibrium total heating/cooling rate by each atmospheric gas in the model are shown in figure 4.11. According to this figure, the most important gas for maintaining the radiative convective equilibrium temperature profile of the lower atmosphere is water vapor. Figure 4.12 shows the temperature profiles of experiment 2, 3 and the real atmosphere. Both experiments 2 and 3 produce very realistic temperature profiles. However, there are still some small disagreements between experiment 3 and the real atmosphere which are probably caused by the existence of clouds in the real atmosphere which tend to cut down energy into and out of the atmosphere and thus altering the final equilibrium atmospheric temperature profile.

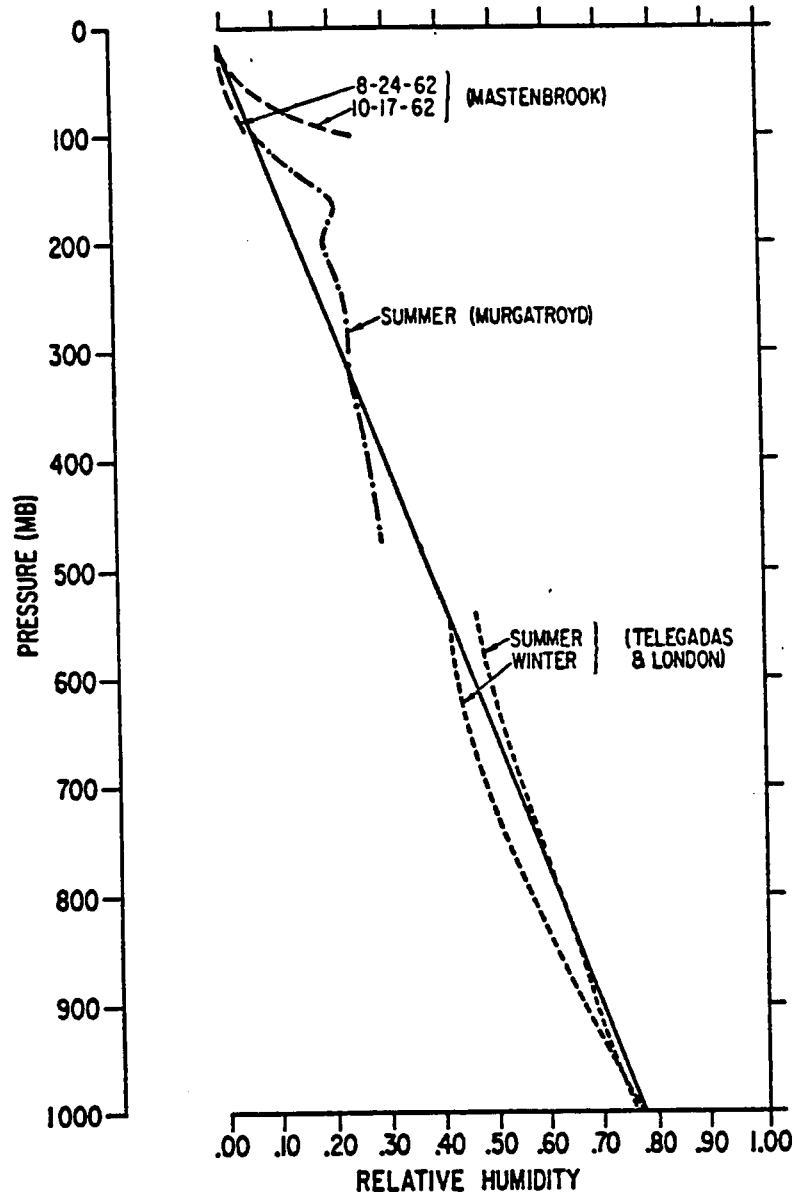


Figure 4.10: Vertical distribution of relative humidity (Mastenbrook, 1963; Murgatroyd, 1960; Telegadas and London, 1954) (after Manabe and Weatherald, 1967).

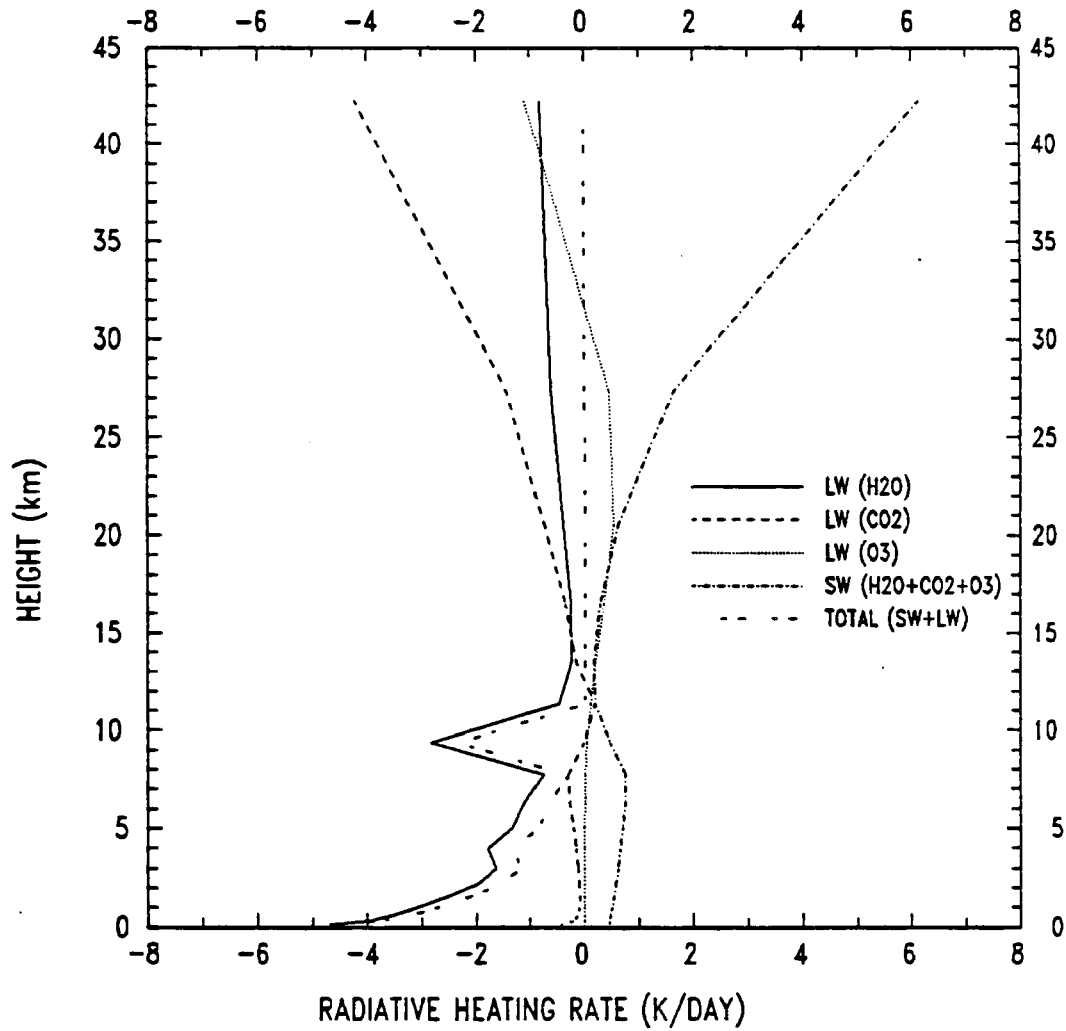


Figure 4.11: Vertical profiles of various equilibrium radiative heating rate.

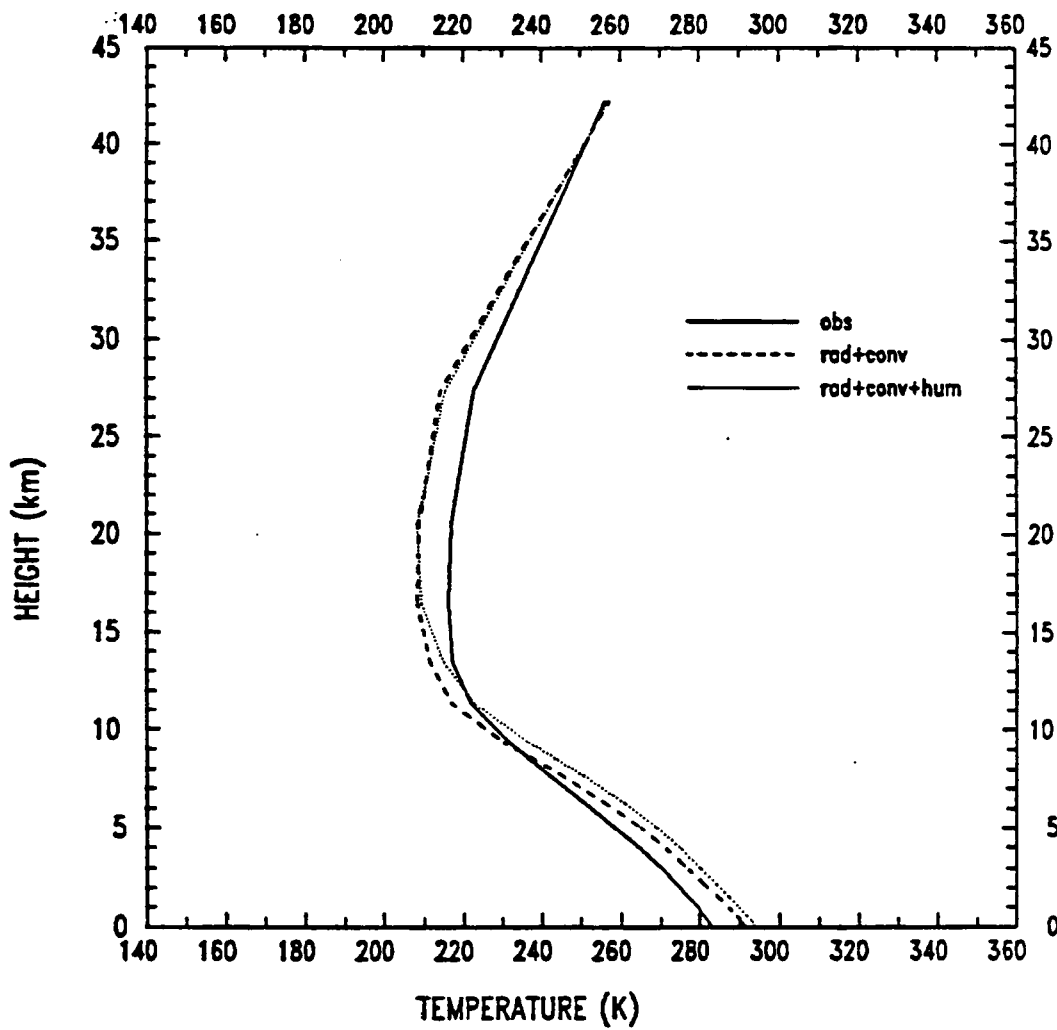


Figure 4.12: Temperature profile from real atmosphere (solid), experiment 2 (dash), and experiment 3 (dot).

## 4.5 Model Sensitivities

The sensitivity of the radiative convective atmosphere model with a fixed relative humidity to change in solar input,  $CO_2$  content, surface albedo value, and cloudiness is now examined.

### 4.5.1 Solar input

There is little argument that solar input is one of the greatest climate modulators of the earth-atmospheric system. In order to evaluate the effect of the solar forcing upon the climate of the earth's surface, a series of computations of equilibrium temperature was performed. Figure 4.13 show the dependence of the surface equilibrium temperature upon the solar input. According to this figure, the change in equilibrium surface temperature is not symmetry in its response to changing solar inputs. The temperature is more sensitive to decrease of solar input than to an increase. Thus a decrease in solar input may have a larger impact on the earth's climate than that from a comparable solar increase. As a reference, the vertical distributions of equilibrium temperature corresponding to various values of the solar input are shown in figure 4.14.

### 4.5.2 Carbon dioxide

Carbon dioxide is another important climate modifier. The increasing carbon dioxide level in the atmosphere due to anthropogenic and natural causes and the impact of this increase on the earth's climate has been a subject of considerable discussion (e.g., Manabe and Weatherald (1967), Rasool and Schneider (1971), Manabe (1971), Schneider (1974), Schneider and Dennett (1975) ,etc.). A number of radiative convective equilibrium computations were performed to test the model sensitivity to changing  $CO_2$  amount. Figure 4.15 shows the vertical distributions of equilibrium temperature corresponding to the four different  $CO_2$ , i.e., 150, 300, 600, and 900 ppm contents by volume. Generally the larger the mixing ratio of carbon dioxide, the warmer is the equilibrium surface temperature and the colder is the equilibrium temperature of the stratosphere. The results are similar to previous study by Manabe and Weatherald (1967), but the sensitivity of equilibrium

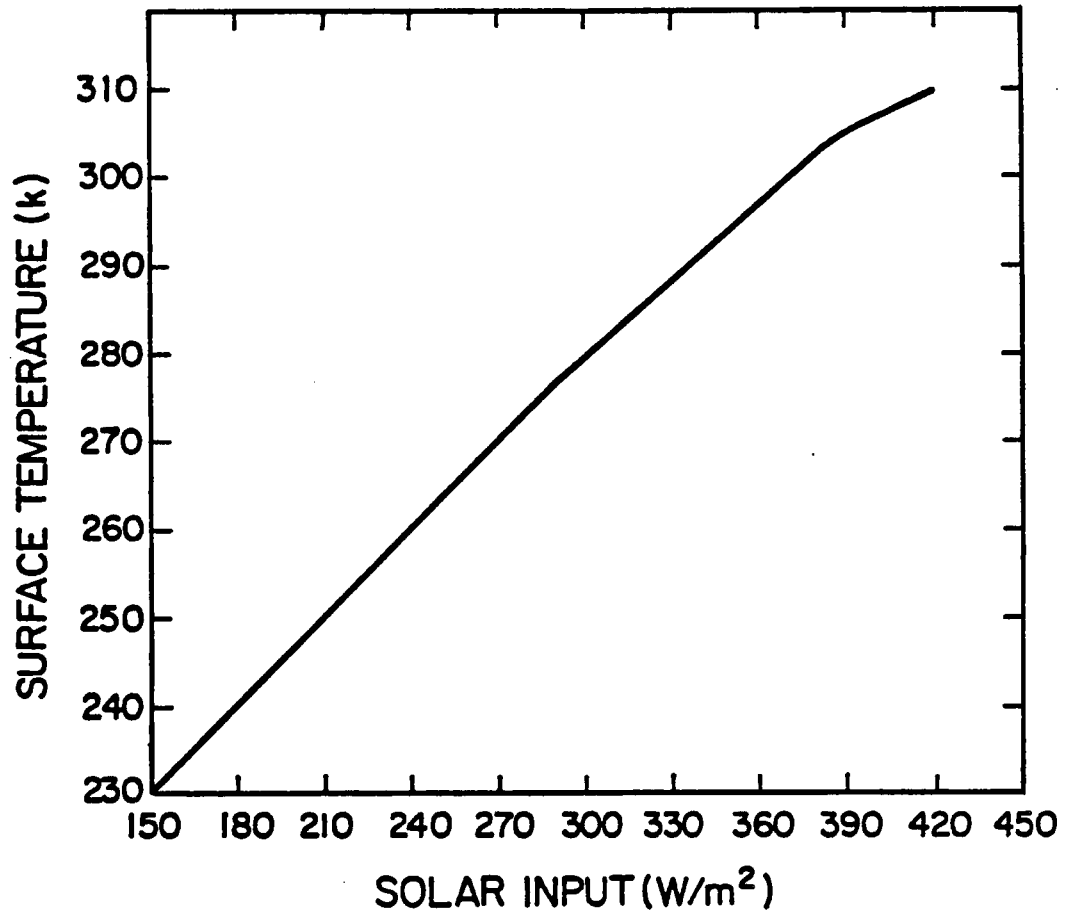


Figure 4.13: Solar input and surface temperature of radiative convective equilibrium.

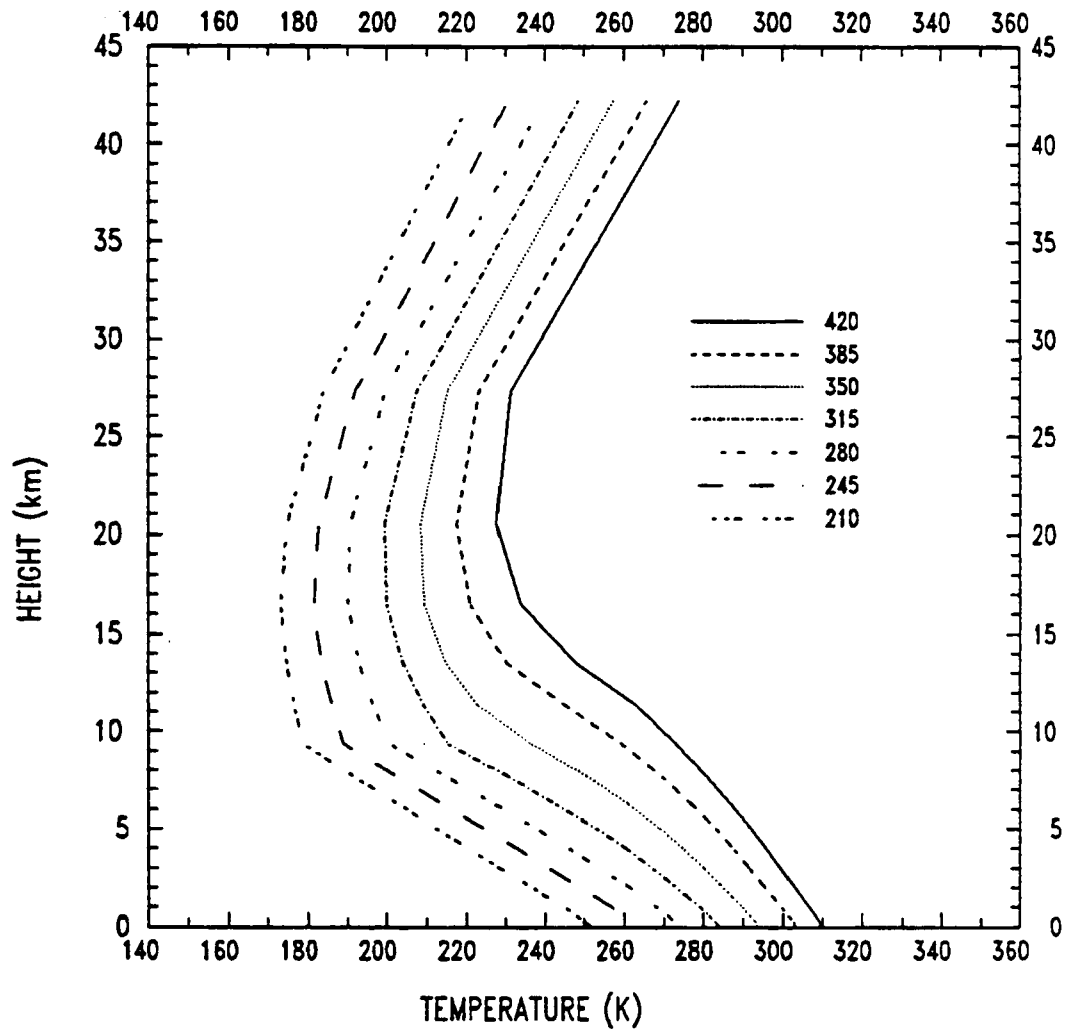


Figure 4.14: Vertical distribution of radiative convective equilibrium temperature of the atmosphere for various values of solar input.

surface temperature change are slightly smaller for our model, probably due to different initial inputs. Table 4.4 shows the equilibrium surface temperature corresponding to various  $CO_2$  contents of the atmosphere obtained from the model described here and from the result of Manabe and Weatherald (1967).

Table 4.4: Equilibrium and change of equilibrium temperature (K) of the earth's surface corresponding to various  $CO_2$  content of the clear atmosphere.

$CO_2$ Content (ppm)	$T_s(X)$	$T_s(X) - T_s(300)$	
		our	other*
150	291.59	-2.02	-2.80
300	293.61	0.00	0.00
600	295.68	2.07	2.92
900	296.58	2.97	-

\*Results obtained from Manabe and Weatherald (1967).

#### 4.5.3 Surface albedo

Surface albedo is another important parameter in any climate studies of the earth surface. The high surface reflectivity of snow and ice is a dominant factor in the climate of polar regions. But, the extent of the snow and ice cover of the earth's surface depends strongly upon surface temperature. Thus, if lowering the planetary temperature would lead to a longer lasting and more extensive snow and ice cover, this would increase the planetary albedo, causing a decrease in the amount of solar energy absorbed by the earth-atmosphere system, and would thereby lower the temperature further. A series of equilibrium states of the atmosphere were therefore computed using various values of surface albedos. Figure 4.16 shows the results of these studies. These results are also similar to the early studies from other investigators. Table 4.5 shows the equilibrium surface temperature as a function of surface albedo value. Generally speaking the effect of surface albedo is maximum near the surface and it decreases significantly with height. The larger the surface albedo value, the colder the temperature will be for the earth surface.

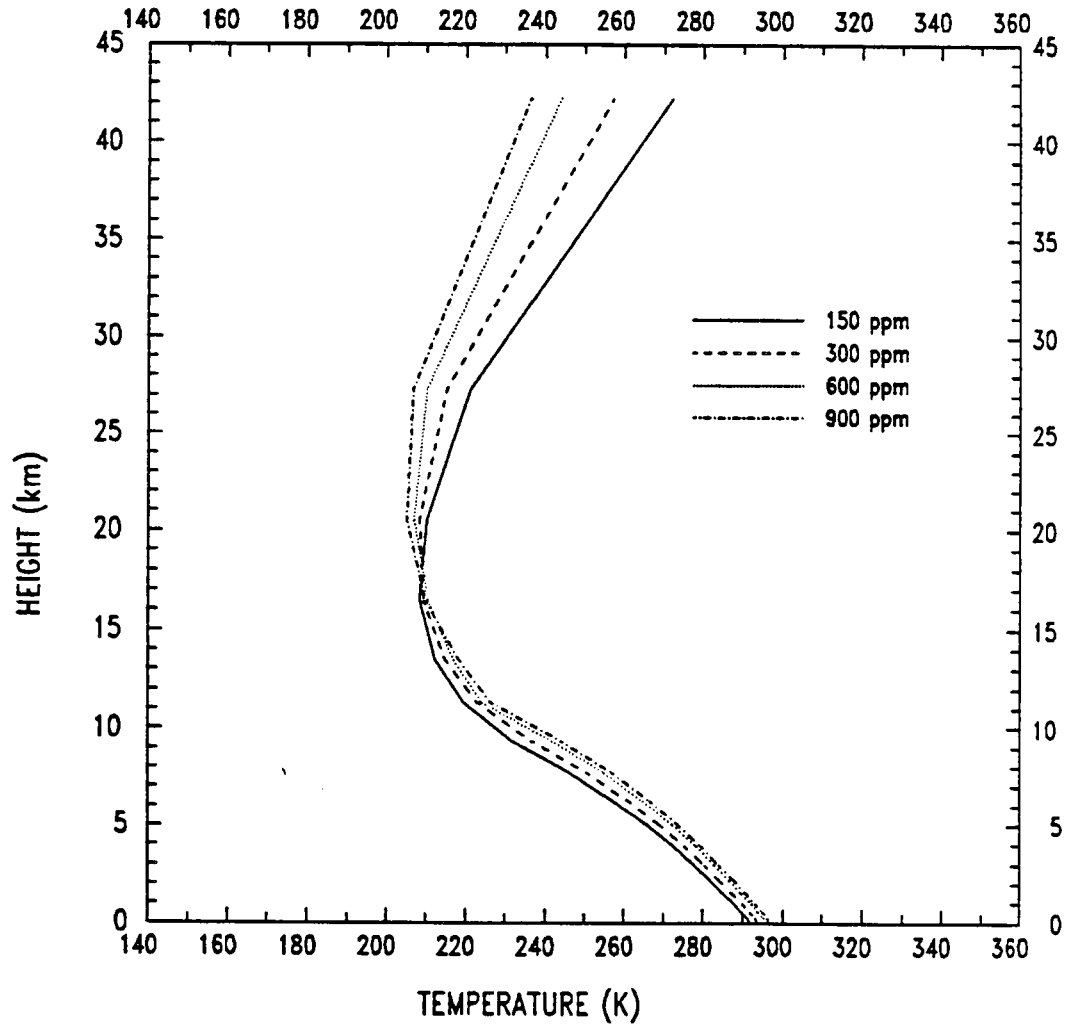


Figure 4.15: Vertical distributions of temperature in radiative convective equilibrium for various values of  $CO_2$  content.

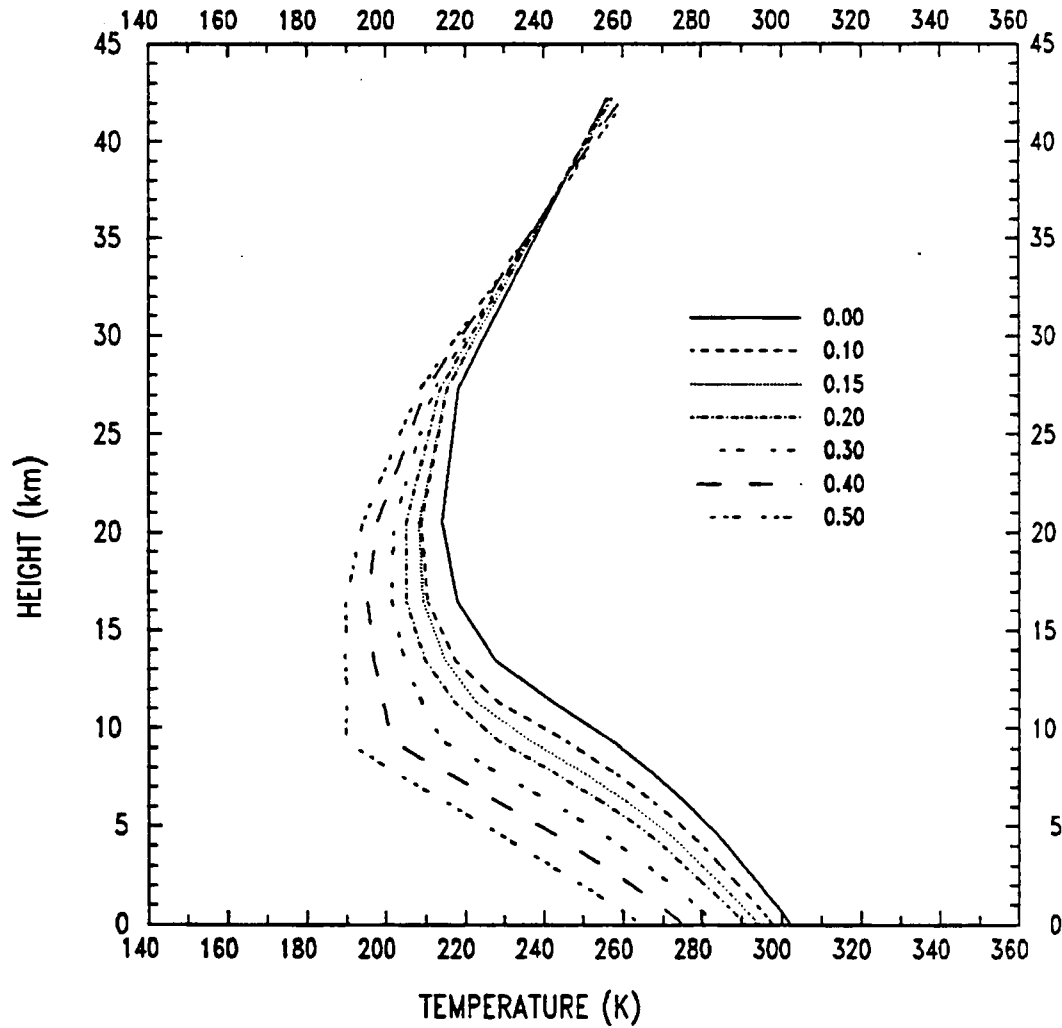


Figure 4.16: Vertical distributions of radiative convective equilibrium for various values of surface albedo.

Table 4.5: Equilibrium and change of equilibrium temperature (K) of the earth's surface corresponding to various values of the surface albedo.

Albedo	$T_s(X)$	$T_s(X) - T_s(15)$
0.0	301.98	8.37
5.0	299.67	6.06
10.0	297.30	3.69
15.0	293.61	0.00
20.0	290.16	-3.45
25.0	286.74	-6.87
30.0	282.96	-10.65
40.0	274.48	-19.13
50.0	263.78	-29.83

#### 4.5.4 Cloud effects

As discussed in Chapter 2, clouds are one of the most important modulators of the earth climate system. Their effects on the equilibrium temperature profile of the atmosphere is investigated by using different cloud types. Table 4.6 summaries the liquid/ice water paths used in the studies. The equilibrium temperature profiles obtained from these studies are presented in figure 4.17 and summarized in table 4.7 in terms of surface, planetary temperature and downward radiative energy incident on the surface. The equilibrium temperature profile for the cloud case does not show a temperature inversion at the cloud layer as suggested by Stephens and Webster (1981). The reason for the lack of inversion is that the temperature at the cloud base is raised significantly by convective adjustment process and thus erasing the inversion profile produced by radiative forcing. Beside from this minor disagreement, the results for all cloud studies agree well with other studies (Manabe and Weathrald, 1967; Stephens and Webster, 1981; and, Liou, 1986). It is shown that the presence of low and middle cloud produce a general decrease in surface temperature due to a significant decrease of both solar and atmospheric energy to the surface. For high cloud (cirrus) the effect is opposite and it tends to warm the surface. This warming is caused by the net increase in downward flux of energy at the surface (shown in table 4.7) and it is mainly due to the large increase in atmospheric radiation, which overcome the decrease in solar energy into the surface. On the other hand the planetary temperature is less sensitive to cloud forcings having the same total liquid/ice water

content. These results suggest that cloud tends to decouple the surface and the planetary radiative budgets. These findings are again consistent with early results by Stephens and Webster (1984), in which they first described these effects.

Table 4.6: Setups for the clouds studies

Cloud Type	Level	Position (Km)	Liquid/Ice Water Path (g/m <sup>2</sup> )
Clear	—	—	0.0
Low	15	0.77-1.25	14.0
Middle	11	3.45-4.47	14.0
High	8	6.96-8.49	14.0
High	8	6.96-8.49	5.0

Table 4.7: Equilibrium temperature (K), downward energy budget (W/m<sup>2</sup>) at the surface, planetary temperatures (K) and difference in flux (W/m<sup>2</sup>) between clear and cloud cases for various cloud studies.

Type	T <sub>s</sub>	T <sub>p</sub>	LW	SW	Total	CLD-CLR
Clear	293.61	263.87	356.48	203.29	559.77	0.00
Low	283.42	255.33	339.55	150.47	490.02	-69.75
Middle	289.26	253.16	356.69	148.01	504.70	-55.07
High14	297.85	258.46	432.45	161.84	594.29	34.52
High05	298.79	262.03	421.75	190.02	611.77	52.00

#### 4.6 Summary of the model's performance

The atmospheric model with fixed relative humidity and convective adjustment performs quite well and provided sensitivities similar to many other studies. It was found that

1. the increase in CO<sub>2</sub> content and solar input will create a surface warming;
2. the increase in surface albedo will cause a surface cooling;
3. the present of low and middle cloud will decrease the surface temperature while high cloud has a opposite effect and will tend to warm the surface (for the liquid water paths assumed), and

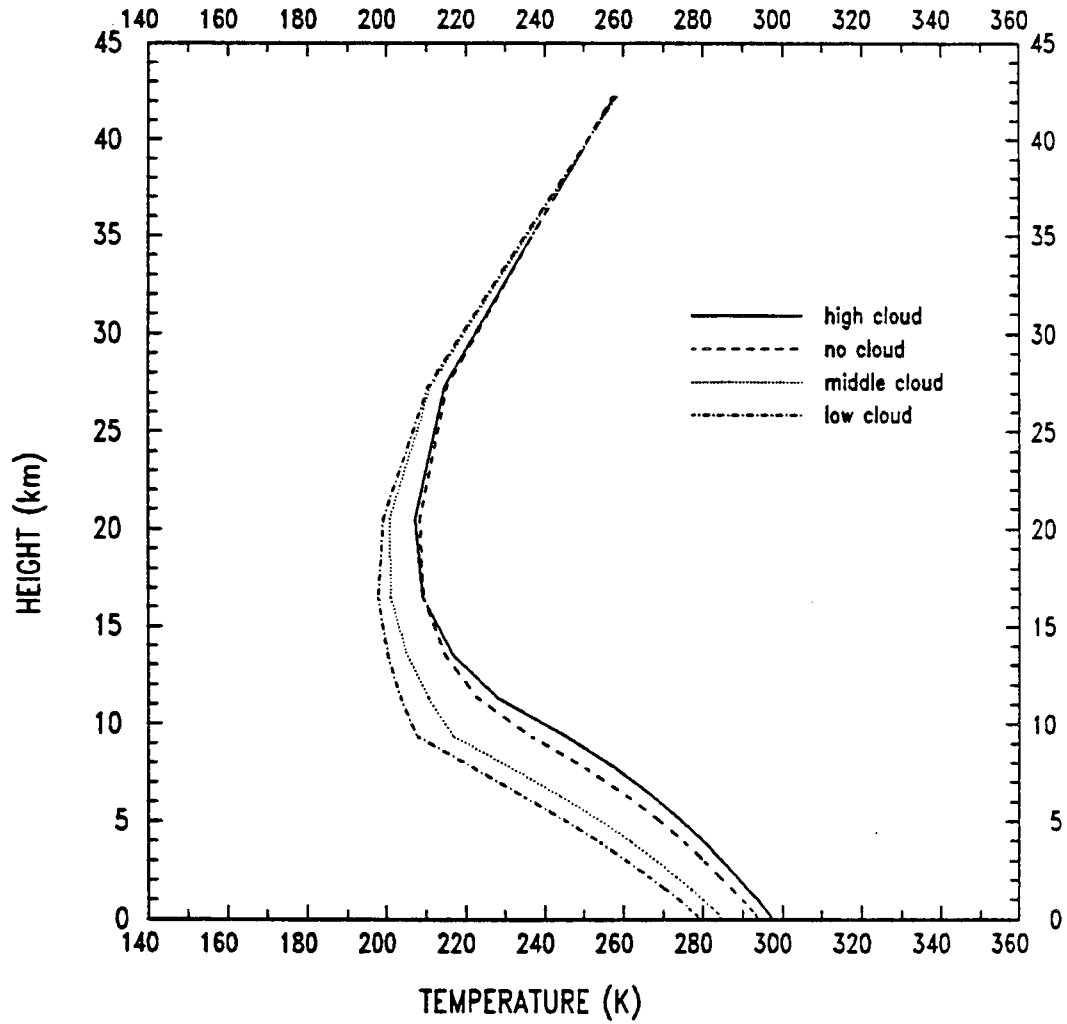


Figure 4.17: Vertical distribution of radiative convective equilibrium temperature for various types of cloud condition.

4. cloud also decouples the surface and planetary radiative budgets.

These result are in good agreement with other studies notably those of Manabe and Weatherald (1967) and Stephens and Webster (1981).

Since the change in solar input,  $CO_2$  mixing ratio, and cloudiness can change the downward flux of energy at the surface, which is the primary energy source for the ocean system, changes in these parameters therefore can be expected to have a significant impact on the energy budget and the temperature profile of the ocean. These effects will be investigated further in Chapter 6 using a coupled atmosphere-ocean model.

## Chapter 5

### PERFORMANCE OF THE OCEAN MODEL.

Since the proper behavior of the mixed layer ocean model is important to the present study, a careful examination of its performances is necessary to assess the reality of the model. In this chapter the ocean model is extensively tested. First, the model's simulated seasonal cycle under mid-latitude conditions is compared to real oceanic data of Defant (1961). The behavior of the model under annual/mean conditions (i.e. the annual cycle are replaced by their respective mean values.) is then considered. The problems associate with running annual/mean ocean model are discussed and a new hybrid annual model is presented to overcome these problems. Sensitivity experiments are presented to evaluate the new model and a summary of the performance of the new model is provided.

#### 5.1 Input conditions and computational method.

The inputs to the mixed layer ocean model defined in chapter 3 can be separated into two categories, the atmospheric inputs and the internal oceanic inputs. The atmospheric inputs to the ocean are simply the top-boundary terms, which include the surface solar and atmosphere radiation, surface air temperature, surface water mixing ratio content, and surface wind speed. The internal oceanic inputs contain elements associated with the characteristics of the mixed layer plus the lower-boundary inputs below the mixed layer. These factors include the attenuation for solar radiation, the fraction of turbulent energy transfer to the mixed layer from the atmosphere, the sea surface temperature, the mixed layer depth and temperature, lapse rate and vertical velocity below the mixed layer. Table 5.1 summarizes the annual/mean values of these inputs for typical mid-latitude clear sky condition.

Table 5.1: Annual/mean inputs for the ocean model according to their categories.

Atmospheric Inputs	Internal Oceanic Inputs
Vis. radiation - 110w/m <sup>2</sup>	Extinction length:
Nir. radiation - 110w/m <sup>2</sup>	Vis. - 20m <sup>-1</sup>
Atm. radiation - 360w/m <sup>2</sup>	Nir. - 1m <sup>-1</sup>
Air temperature - 292.9K	Surface temperature - 296K
Air moisture - 10.0g/Kg	Mixed layer depth - 100m
Air wind speed - 1.0m/s	Fractional mixing - .0012
	Below the mixed layer :
	Temperature - 294K
	Temp. gradient - .02K/m
	Vertical velocity - small

For the seasonal cycle experiment conducted below, the atmospheric inputs are represented by the following simple harmonic functions

$$U = U_m - U_a \sin(2\pi T)$$

$$AT = AT_m + AT_a \sin(2\pi T)$$

$$AQ = AQ_m + AQ_a \sin(2\pi T)$$

$$FS = FS_m + FS_a \sin(2\pi T)$$

$$FL = FL_m + FL_a \sin(2\pi T)$$

$$T = \frac{\text{\#of actual timestep}}{\text{\#of timestep in year}} \quad (5.1)$$

where  $U_m, AT_m, AQ_m, FS_m, FL_m$  are the surface annual/mean values of wind speed, air temperature, water vapor mixing ratio, net downward shortwave flux, and net downward longwave flux, respectively.  $U_a, AT_a, AQ_a, FS_a, FL_a$  are the corresponding seasonal fluctuations (or the amplitudes) for the above quantities.  $T$  is the time function which controls the variations of the harmonic motions. Table 5.2 shows the typical mid-latitude values for the fluctuations terms. For the annual/mean experiment, these seasonal fluctuations terms are assumed to be zero.

Using the governing equations presented in chapter 3, the state of the ocean was calculated by forward numerical integration with time step of 15 minutes. This small

Table 5.2: Seasonal fluctuation for the atmospheric inputs.

Name	Fluctuation
Vis. radiation	40w/m <sup>2</sup>
Nir. radiation	40w/m <sup>2</sup>
Atm. radiation	30w/m <sup>2</sup>
Air temperature	5K
Air moisture	3g/Kg
Air wind speed	0.5m/s

model time step, which is obtained by trail and error, is necessary in order to prevent numerical instability. A discussion of this instability is presented in Appendix A. The seasonal cycle experiment began its integration at vernal equinox and was integrated over a period of ten years. This long integration time was necessary to insure that the final solutions of the model were free of the influence of initialization parameters. The exit condition for the annual/mean experiment was chosen such that the rate of change of mixed layer temperature with time is equivalent to 1 K per 100 years. This condition again insures a final solution independent of initial conditions.

## 5.2 Evaluation of the model's seasonal cycle.

Using inputs similar to those introduced in section 5.1, a seasonal simulation was run for ten years. The time-evolution of the model's mixed layer depth and temperature during these ten years is shown in figure 5.1 and 5.2. The model's solutions shown in these diagrams appear to be stable after six years of integration with the final mixed layer depth and temperature values relatively free of initial conditions.

### 5.2.1 The mixed layer depth.

The mixed layer depth (shown in figure 5.1) displays a distinct and repetitive annual cycle. Note that the amplitude of the first cycle is overestimated due to the chosen input parameters. This amplitude decays and finally settles down to a stable value after 6 years of integration. The distribution of the mixed layer depth over any one year is found to be asymmetric between the heating and cooling seasons, with the most rapid deepening occurring in the autumn, and the greatest depth achieved in the winter, after which

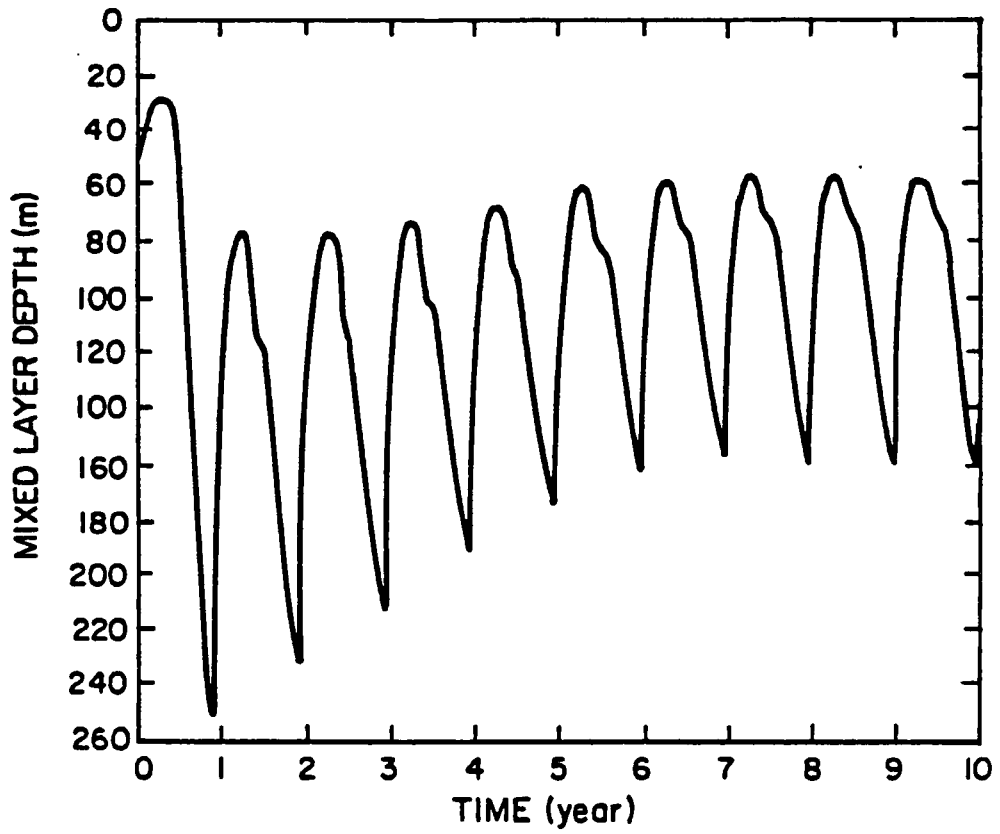


Figure 5.1: The approach to steady state mixed layer depth for seasonal model.

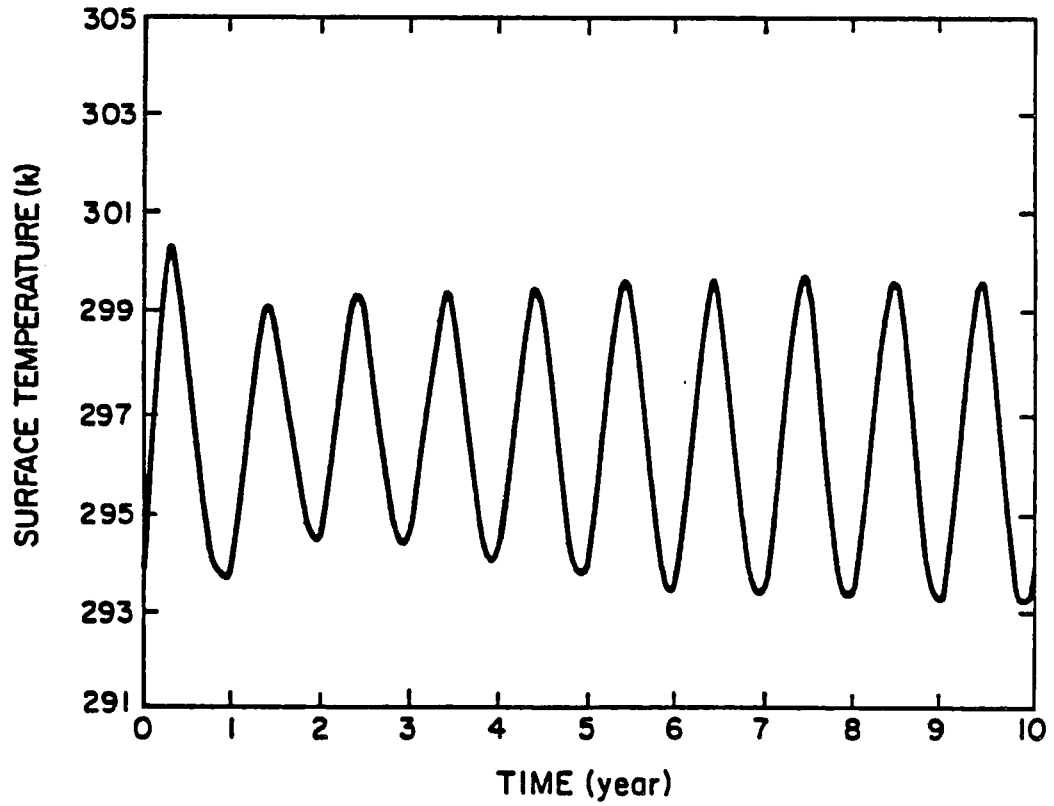


Figure 5.2: The approach to steady state solution for sea surface temperature for seasonal model.

shallowing takes place until the next summer. One other interesting aspect of figure 5.1 is that there is a clear distinction, indicated by a discontinuity, between the transition from one regime (wind or heat) into the other. At the tenth year of integration, the maximum and minimum mixed layer depth is 162 m and 57 m, respectively, and the annual average mixed layer depth of the seasonal model is 94 m. These values are very reasonable when compared to the actual annual/mean mixed layer depth, which has typical mid-latitude value of about 100 m (refer to table 5.3).

Table 5.3: The mixed layer/quasi-isothermal top layer temperature ( $^{\circ}\text{C}$ ) in the Atlantic Ocean (after Defant, 1961).

Mean Geographical Depth(m)	24° S. 16° W.	15° S. 15° W.	9° S. 17° W.	0° S. 22° W.	8° N. 23° W.	18° N. 36° W.
0	20.36	24.10	24.40	26.50	25.80	22.78
25	20.32	24.44	24.36	26.43	25.82	22.86
50	20.38	24.45	24.28	26.28	25.43	22.91
75	20.37	23.46	23.79	22.77	24.55	22.65
100	20.30	20.65	20.32	17.02	19.77	22.50
150	17.22	17.10	14.60	13.42	12.98	20.22

### 5.2.2 The mixed layer temperature.

The mixed layer temperature predicted by the model and shown in figure 5.2 also shows a distinct oscillation between seasons. Similar features exist between mixed layer temperature and depth. The pattern again stabilized after 6 years of integration. The distribution of the surface temperature, however, is more symmetric between the heating and cooling seasons with maximum and minimum values of 299 K and 293 K respectively giving an annual range of 6 K. When compared to the actual oceanic temperature variation at mid-latitudes illustrated in figure 5.3 and table 5.4, it is evident that the model is capable of predicting the annual cycle and its amplitude accurately.

Table 5.4: Annual sea surface temperature variations ( $^{\circ}\text{C}$ ) (after Defant, 1961).

Latitude	Equator	10°	20°	30°	40°	50°
Oceans	2.3	2.4	3.6	5.9	7.5	5.6

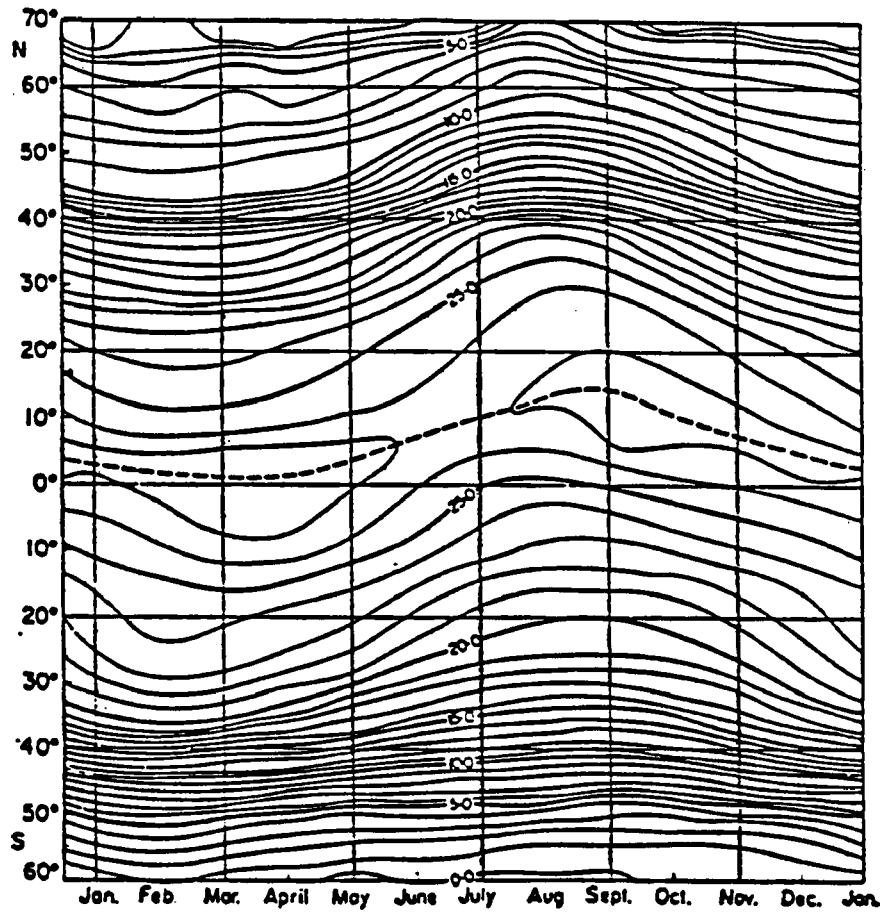


Figure 5.3: Isopleths of surface temperature in the Atlantic Ocean after Defant, 1961).

### **5.3 Annual/mean simulations.**

#### **5.3.1 Problems in running the annual model.**

The ocean model with the corresponding seasonal input mean conditions described in section 5.2, together with the exit condition prescribed in section 5.1, was used to simulate the annual mean properties of the ocean. The model results, however, do not compare as favorably with the observations as in the previous experiment. In fact, the equilibrium mixed layer depth predicted by this model after about 14.9 years of integration is exceeded 277 m which is much too deep according to the data of table 5.3. The equilibrium temperature, in contrast, is about 297.0 K which is a reasonable value compared to the seasonal results. These results suggest that the mixed layer is artificially heated in the annual model experiment. Examination of the model's equations suggest that there may be some problems when applying fixed annual/mean conditions. These difficulties lie in the fact that all input variables in this experiment are fixed in time in the annual study and that the response of the mixed layer properties is dependent on these inputs in a nonlinear manner. The decrease of mixed layer depth in the heat-dominated region depends on the variations of these inputs with time. Thus if the mixed layer model over predicts the mixed layer depth in the wind-dominated region, it can never bounce back to the correct annual value since the decrease of mixed layer depth in the heat-dominated region can never occur.

#### **5.3.2 A hybrid annual model for studying the mean ocean condition.**

The shortcoming of the model in studying the annual/mean condition of the ocean is an unfortunate consequences of the formulation of the mixed layer model. Further study of the model equations and annual results (see Appendix B) suggests that the incorporation of the solar seasonal cycle, which is one of the important forcing of the mixed layer model, into the annual/mean study may help to control the excess deepening of the mixed layer depth. We will refer to the method of imposing a seasonal cycle on the atmospheric inputs (which are to be predicted by the annual mean atmospheric model) as a hybrid model. This hybrid model basically contains the same structure as the previous annual

ocean model but also allows the solar radiation to vary annually according to equation 5.1. The final annual/mean states of the ocean model are then obtained by averaging over the annual cycle predicted by the model after equilibrium is reached.

The resultant mixed layer depth and surface temperature predicted from this hybrid model are shown in figure 5.4 and 5.5 for 10 years of integration. The evolution of these parameters is similar to that of the full seasonal model although the annual trends and fluctuations are somewhat smaller due to neglect of other forcings. After the tenth year of integration, the surface temperature oscillates between 294 and 297 K while the mixed layer depth fluctuates from 57 to 123 m. These give an annual/mean values of 296 K and 82 m respectively which agree better with the observations than the results of the previous annual/mean experiment. The most remarkable improvement of this hybrid model is in its ability to control excesses deepening of the mixed layer depth.

#### **5.4 Sensitivity experiments with the new ocean model.**

The sensitivity of the new hybrid ocean model to changes in the model parameters is now investigated. The effects of oceanic radiation extinction lengths, temperature lapse rates below the mixed layer, turbulent parameters, and atmospheric forcing, such as solar radiation, longwave radiation, atmospheric temperature and moisture inputs, on the model predictions are now considered.

##### **5.4.1 Oceanic radiation parameterization.**

In order to assess the sensitivity of the model to the oceanic radiation forcing, three experiments were conducted in which the values of the extinction lengths were changed. The setups of these experiments and results obtained are outlined at table 5.5. According to the results summarized in this table, the effect of altering radiation extinction values produces a significant influence on the thermal structure of the mixed layer. The greatest effects of these changes result from altering the visible extinction value while changes in the near infrared extinction value have very little effect on the mixed layer structure. A 25% decrease in both visible and near infrared extinction values or just visible extinction values alone can result in a 15% decrease in mixed layer depth. The change in surface

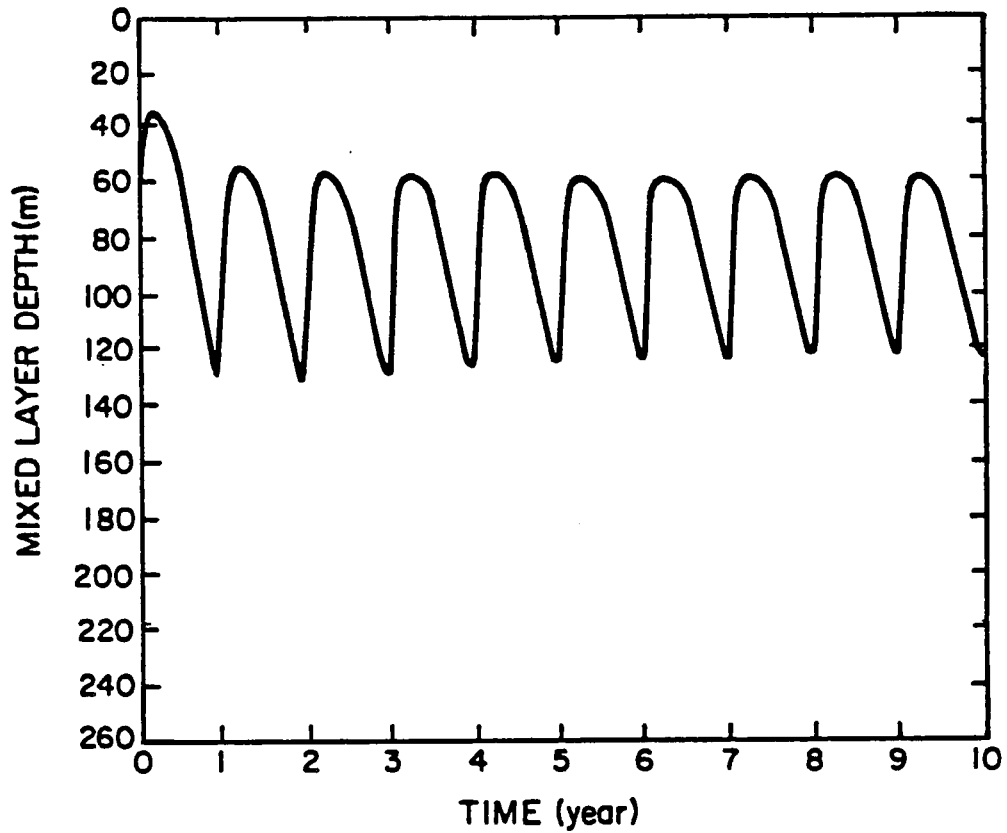


Figure 5.4: The approach to steady state mixed layer depth for hybrid annual/mean model.

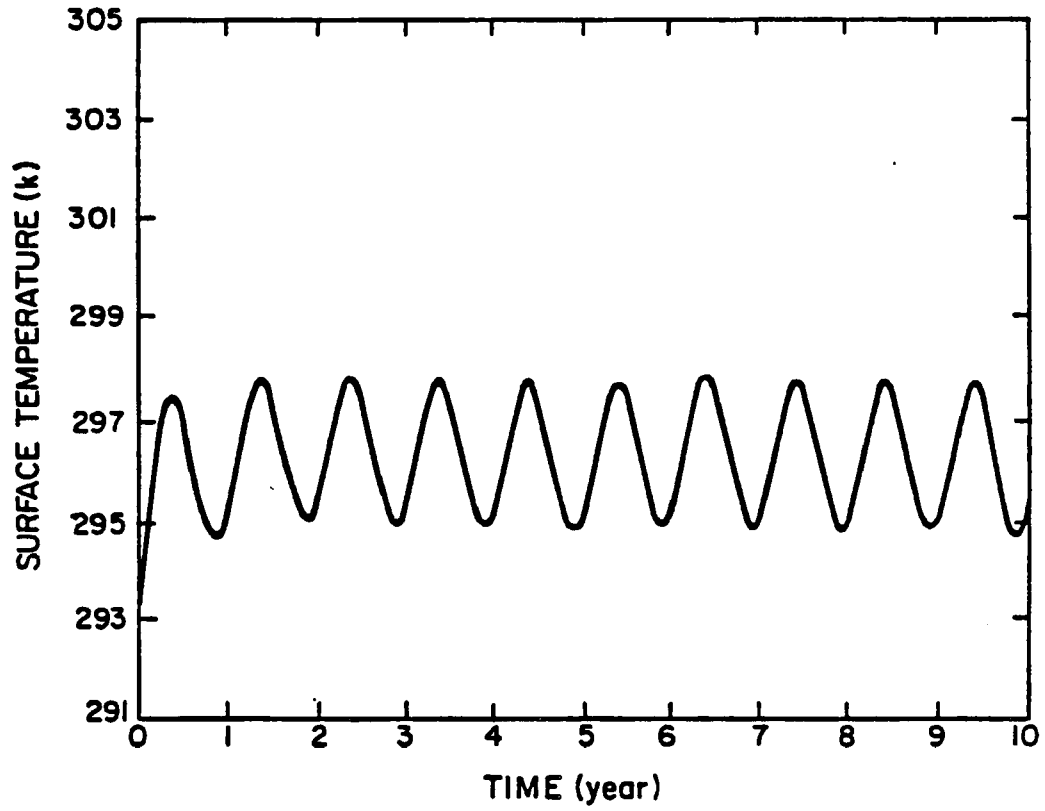


Figure 5.5: The approach to steady state solution for sea surface temperature for hybrid annual/mean model.

temperature, however, is negligible and can be view as constant. But the overall heat content of the upper ocean, which is related to the product of these two terms, is changed significantly. The decrease in mixed layer depth can be explained very simply. Radiation is absorbed over much shorter distances when the extinction is increased. This causes the upper ocean to heat up much faster, thus making it more difficult for turbulent eddies to overcome the large buoyancy force that results. The end effect is a much shallower mixed layer.

Table 5.5: Experiment setups and results for studying oceanic radiation extinction length.

Setup	Vis Extinction ( $m^{-1}$ )	Nir Extinction ( $m^{-1}$ )	$T_s$ (K)	H(m)
normal	20.0	1.00	296.3	81.8
1	20.0	0.75	296.3	81.8
2	15.0	1.00	296.4	69.8
3	15.0	0.75	296.4	69.8

The explanation given above is a very simple one and, in actual circumstances, the response of the ocean will be more complicated by other interactions such as by currents, and upwelling.

#### 5.4.2 Temperature gradient below the mixed layer

Another important parameter of the ocean model is the temperature gradient just below the mixed layer. This parameter determines the buoyancy forces that the mixed layer encounters as it expands downward. Three sets of experiments are performed and their results are summarized in table 5.6. As expected from intuition, the larger/smaller the temperature gradient, the harder/easier it is for the mixed layer to advance downward against the buoyancy force and the mixed layer thus becomes shallower/deeper than the normal condition as a result. According to the results contained in the table, a 50% increase/decrease in the temperature gradient will result in a 8%/17% decrease/increase in the mixed layer depth. The surface temperature however is less sensitive to the changes and it can be considered to be constant.

Table 5.6: Same as table 5.5 except for temperature gradient (lapse rate) below the mixed layer.

Setup	Lapse Rate(K/m)	$T_s$ (K)	H(m)
normal	0.02	296.3	81.8
1	0.01	296.5	95.9
2	0.03	296.2	75.3

#### 5.4.3 Turbulent parameterization

In this section, the influence of the turbulent parameterization on the mixed layer properties is examined. The available turbulent kinetic energy that are used for mixing in the ocean is some fraction of the atmospheric turbulent kinetic energy 10 m above the ocean surface. According to Turner (1969), Kato and Phillips (1969), and Denman (1973), this fraction ranges between 0.1% to 0.15%. Three experiments were run with different assumed values of this fraction and their results are shown in table 5.7. According to this table the results of the simulation are largely insensitive to the values of this fraction given above. Thus for all purpose, a constant of 0.12% will hereafter be used to represent mean conditions.

Table 5.7: Same as table 5.5 except for turbulent parameterization constant.

Setup	Constant(%)	$T_s$ (K)	H(m)
normal	0.12	296.3	81.8
1	0.10	296.3	81.8
2	0.15	296.3	81.9

#### 5.4.4 Solar and atmospheric radiation inputs

The effects of downward flux of solar and atmospheric radiation on the mixed layer simulations are also investigated. Table 5.8 and 5.9 show experiments results using different input fluxes. The effects of these two different forcings on the simulations are very similar. As the amount of input solar/atmospheric radiation increases, the mixed layer increases in both depth and temperature.

Table 5.8: Same as table 5.5 except for solar radiation input.

Setup	Vis(W/m <sup>2</sup> )	Nir(W/m <sup>2</sup> )	T <sub>s</sub> (K)	H(m)
normal	110.0	110.0	296.3	81.8
1	90.0	90.0	294.7	78.0
2	130.0	130.0	297.8	86.2

Table 5.9: Same as table 5.5 except for atmosphere radiation input.

Setup	Atm Rad(W/m <sup>2</sup> )	T <sub>s</sub> (K)	H(m)
normal	360.0	296.3	81.8
1	340.0	295.1	75.8
2	380.0	297.1	81.9

#### 5.4.5 Atmospheric wind speed, water vapor content, and temperature.

The surface wind speed is directly proportional to the amount of available turbulent kinetic energy for mixing. The effects of increasing wind speed on the mixed layer structure are shown in table 5.10. As expected, the mixed layer increases in depth with decreasing surface temperature as the wind speed increases since there is more available turbulent kinetic energy to mix the colder deep ocean water with the warm surface water.

The effects of atmospheric water vapor content and temperature are also demonstrated in table 5.11 and 5.12. Generally speaking, the effects of atmospheric-oceanic water vapor content differences are more important due to release of latent energy than are the sensible heat processes which are due to convection and conduction caused by atmospheric-oceanic temperature differences. In the former case, the effects are clearly shown by the increase/decrease in surface temperature as the atmospheric water vapor content increases/decreases. An increase/decrease in atmospheric water vapor content causes a downward/upward flux of latent heat transfer of energy at the air-sea interface, and therefore warms/cool the mixed layer/surface temperature. A similar explanation can be offered for the case of sensible heat transfer of energy between the two media although the change is much smaller. In both experiments, the mixed layer depth remains relatively unchanged.

Table 5.10: Same as table 5.5 except for atmosphere wind input.

Setup	Wind Speed(m/s)	T <sub>s</sub> (K)	H(m)
normal	1.0	296.3	81.8
1	2.0	295.2	82.4
2	3.0	294.3	83.8

Table 5.11: Same as table 5.5 except for atmosphere water vapor content input.

Setup	Water Vapor(g/Kg)	T <sub>s</sub> (K)	H(m)
normal	10.0	296.3	81.8
1	8.0	294.9	81.8
2	12.0	297.6	82.0

Table 5.12: Same as table 5.5 except for atmosphere temperature input.

Setup	Temperature(K)	T <sub>s</sub> (K)	H(m)
normal	292.9	296.3	81.8
1	289.9	296.1	81.8
2	295.9	296.4	81.9

#### 5.4.6 Summary of the new hybrid annual ocean model

In this section, the performance of the new hybrid ocean model is summarized.

1. It was found that any changes in the internal oceanic inputs have an effect only on the mixed layer depth of the model. The changes in mixed layer temperature caused by these inputs are relatively small. Thus the changes in oceanic characteristic can not affect the annual surface temperature.
2. On the other hand, the ocean model is more sensitive to changes in atmospheric inputs since they represent the main forcings by which the oceanic mixed layer is driven. Both the simulated mixed layer temperature and depth were shown to be significantly influenced by changes in these inputs.

## Chapter 6

### JOINT EQUILIBRIUM ATMOSPHERE-OCEAN MODEL

One of the most interesting and yet mysterious problems in the continuing research of the earth's climate is the role of ocean in maintaining the equilibrium state of climate system. As mentioned in Chapter 3 the ocean with its high heat capacity and large surface area is a very effective thermal energy reservoir. Therefore, it serves to reduce the contrast between the summer and winter seasons. Figure 6.1 shows the rate of heat storage for both the atmosphere and the ocean. The rate of oceanic heat storage is not only somewhat larger than that of the atmosphere but has a more complex meridional and seasonal structure. The ocean also transports relatively large amounts of heat towards the pole in spring and winter and towards the equator in summer as compared to its atmospheric counterpart (shown in Figure 6.2), thus they are at least as important as the atmosphere in fulfilling the heat transport requirements of the planetary heat balance. Many unsolved problems in the atmosphere (such as the El Nino Southern Oscillation (ENSO) and 30 to 40 oscillations in the tropical atmosphere) are ultimately tied to the ocean and to the nature of how the storage of energy in the ocean is returned to the atmosphere. In order to understand these phenomena, we must study these two systems as a coupled unit. Model studies of the coupled atmosphere and ocean have been attempted in the past particularly to study air-sea interaction processes among others. However, most tend to be very complex making it difficult to interpret the results and to isolate the role of individual elements of the climate system. Apart from these complexities, the results from such complex model also depend, to a large extent, on the assumption about the interaction processes that occur at the atmosphere-ocean interface. Therefore some investigators turned their efforts to simpler 1-D models (eg. Hunt and Wells, 1979) to

study these interactions. In this chapter, a simple 1-D coupled atmosphere-ocean model is formulated as a combination of the atmosphere and the ocean model introduced in the previous chapters to study the equilibrium temperature structure and heat storage of the ocean system and to investigate the sensitivity of the equilibrium state to a change in characteristics of the atmosphere. The coupled model described in the following section represents a first approximation to the complicated nonlinear interaction between the atmosphere and the ocean.

## **6.1 Basic considerations in connecting the two systems**

In order to connect the two systems together, there are a few basic problems that need to be addressed. These problems arise from the different structure and the behavior of the two separate models. It is important to keep these points in mind throughout this chapter since they are relevant to the way the coupling process is achieved and thus how results of this chapter might be interpreted.

### **6.1.1 The different structure of the two models**

It is important to understand that the atmosphere model and the ocean model introduced in the previous chapters are based on completely different physical laws. The atmospheric model is derived from principle of radiative transfer and includes a simple parameterization of dynamical effects of convection. The ocean model, on the other hand, is based on turbulent kinetic theory and on the conservation of thermal energy and treats radiation by way of a simple parameterization. Even though the two models work very well independently, there is no guarantee that the coupled atmosphere-ocean model will perform properly. Therefore special care was adopted in designing the coupling of these two models.

### **6.1.2 The models' behavior**

As discussed in Chapter 4, the ocean model is incapable of simulating a realistic annual condition without an annual cycle in surface radiation input. The atmospheric model, on the other hand, is constructed to simulate only the annual/mean condition. An

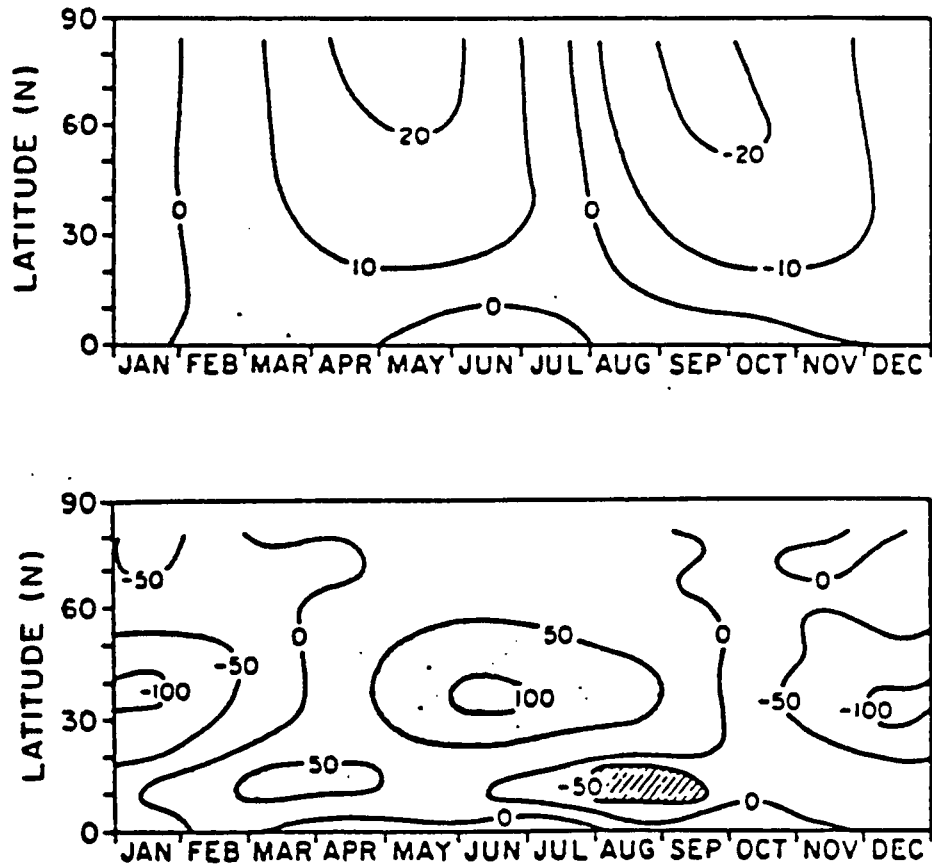


Figure 6.1: Rate of heat storage ( $wm^{-2}$ ) in the atmosphere (top) based on radiosonde data and in the ocean (bottom) based on hydrographic stations and BT data. (Redrawn from Oort and Vonder Haar, 1976.)

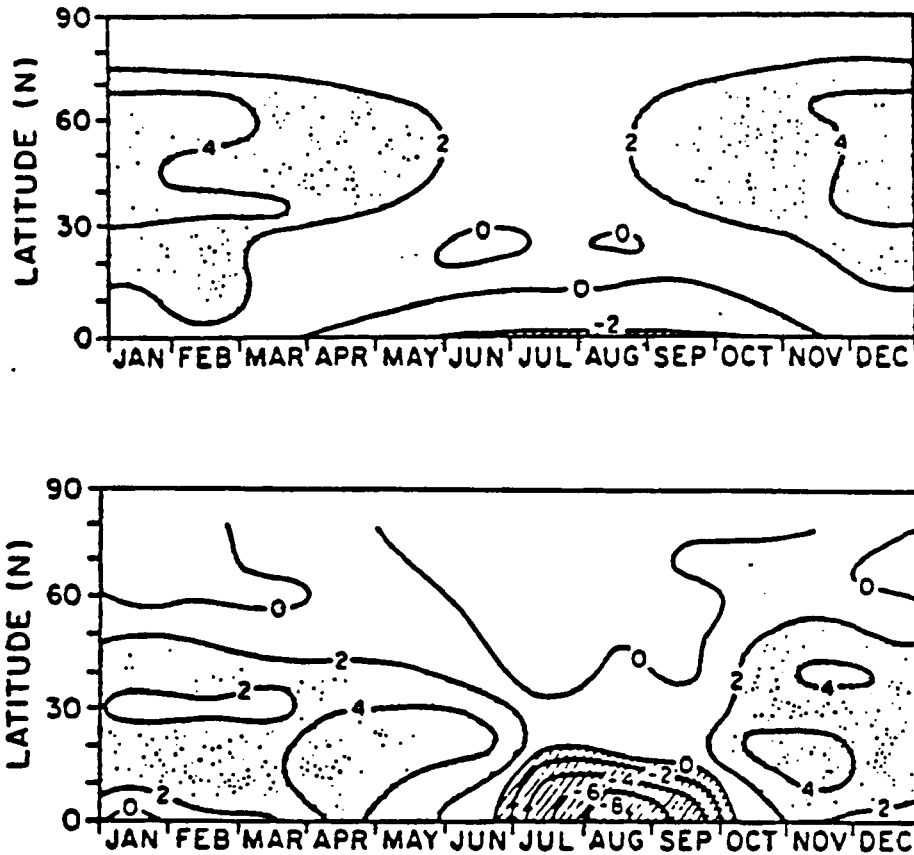


Figure 6.2: Northward flux of energy ( $10^{15}W$ ) in the atmosphere based on radiosonde data and in the ocean computed as a residual in the earth's heat balance. (Redrawn from Oort and Vonder Haar, 1976.)

introduction of the annual cycle in solar radiation input to the atmospheric model is not feasible since the model cannot reach a complete equilibrium state.

An even more serious problem is that the ocean model does not resolve the temperature behavior of the deep ocean (which is believed to be governed by large scale dynamical processes). A pseudo energy source may be added to the system indirectly from below the mixed layer due to neglect of this deep ocean structure. Thus some sort of simple parameterization scheme is required to insure energy conservation in the final equilibrium state of the coupled atmosphere-ocean model.

The mixed layer model did not include sea ice, thus we are also limited in to applications of the model to problems that have temperature responses above freezing.

## **6.2 Theory and assumptions of the coupled system**

The methods for coupling the atmosphere and the ocean model together are now discussed in this section. Since we are interested in studying the equilibrium state of the system and its sensitivities to different external changes, a further simplification is presented to solve some of the problems outlined in the last section (i.e., coupling the annual/mean atmosphere model with an annual cycle ocean model). Two simple parameterization schemes will be introduced to insure energy conservation in the equilibrium coupled atmosphere-ocean system. Finally, a useful new parameter, heat content per unit area, is introduced and will be used to examine the response of the coupled atmosphere-ocean model.

### **6.2.1 Coupling methods**

This study adopts the simple approach of Hunt and Wells (1979) who coupled an atmosphere model to an ocean surface by specifying a fixed anemometer level wind speed appropriated to ocean condition. This permitted sensible and latent heat fluxes between the ocean and the atmosphere to be computed via the bulk aerodynamic formulae introduced in Chapter 3. These fluxes were then assumed to be totally assimilated into the lowest atmospheric model and subsequently were redistributed by the convective parameterization. The ocean model was coupled to the atmosphere in a similar fashion by

using the the surface radiation, temperature, and moisture quantities obtained from the atmospheric model.

### **6.2.2 Equilibrium state of the coupled system**

#### **Basic consideration of equilibrium state**

According to the definition, the equilibrium state of any system occurs when the energy received by the system matches to the energy released by the same system. For the 1-D coupled atmosphere-ocean system, there are only two possible boundaries in which energy either enter into or escape from the system. These boundaries are, of course, the top of the atmosphere and the base of the ocean. Since there are no theoretical energy source/sinks at the bottom of the ocean, the only energy source/sink of the entire system must be located at the top of the atmosphere. At equilibrium, the net incoming solar radiation into the coupled system must be balanced by the net outgoing longwave radiation released by the same system at the top of the atmosphere.

#### **Introduction of assumption**

Since the direct coupling of the annual/mean atmospheric model and the annual cycle ocean model is impossible to achieve, we are therefore forced to take an alternative approach to obtain the equilibrium state of the coupled annual/mean atmosphere-ocean model. This approach assumes that the equilibrium atmosphere obtained from the surface-atmosphere model remains unchanged in the final equilibrium state of the coupled atmosphere-ocean system. This equilibrium assumption is valid as long as the following requirements are met:

1. the lower energy boundary condition of both system remain unchanged (i.e., no energy input at the base of the system),
2. surface albedo remains unchanged at the interface of the coupled atmosphere-ocean system as compared to the surface-atmosphere system. This requirement ensures the conservation of the net incoming solar radiation at the top of the atmosphere model for the surface-atmosphere model or the coupled atmosphere-ocean model,

3. the net downward flux of radiation at the air-sea interface equals the net upward flux of energy, including radiation, sensible and latent heat, at the interface.

Using these assumptions, a further simplification can be made in obtaining the equilibrium state of the coupled atmosphere-ocean model. Basically, these assumptions allow decoupling of the atmosphere-ocean model in determining the final equilibrium states. Thus the equilibrium state of the atmosphere is deduced independently from the ocean system. Once the equilibrium state of the atmosphere is obtained, the equilibrium state of the ocean can then be calculated by using the equilibrium surface forcings from the atmospheric model. The final equilibrium condition of the coupled atmosphere-ocean system is then obtained by combining the two equilibrium profiles together.

### **6.2.3 Energy conservation parameterization**

#### **Methodology**

In order to prevent the calculation of an unrealistic oceanic equilibrium profile due to unresolved deep ocean structure such as an equilibrium oceanic surface temperature higher than the equilibrium surface temperature obtained from the atmospheric model, the following parameterizations are employed. These parameterizations force energy conservation at the top of the equilibrium coupled model by adjusting the oceanic surface temperature back to the surface temperature predicted by the equilibrium atmospheric model. If the oceanic surface temperature is the same as the atmospheric surface temperature, then no adjustment is made.

#### **Theoretical consideration**

The basis for the adjustments is analogous to that of convective adjustment of the atmosphere. The excess energy in the mixed layer is a result of the pseudo energy inputs into the mixed layer from the deep ocean. In order to cancel this pseudo source, the deep oceanic temperature structure or the mixed layer structure must be rearranged in such a way that this pseudo source is adjusted back to zero. This is done either through an adjustment in mixed layer depth or in the entire mixed layer temperature until the

oceanic surface temperature adjusts back to the same value as predicted by the equilibrium atmospheric model. Even though the product of these two methods are the same, they rely on a completely different interpretation of the location of the pseudo energy.

A. Parameterization 1: Mixed layer height adjustment.

This adjustment involved redefining the mixed layer depth through the following formula.

$$\int_{H_{old}}^0 T_{old} dz = \int_{H_{new}}^0 T_{new} dz \quad (6.1)$$

where  $T_{old}$ ,  $H_{old}$ ,  $T_{new}$ , and  $H_{new}$  are the non-adjusted mixed layer temperature and depth and the adjusted mixed layer temperature and depth, respectively. This adjustment assumes that the pseudo energy is being stored in the mixed layer and therefore must be removed from the mixed layer via an energy parameterization. A pictorial representation of this approach is provided in Figure 6.3. The two shaded areas represent an equal partition of energy.

B. Parameterization 2: Mixed layer temperature adjustment.

An alternative adjustment can be used to replace the above method. This method involved moving the entire mixed layer temperature back to match the equilibrium atmosphere surface temperature. This adjustment assume the pseudo energy is being stored in the deep ocean, and therefore must be removed from the deep ocean. This method is pictorial represented in Figure 6.4 where the two shaded areas again represent equal partition of energy.

#### 6.2.4 Definition of heat storage

One of the useful parameter in differentiating effects of the 1-D coupled atmosphere-ocean model to specific external changes is the global oceanic heat storage per unit area for the mixed layer. It is defined as the amount of stored energy per unit area. It is mathematically represented for a global average mixed layer ocean as

$$C = \int_H^0 \rho_o C_{p,w} T dz \simeq \rho_o C_{p,w} T_s H \quad (6.2)$$

where  $\rho_o$  is the density of the mixed layer,  $C_{p,w}$  is the specific heat of water at constant pressure,  $T_s$  is the temperature of the mixed layer, and  $H$  is the mixed layer depth. The

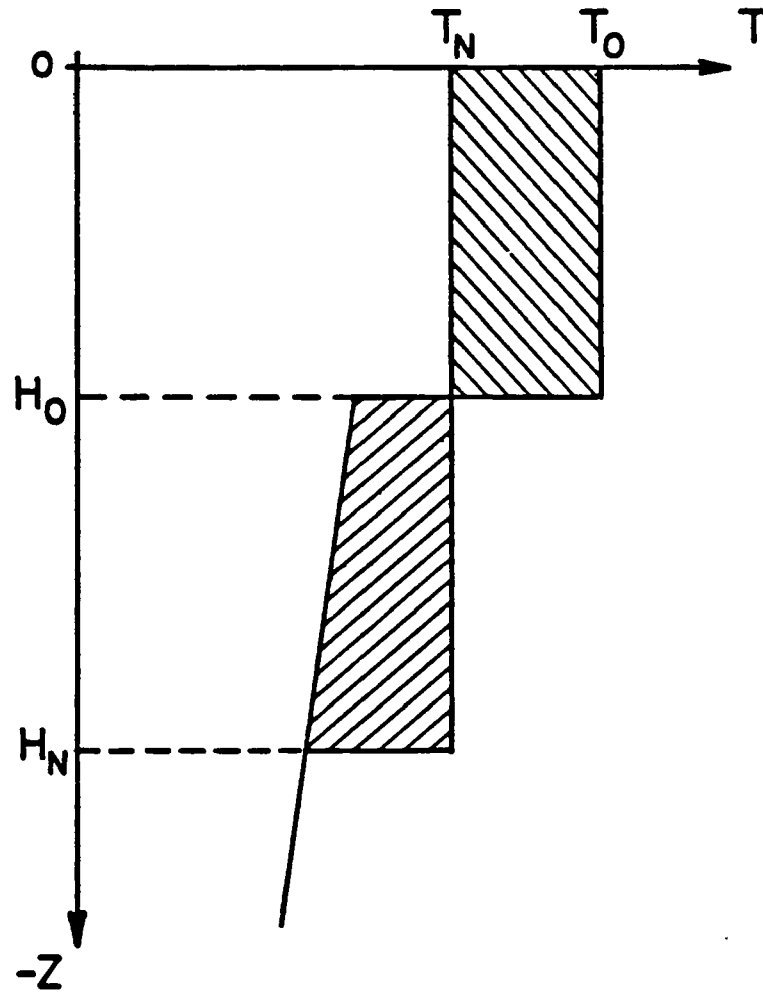


Figure 6.3: Schematic representation of energy adjustment process (method 1).



difference in this storage term between the clear sky and other cases indicates the amount of change of energy in the ocean system that could be associated with those specific external changes. These differences are defined by

$$\Delta C_{case} = \rho_o C_{p,w} \left[ (T_s H)_{case} - (T_s H)_{clear\ sky} \right] \quad (6.3)$$

### 6.3 Performance of the coupled model

#### 6.3.1 Input values and method of computations

Unless specified otherwise, we will adopt the set of atmospheric equilibrium results from Chapter 4 as the surface inputs to the ocean model. The rest of the initial inputs to the ocean model remain the same as those described in Chapter 5 with the exception that the initial mixed layer depth is set to be 80 m. The hybrid annual/mean ocean model is then integrated forward in time for ten years. The model results at the tenth year of integration are then averaged to obtain the equilibrium annual/mean results. If the model oceanic surface temperature is different from the model atmospheric surface temperature, the energy parameterization is used to obtain the final temperature profile of the coupled system. In the following analysis, only the model equilibrium ocean structures are shown since the equilibrium atmospheric profiles have already been presented in Chapter 4.

#### 6.3.2 Clear sky condition

Table 6.1 lists the results of equilibrium calculations for clear sky conditions. The mixed layer temperature, depths and heat storage are presented for the two different parameterization schemes discussed above. The mixed layer structures are very similar and significant differences between the equilibrium states were only found in the deep ocean. The mixed layer temperatures are the same value as the atmospheric model. The equilibrium mixed layer depth varies from 80 to 81 m for the two different parameterizations. The absolute difference in heat content is about  $1 \times 10^9 \text{ J/m}^2$ .

#### 6.3.3 Sensitivity studies with $CO_2$ , solar constant, and cloud

Table 6.1: Equilibrium ocean model under clear sky condition.

	$T(K)$	$H(m)$	$C \times 10^{11}(J/m^2)$
Method 1	293.61	81.10	1.0043805
Method 2	293.61	80.28	0.9942252

### Carbon dioxide

The sensitivities of the model equilibrium to different assumed values of  $CO_2$  content are illustrated in Table 6.2 and 6.3. According to these results, the changes in  $CO_2$  have a very small effect on the mixed layer depth. The equilibrium values remain relatively constant and the changes are within 0.25 m. This indicates that most of the energy involved in these processes are used in heating/cooling the entire ocean. The amount of energy involved in these processes can be illustrated by examining the changes in heat content of the mixed layer. As shown in the same table, decreasing/increasing  $CO_2$  content will decrease/increase the equilibrium heat content of the mixed layer.

Table 6.2: Same as table 6.1 except for various  $CO_2$  content using Method 1.

Case	$T(K)$	$H(m)$	$C \times 10^{11}(J/m^2)$	$\Delta C \times 10^8(J/m^2)$
1/2 $CO_2$	291.59	81.04	0.9967325	-7.64797
normal	293.61	81.10	1.0043805	-
2x $CO_2$	295.68	81.21	1.0128334	8.45290
3x $CO_2$	296.58	81.27	1.0166669	42.2864

Table 6.3: Same as table 6.1 except for various  $CO_2$  content using Method 2.

Case	$T(K)$	$H(m)$	$C \times 10^{11}(J/m^2)$	$\Delta C \times 10^8(J/m^2)$
1/2 $CO_2$	291.59	80.22	0.9866471	-7.57811
normal	293.61	80.28	0.9942252	-
2x $CO_2$	295.68	80.40	1.0027313	8.50606
3x $CO_2$	296.58	80.45	1.0064089	12.1837

### Solar inputs

For the solar inputs, the equilibrium model results are completely different than those of the carbon dioxide changes. For the four solar inputs values tested in this section, the

mixed layer depth shown in table 6.4 and 6.5, has varied more than 8 m. The higher/lower the solar inputs, the deeper/shallow the mixed layer will become. The largest change in mixed layer heat content are found in these group of tests.

Table 6.4: Same as table 6.1 except for various solar input using Method 1.

Case	$T(K)$	$H(m)$	$C \times 10^{11}(J/m^2)$	$\Delta C \times 10^8(J/m^2)$
420.00	309.60	88.84	1.1601552	155.775
385.00	302.90	84.29	1.0769162	72.5357
normal	293.61	81.10	1.0043805	-
315.00	283.64	79.08	0.9461080	-58.2725

Table 6.5: Same as table 6.1 except for various solar input using Method 2.

Case	$T(K)$	$H(m)$	$C \times 10^{11}(J/m^2)$	$\Delta C \times 10^8(J/m^2)$
420.00	309.60	88.35	1.1537563	159.531
385.00	302.90	83.57	1.0677172	73.4920
normal	293.61	80.28	0.9942252	-
315.00	283.64	78.44	0.9384511	-55.7742

## Clouds

The equilibrium model inputs and results for varies type of cloud condition are shown in table 6.6, 6.7 and 6.8. The present of low and middle cloud tends to cause a decrease in the heat content of the mixed layer by decrease both the mixed layer temperature and depth. Such decreases are ultimately tied to the significant decrease of total net downward flux of energy at the surface. High thin cloud, however has a opposite effect. It increases the heat content of the mixed layer. This rise in the mixed layer heat content is largely due to the increases in the mixed layer temperature which overcompensates the decreases in the mixed layer depth caused by decreasing in downward surface flux of solar radiation. The increase in this mixed layer temperature can also be explained by the increasing in total net downward flux of radiation.

Table 6.6: Cloud parameters and surface downward flux of radiation ( $W/m^2$ ) for different cloud studies.

Type	Position (Km)	$W(g/m^2)$	LW	SW	Total	cld-clr
Clear	-	0.0	356.48	203.29	559.77	0.00
Low	0.77-1.25	14.0	339.55	150.47	490.02	-69.75
Middle	3.45-4.47	14.0	356.69	148.01	504.70	-55.07
High	6.96-8.49	5.0	421.75	190.02	611.77	52.00

Table 6.7: Same as table 6.1 except for various cloud inputs using Method 1.

Case	$T(K)$	$H(m)$	$C \times 10^{11}(J/m^2)$	$\Delta C \times 10^8(J/m^2)$
normal	293.61	81.10	1.0043805	-
low	283.42	80.19	0.9586438	-45.7367
middle	289.26	79.39	0.9686363	-35.7442
high	298.79	80.13	1.0098754	5.49486

Table 6.8: Same as table 6.1 except for various cloud inputs using Method 2.

Case	$T(K)$	$H(m)$	$C \times 10^{11}(J/m^2)$	$\Delta C \times 10^8(J/m^2)$
normal	293.61	80.28	0.9942252	-
low	283.42	78.83	0.9423855	-51.8397
middle	289.26	78.67	0.9598516	-34.3736
high	298.79	79.41	1.0008012	6.57596

#### 6.4 Summary of the equilibrium coupled model sensitivities and their climatic implications

The equilibrium coupled atmosphere-ocean model was formulated in this chapter using a simple coupling process and energy parameterization. An equilibrium assumption is made to allow first order examination of the entire system. The resultant equilibrium model is used to test the sensitivity of the coupled atmosphere-ocean system to different external forcings. It is found that:

1. the change in  $CO_2$  content has very little effect in altering the mixed layer depth, but has a distinct effect on the mixed layer temperature,

2. the mixed layer depth, however, is more sensitive to change in solar input. The energy for this case is used to alter the mixed layer depth and warm or cool the entire ocean,
3. the mixed layer depth and temperature are both sensitivity to cloud forcing. The mixed layer depth decreases in the presence of clouds due to the decrease in the downward shortwave flux whereas the mixed layer temperature behavior depends more on the total downward net flux of energy (i.e., the combination of the shortwave and longwave fluxes) at the surface,
4. the model sensitivity is much the same for the two energy parameterization schemes, and either one method can be used to assess the change in mixed layer heat content due to different external forcings,
5. it seems that the mixed layer depth is much more sensitive to change in surface solar radiation inputs caused by changes in cloud forcing or solar inputs at the top of the atmosphere model while the change in surface longwave radiation inputs caused by changes in  $CO_2$  content is not as important in altering the mixed layer depth,
6. the changes in both mixed layer depth and temperature can have important significance in the biological cycle (i.e., production of phytoplankton, the largest biomass community in the marine environment) of the ocean, which in term can feed back to changing the internal characteristic ( such as the solar attenuation) of the ocean system,
7. the changes in internal oceanic features, such as extinction length, can significantly alter the mixed layer depth according to the results of the early chapters and thus can feedback to the biological cycle and further alter the structure of the ocean,
8. the feedback process between the the oceanic extinction length, the biological cycle, and the other components of the climate system (i.e., the atmosphere) may be possible and the outcome of this process in term of climatic changes need to be further studied using more advance models, and

9. the amount of energy associated with the change in equilibrium heat content of the ocean from different external forcings may be important in explaining some of the transient features of our climate.

## Chapter 7

### SUMMARY, CONCLUSION, AND RECOMMENDATIONS

Natural climatic variations have played an important role in man's history (eg, Claiborne, 1974). The influence of anthropogenic materials and technologies on the climate system have further complicated the comprehension of climatic changes. The usual approach in studying the climate system and its response to given changes in parameters is to employ some form of climate model. These models are usually based on the mathematical description of the atmospheric circulation and the physical processes of importance (such as radiation). Climate models range from relatively simple 1-D models to very complex mathematical systems that contain the full 3-D behavior of the entire system and are known as General Circulation Models (GCM).

Simple 1-D models are used frequently in climate studies since they are able to isolate some of the important physical processes that determine the broad features of the climate. Extensive climate studies using this type of model have uncovered many of the characteristics and behaviors of the climate system that are not greatly different from those determined from more complex climate models. However, these classic 1-D studies are somewhat incomplete, as are many more elaborate models, due to the omission of the effect of the ocean system.

The inclusion of the effects of an ocean in a climate model is not a trivial task since there are many unsolved problems that first needed to be resolved (the complete understanding of the deep ocean structure for example). Early 3-D coupled atmosphere-ocean models indicated that the ocean played an important role in the determining of the atmospheric circulation. However, these models had a few setbacks. Besides having problem in reaching a true "climatic equilibrium", these models were just as complex as

the real system and it is difficult to determine the significance of the individual processes in these models. Therefore there is a need to construct simpler models to examine the structure of a simple equilibrium coupled atmosphere-ocean system and its sensitivity to possible imposed external changes.

The objectives of this study were first to construct a set of simple models to simulate the 1-D structure for both the atmosphere and the ocean separately. These models were tested to insure proper performance and also to realize their limitations. These two model were then coupled together to examine the equilibrium structure of the ocean-atmosphere system under annual/mean conditions and its sensitivity to changes in  $CO_2$  content, solar inputs, and cloud forcings. These objectives were achieved and their results were summarized in the following sections.

### 7.1 1-D convective-radiative atmosphere model

The construction of this 1-D atmosphere model was based on the equation of radiative transfer and the incorporation of dynamical convection using a parameterization scheme. The radiative temperature change in the atmosphere is caused by an imbalance of radiative fluxes in the atmosphere. This imbalance resulted from differences in optical properties of the atmospheric constituents. In this study, these radiative fluxes were calculated using the equation of radiative transfer. Three radiative dominant gases ( $CO_2$ ,  $O_3$ , and  $H_2O$ ) were modeled for the clear sky atmosphere in addition to Rayleigh scattering by gas molecules and small aerosols. The effect of cloud were also modeled by using an simple technique.

In the longwave radiative transfer model, scattering was neglected and the radiative fluxes due to different gases were calculated using the broadband emissivity approach with pressure corrected optical paths for each of the gases. Cloud absorption in the longwave was parameterized using a simple method which related the cloud emissivity to cloud liquid/ice water content. For the shortwave model, the radiative fluxes were calculated using a 2 band 2-stream model. These two separate bands covered the visible and the near infrared regions and the shortwave optical properties of the different gases and associated Rayleigh scatter were generated using a parameterization technique. Cloud

was also modeled by relating its shortwave optical properties with the mean solar zenith angle and cloud liquid/ice water content. Finally the effect of convection was incorporated into the radiation model using convective parameterization for better simulation of the atmospheric temperature structure in the troposphere.

## **7.2 The performance of the model atmosphere**

The behavior of the 1-D convective radiative atmosphere model was found to be very similar to many other early studies and seems capable of simulating the global annual/mean structure of the atmosphere. The following is the summary of the performance of the model:

1. The pure radiative atmospheric model tended to produce a super-adiabatic lapse rate at the troposphere indicating the importance of convective processes in this region of the atmosphere. The radiative thermal relaxation time of the model was found to be about 1 year;
2. the convective radiative atmosphere model gave a better simulated temperature structure since the excess amount of energy at the surface was allowed to be transferred to the free atmosphere through a parameterization of dynamical convection;
3. the convective radiative thermal relaxation time for a fixed relative humidity model was found to be 70 percent longer than that for a fixed absolute humidity model due to feedback process between temperature and moisture;
4. model sensitivity to solar energy inputs suggested an asymmetric response in which a decrease in solar inputs might cause a larger impact on the earth's climate than would an equal increase in solar input;
5. the increase/decrease of  $CO_2$  content of the atmosphere tended to warm/cool the earth's surface while the same forcing produced an opposite effect in the stratosphere;
6. the effect of surface albedo was maximum near the earth surface and decreased with height, the larger the surface albedo, the colder the surface temperature;

7. low and middle clouds cooled the earth surface by reducing the net surface downward energy flux. Thin high cloud, on the other hand, tended to give surface warming by significantly increasing the downward longwave flux at the surface and overcompensating the decrease in downward surface shortwave flux. These results depend on the assumed value of the cloud liquid/ice water path, and
8. cloud was also found to decouple the surface and the planetary radiative budget.

### 7.3 Overview of the mixed layer ocean model

This study only modeled the upper mixed layer of the ocean. The deep ocean was viewed as a thermal reservoir. The reason for this treatment was due to the lack of a suitable theory about the deep ocean structure.

The oceanic mixed layer model was based on the conservation of thermal energy and turbulent kinetic energy theory. The model's equations, derived from these two laws, were used to calculate the temperature structure of the mixed layer ocean during two different periods of the year. The model treated the surface transfer of sensible and latent energy by a simple parameterization scheme using a bulk aerodynamic theory based on a drag coefficient and some specific sea surface wind speed. The mean available turbulent kinetic energy, which drove the mixing processes of the ocean mixed layer, was taken to be proportional to the surface input of turbulent kinetic energy from the atmosphere, which was related to the surface wind speed. The surface inputs of solar radiation were divided in two separate bands, the visible, and the near infrared to be consistent with the treatment of solar radiation in the atmosphere. The extinction of the solar radiation with depth in the ocean was modeled using a simple Beer law's type of formulation with a e-folding length for radiation appropriate to the two solar bands. The upward flux of surface longwave radiation was modeled using blackbody emission at the sea surface temperature.

### 7.4 Ocean model behavior

Although the mixed layer model worked exceptionally well in simulating the annual cycle of the mixed layer, the simulation of the annual/mean condition was a disappointment with a predicted equilibrium mixed layer depth in excess of over 270 m. Further

analysis suggested that a hybrid annual/mean model with incorporation of a surface solar radiation annual cycle might be useful in correcting such problem. The behavior of this hybrid annual/mean model is summarized as follows:

1. The change in extinction value in the visible band had the most dominate effect in altering the mixed layer depth. The effect on the mixed layer temperature, however, was very small;
2. the change in temperature structure below the mixed layer influenced the predicted mixed layer depth, but the surface temperature remained unchanged;
3. the effect of mean available kinetic turbulent energy on the mixed layer structure was small and can be neglected;
4. the change in solar and atmospheric energy inputs into the ocean can affect both the mixed layer depth and the temperature;
5. the surface wind speed had a negative effect on the surface temperature, the higher the wind speed, the lower the temperature of the surface;
6. the effects of atmospheric moisture were found to be more significant than those of atmospheric temperature due to the large amounts of energy associated with latent heating;
7. the change in internal characteristics of the ocean (such as extinction length, temperature lapse rate below the mixed layer) only affected the mixed layer depth with the surface temperature remaining unchanged;
8. however, significant changes in both surface temperature and mixed layer depth resulted from changes in surface atmospheric inputs.

#### **7.5 Conclusions drawn from the joint equilibrium atmosphere-ocean model**

Even though there were many problems associated with coupling the model atmosphere and ocean together, this study attempted to examine the issues of the approach to

an equilibrium of a coupled model and its sensitivity to external forcings. Some assumptions were introduced in order to achieve this objective. These assumptions were based on definition of energy conservation and the state of equilibrium. A new variable, heat content, was introduced to provide a more quantitative discussion of the coupled model results. The following summarizes the equilibrium assumptions and new results of the atmosphere-ocean model:

1. The equilibrium thermal structure of the atmospheric part of the coupled atmosphere-ocean model remained unchanged from those provided by the atmosphere model alone;
2. it was found that the change in  $CO_2$  content of the atmosphere had a very little effect on the oceanic mixed layer depth. The change was basically associated with altering the oceanic mixed layer temperature;
3. the oceanic mixed layer depth and temperature, on the other hand, were sensitive to change in solar energy inputs at top of the atmosphere. As the solar energy increases, the extra radiation was used to heat up the ocean and also to push the oceanic mixed layer downward against the natural buoyancy forces of the ocean, and
4. cloud can also alter the oceanic mixed layer depth and temperature by changing the partitions of surface inputs radiation budget. The present of cloud had a negative effect on the oceanic mixed layer depth since it decreased the surface inputs of solar radiation, which was the primary source of energy for the ocean system. The oceanic mixed layer temperature, however, depended on the surface inputs of net radiation (solar plus infrared). It increased/decreased as the net surface radiation increases/decreases.

#### **7.6 Recommendation for possible future research**

The results obtained from this study, using a simple coupled model, are limited due to neglect of many physical important processes in the ocean system. However, it does give first order examination of the equilibrium that is reached by a coupled atmosphere-ocean model. It identifies that

1.  $CO_2$  content of the atmosphere,
2. solar energy inputs at the top of the atmosphere, and
3. cloud forcings

are very important parameters for the equilibrium coupled model. They alter both the mixed layer depth and temperature of the ocean system.

#### 7.6.1 Possible future research topics

The following is a list of some possible future research areas that follow from the present study:

1. The change in the oceanic mixed layer depth and temperature are known to have a significant effect in the biological cycle of the ocean, which in turn can change the internal characteristic (eg, oceanic radiation extinction length) of the mixed layer. Therefore, possible feedback processes between  $CO_2$ , solar inputs, cloud forcing, the biological cycle in the mixed layer ocean, and the internal characteristic of the mixed layer cannot be overlooked and needs further study.
2. The deep ocean system utilizes only the surface inputs of solar radiation. The infrared radiation, on the other hand, is completely absorbed by the upper few centimeters of the mixed layer. The full understanding of how the deep ocean system is influenced by the surface inputs of radiation and how this energy is feeds back into the atmospheric circulation is intriguing.
3. Cloud can significantly alter the partition of the surface radiation budget between the solar and infrared radiation, therefore it can have a large impact on the energy budget of the deep ocean. This effect demands some considerable future research.
4. The amount of energy released from or absorbed by the ocean can be significant in terms of transient features in the short term climate. The full extent of how these short lived systems affect the short term climate is not known and future research on this matter is necessary.

5. The effects of oceanic mixed layer's annual cycle in stabilizing the coupled atmosphere-ocean system must also be studied in the future to determine its actual effect on the whole system.

#### **7.6.2 Suggestions on future modeling and observational approach to the coupled atmosphere-ocean system**

Many refinements of the present coupled model in this thesis are desirable. These include the formulation of a true annual/mean ocean model based on a better theory. Explicit representation of the evolution of the deep ocean temperature profile is also necessary to examine long term effects of these forcings on climate. Sea ice and salinity are also important parameters that need to be included into a future model. A better parameterization scheme for solar heating in the ocean model is also desirable. Once such a model is established, it can possibly be used as a basis for the development of some form of simple parameterization for the treatment of the mixed layer in more advanced models (such as General Circulation Models). Meanwhile, there is a definite need for more observational studies of the ocean system to provide better global coverage which can be used for constructing and testing more refined theories of the ocean system.

## REFERENCE

- Arhrens, C.D., 1982: *Meteorology Today: An introduction to weather, climate and the environment. West Publishing Company.*
- Chou, M.-D., and A.Arking, 1980: Computation of infrared cooling rates in the water vapor bands. *J. Atmos. Sci.*, **37**, 855-867.
- Claiborne, R., 1970: *Climate, man, and history. Redwood Press.*
- Curtis, A. R., 1952: Discussion of "A statistical model for water vapour absorption" by R. M. Goody. *Quart. J. Roy. Meteor. Soc.*, **78**, 638.
- Defant, A., 1961: *Physical Oceanography, Vol.2. Pergamon Press.*
- Denman, K. L., 1973: A time-dependent model of the upper ocean. *J. Phys. Oceanogr.*, **3**, 173-184.
- Godson, W. L., 1954: Spectral models and the properties of transmission functions. *Proc. Toronto Meteor. Conf., 1953, Roy. Meteor. Soc., Berkshire, UK.* 35-42.
- Goody, R. M., 1964: *Atmospheric radiation, Vol.1., Theoretical basis. Clarendon Press, Oxford.*
- Grant, I., and G. E. Hunt, 1968: Solution of radiative transfer problems in planetary atmosphere. *Icarus*, **9**, 526-534.
- Hunt, G. E., and N. C. Well, 1979: Assessment of the possible future climatic impact of carbon dioxide increases based on a coupled one-dimensional atmospheric-oceanic model. *J. Geophys. Res.*, **84**, 787-791.
- Kato, H., and O. M. Phillips, 1969: On the penetration of a turbulent layer into a stratified fluid. *J. Fluid Mech.*, **37**, 643-655.
- Kraus, E. B., and J. S. Turner, 1967: A one-dimensional model of the seasonal thermocline: II. The general theory and its consequences. *Tellus*, **19**, 98-106.
- Lacis, A. A., and J. E. Hansen, 1974: A parameterization for the absorption of solar radiation in the earth's atmosphere. *J. Atmos. Sci.*, **31**, 118-133.
- Liou, K.-N., 1980: *Introduction to atmospheric radiation. Academic Press.*

- , 1986: Influence of cirrus clouds on weather and climate processes: A global perspective. *Mon. Wea. Rev.*, **114**, 1167-1199.
- Manabe, S., 1971: Estimate of future change of climate due to the increase of carbon dioxide concentration in the air, in *Man's Impact on Climate*, edited by W. H. Matthews, W. W. Kellogg, and G. D. Robinson. *MIT Press*, P256.
- , and K. Bryan, 1969: Climate calculation with a combined ocean atmosphere model. *J. Atmos. Sci.*, **26**, 786-789.
- , and F. Moller, 1961: On the radiative equilibrium and heat balance of the atmosphere. *Mon. Wea. Rev.*, **89**, 503-532.
- , and R. F. Strickler, 1964: Thermal equilibrium of the atmosphere with a convective adjustment. *J. Atmos. Sci.*, **21**, 361-385.
- , and R. T. Wetherald, 1967: Thermal equilibrium of the atmosphere with a given distribution of relative humidity. *J. Atmos. Sci.*, **24**, 241-259.
- McClatchey, R. A., and J. E. A. Selby, 1972: Atmospheric transmittance, 7-30  $\mu\text{m}$ : Attenuation of  $\text{CO}_2$  laser radiation. *Environ. Res. Pap. No. 419, AFCRL-72-0611*.
- , R. W. Fenn, J. E. A. Selby, F. E. Volz, and J. S. Garing, 1973: Optical properties of the atmosphere. *Environ. Res. Pap. No. 354, AFCRL-71-0279*.
- Oort, A. H., and T. H. Vonder Harr, 1976: On the observed annual cycle in the ocean-atmosphere heat balance over the Northern Hemisphere. *J. Phys. Oceanogr.*, **6**, 781-800.
- Paltridge, G. W., and C. M. R. Platt, 1981: Aircraft measurements of solar and infrared radiation and the microphysics of cirrus cloud. *Quart. J. Roy. Meteor. Soc.*, **107**, 367-380.
- Rasool, S. I., and S. H. Schneider, 1971: Atmospheric carbon dioxide and aerosols: Effects of large increases on global climate. *Science*, **173**, 138-141.
- Rodger, C. D., 1967: The use of emissivity in atmospheric radiation calculations. *Quart. J. Roy. Meteor. Soc.*, **93**, 43-54.
- , 1976: Approximate methods of calculating transmission by bands of spectral lines. *NCAR technical note, NCAR/TN-116+1A*.
- Seller, W. D., 1965: Physical climatology. *The University of Chicago Press*.
- Sarachik, E. S., 1978: Tropical sea surface temperature: An interactive one-dimensional atmosphere-ocean model. *Dyn. Atmos. Oceans*, **2**, 455-469.
- Sasamoir, T., J. London, and D. V. Hoyt, 1972: Radiation budget of the Southern Hemisphere. *Amer. Meteor. Soc. Monogr.*, **13**, 9-23.
- Schneider, S. H., 1974: The population explosion: Can it shake climate?. *Ambio*, **3**, 150-155.

- , and R. D. Dennett, 1975: Climate barriers to long-term energy growth. *Ambio*, 4, 65-74.
- , and R. E. Dickinson, 1974: Climate Modeling. *Rev. Geophys. and Space Phys.*, 12, 447-493.
- Seigel, A. D., 1977: Oceanic latent and sensible heat flux variability and air- interaction. *Environ. Res. Pap. CSU*.
- Stephens, G. L., 1978: Radiative properties of extended water cloud: II: Parameterization. *J. Atmos. Sci.*, 35, 2123-2132.
- , 1984: The parameterization of radiation for numerical weather prediction and climate models. *Mon. Wea. Rev.*, 112, 826-867.
- , and P. J. Webster, 1979: Sensitivity of radiative forcing to variable cloud and moisture. *J. Atmos. Sci.*, 37, 435-466.
- , 1981: Cloud and climate sensitivity of simple system. *J. Atmos. Sci.*, 38, 235-247.
- , 1984: Cloud decoupling of the surface and planetary radiative budgets. *J. Atmos. Sci.*, 41, 681-686.
- Thurman, H. V., 1981: Introductory oceanography. *Merrill Publishing Company*.
- Trewartha, G. T., and L. H. Horn, 1980: An introduction to climate. *McGraw-Hill Book Company*.
- Turner, J. S., 1969: A note on wind mixing at the seasonal thermocline. *Deep-sea Res.*, 16 Suppl., 297-300.
- Wallace, J. M., and P. V. Hobbs, 1979: Atmospheric science: An introductory survey. *Academic Press*.
- Walshaw, C. D., and C. D. Rodgers, 1963: The effect of the Curtis-Godson approximation on the accuracy of radiative heating rate calculation. *Quart. J. Roy. Meteor. Soc.*, 89, 122-130.
- Yamanoto, G., M. Tanaka, and S. Asano, 1970: Radiative transfer in water clouds in infrared region. *J. Atmos. Sci.*, 23, 303-313.

## Appendix A

### ON THE NUMERICAL INSTABILITY OF THE OCEAN MODEL

This appendix contains information concerning the numerical instability of the ocean model.

As mention in chapter 5, the time step for the ocean model was set to 15 minutes to avoid prognosis of unrealistic mixed layer depths. This small value is very inappropriate for climate modeling since huge amount of computational resources are required to perform time integration over time scales appropriate for climate studies. Therefore it is necessary to study the behavior of the numerical methods used in the model in order to increase the time step.

In the wind-dominated regime, the governing equations for the mixed layer ocean are

$$\frac{dT_s}{dt} = \frac{2}{h^2} \left[ -(G - D)^* + h \left( H_e^* + H_s^* + F_{nd,ir}^* + F_n^*(0) \right) - \int_{-h}^0 F_n^*(Z) dZ \right] \quad (A.1)$$

$$\left( w + \frac{dh}{dt} \right) = \frac{2 \left[ (G - D)^* + \int_{-h}^0 F_n^*(Z) dZ \right] - h \left[ \left( H_e^* + H_s^* + F_{nd,ir}^* + F_n^*(0) + F_n^*(-h) \right) \right]}{h(T_s - T_{-h})} \quad (A.2)$$

$$\frac{dT_{-h}}{dt} = - \left( w + \frac{dh}{dt} \right) \frac{\partial T_{-h}}{\partial Z} + \frac{\partial F_n^*(-h)}{\partial Z} \quad (A.3)$$

One property of the Runge-Kutta is that is a iterative scheme and its accuracy depends on the number of the iterative loops. The higher the number, the better is the accuracy but the higher is the computational demand. In the calculation of  $h$  from equation A.2, the iterative loops break the real time step into a number of smaller time step and it can be written as

$$t = n\Delta t \quad (A.4)$$

where  $n$  is the number of the iterative loops,  $t$  is the real time step, and  $\Delta t$  is the Runge-Kutta method time step. In this thesis, we referred the Runge-Kutta time step simply as time step. For the analysis performed in this thesis, the real time step is set to be 8 hours as dictated by the atmospheric model while  $\Delta t$  is set to be 15 minutes giving  $n = 32$ . It is possible to increase the computational efficiency of the problem by decreasing the number of iterative loops. Computations were performed in which  $n$  was reduced to 4 and 8 which corresponding to a value of 2 and 1 hour for  $\Delta t$ . The results are very close to the original answer obtained by 15 minutes integration. Thus a 1 or 2 hours time step can be used to save computer time in many cases.

It is also noted that we also have an option to change the real time step  $t$  along with the Runge-Kutta time step  $\Delta t$ . Calculations were also performed using a larger value of  $t$ . It is shown that a reasonable result can be obtained if this real time step is of order of 2 days and the Runge-Kutta time step is of order of 1 day. The solutions of  $T_s$  began to diverge from the original solutions for value greater than this time step. Analysis of these results showed that this divergence of the solution is associated with the forward integration in equation A.1 and the time step used rather than due to Runge-Kutta method in equation A.2 since  $h$  is still very well reproduced in these computations while  $T_s$  diverges from the original solutions.

On the basis of these analyses and given the application of the model to study the relative difference between two climate states, it is proposed that the following time step  $t = 1\text{day}$  and  $\Delta t = 4\text{hours}$  be employed in integrating equation A.1 to A.3.

## Appendix B

### CONSTRUCTION OF THE HYBRID ANNUAL/MEAN OCEAN MIXED LAYER MODEL

This appendix illustrates the analysis technique used in deriving the hybrid annual/mean ocean mixed layer model.

The equation controlling the mixed layer depth of the wind-dominated region is

$$\left( w + \frac{dh}{dt} \right) = \frac{2 [(G - D)^* + \int_{-h}^0 F_n^*(Z) dZ] - h \left[ (H_e^* + H_s^* + F_{nd,ir}^* + F_n^*(0) + F_n^*(-h)) \right]}{h(T_s - T_{-h})} \quad (B.1)$$

For  $w = 0$ , the mixed layer depth will advance downward as long as the first term on the right-hand side of the equation is greater than that of the second term. For the annual/mean study, the sensible heat, latent heat, and net downward flux of longwave radiation tend to transfer energy from the surface to the atmosphere, and therefore, the first three factors terms in that second term in parenthesis will also contribute to the increase of mixed layer depth. The advancement of the mixed layer depends completely on the magnitude of the remaining second term in parenthesis. Since the last term in this parenthesis term is small compared to that of the surface solar radiation term, it is therefore seems important to allow the surface solar radiation term to vary annually in order to control the extend of the mixed layer depth. As the mixed layer starts to decrease in value, we then switch to the next set of equation describing the heat-dominated region of the ocean model.

$$\begin{aligned}
& -h \frac{d}{dt} (H_e^* + H_s^* + F_{nd,ir}^*) + 2 \frac{d}{dt} \left[ \int_{-h}^0 F_n^*(z) dz \right] \\
& \left. -h \frac{d}{dt} F_n^*(0) - h \frac{d}{dt} F_n^*(-h) \right\} \quad (B.2)
\end{aligned}$$

For a annual/mean study, the first term of the right hand side is zero. The second term gives very slow positive changes with time and it has a effect of increasing the mixed layer depth. The rest of the terms on the right hand side are also zero for the annual/mean study since the surface inputs are constant in time. In order to allow further decrease in mixed layer depth, an annual cycle of the surface radiation term must also be incorporated in this equation. This annual cycle of surface solar radiation allows the model to flip back into the wind-dominated region and therefore insures that the model cannot predict a mixed layer depth that is too shallow.

